CHALMERS
UNIVERSITY OF TECHNOLOGY

Large Scale V2G Simulations for Frequency Stability

Modelling and Testing of V2G for Frequency Ancillary Service in the Nordic Power System

Master Thesis in Electric Power Engineering

Mahantha Ampavatina Kambagiri

Department of Electrical Engineering
CHALMERS UNIVERSITY OF TECHNOLOGY
Gothenburg, Sweden 2023

Master Thesis 2023

Large Scale V2G Simulations for Frequency Stability

Modelling and Testing of V2G for Frequency Ancillary Service in the Nordic Power System

Mahantha Ampavatina Kambagiri

CHALMERS

Department of Electrical Engineering
Division of Electric Power Engineering
Chalmers University of Technology
Gothenburg, Sweden 2023

Large Scale V2G Simulations for Frequency Stability
Modelling and Testing of V2G for Frequency Ancillary Service in the Nordic Power System

Mahantha Ampavatina Kambagiri

Department of Electrical Engineering
Division of Electric Power Engineering
Chalmers University of Technology
SE - 412 96 Gothenburg
Telephone 031-772 10 00

Thesis supervisor
Mattias Persson
RISE Research Institutes of Sweden AB
mattias.persson@ri.se

Thesis examiner
Peiyuan Chen
Department of Electrical Engineering
Division of Electric Power Engineering
Chalmers University of Technology
SE - 412 96 Gothenburg
Telephone 031-772 10 00
peiyuan.chen@chalmers.se

Typeset in LaTeX
Gothenburg, Sweden 2023

Abstract

The rise in integration of renewable energy sources is reducing the power system inertia, causing an issue with the frequency stability of the system. Low inertia makes the system more sensitive to disturbances, where even a small disturbance can lead to large frequency deviations which can go outside the frequency band. Ancillary services are needed as frequency regulation is becoming more and more important and prices for frequency regulation go up in the Nordic region. This thesis investigated the potential of providing ancillary services using the Vehicle-to-Grid (V2G) technology in a low-inertia power system dominated with renewable energy sources.

In this thesis, a preliminary aggregated V2G model was developed, that can provide ancillary services such as Frequency Containment Reserve for disturbances, up-regulation (FCR-D up) and Fast Frequency Reserve (FFR) according to the technical requirements laid out by ENTSO-E. The delays pertaining to communication and hardware response were considered. Considering the Simulink V2G model as a reference for validation and comparison of results, an aggregated user-written model was built in PSS®E.

Prequalification testing of the aggregated V2G model in both Simulink and PSS®E for the provision of FCR-D up indicated that they fulfilled the technical requirements and qualified to provide 100% of their capacity. However, when the communication and hardware response delays were introduced, the prequalified capacity reduced as the delays increased. No delays were considered for the provision of FFR as fixed activation times are stated in the requirements. The prequalification tests for FFR showed that the models fulfilled all the requirements and were qualified to provide FFR service.

The developed V2G models were implemented in power system models to provide frequency support in Simulink and PSS®E. Two scenarios with different inertia, representing the present and future power system, were considered to assess the impact of the models. When providing FCR-D support, the frequency nadir improved when the delays were short for both higher and lower inertia cases in Simulink and PSS ®E. However, as the delays increased, they resulted in frequency overshoots, which induced frequency oscillations in the lower inertia cases.

When providing FFR support to the power system models, the frequency nadir improved for both higher and lower inertia cases. The improvement was observed to be higher for the low inertia case as compared to the higher inertia with the FFR quantity and the disturbance being the same in both Simulink and PSS®E.

Keywords– Ancillary service, V2G technology, user-written modelling, prequalification testing, Nordic power system

Acknowledgements

This master thesis was carried out in collaboration with RISE Research Institutes of Sweden AB, Gothenburg, Sweden and the Division of Electric Power Engineering at Chalmers University of Technology, Gothenburg, Sweden.

I wish to express my gratitude to my supervisor Mattias Persson, for providing an opportunity to work with RISE. His guidance and constructive feedback were very helpful throughout the work.

I would also like to thank my examiner Peiyuan Chen, for his valuable recommendations.

Special thanks to Børge Lund for all the engaging discussions and constant support. His comprehensive knowledge is impeccable and I am really glad that I had the chance to work alongside him.

My extended gratitude to the whole Elkraftsystem team at RISE for being so welcoming and making my office time enjoyable.

Lastly, I would like to thank my family and friends for keeping me motivated and reminding me to stay relaxed.

Mahantha Ampavatina Kambagiri
Gothenburg, June 2023

List of Acronyms

RISE	Research Institutes of Sweden
TSO	Transmission System Operator
SOA	System Operation Agreement
ENTSO-E	European Network of Transmission System Operators for Electricity
EV	Electric Vehicle
V2G	Vehicle-to-Grid
SCALE	Smart Charging ALignment for Europe
FFR	Fast Frequency Reserve
FCP	Frequency Containment Process
FCR	Frequency Containment Reserve
FRR	Frequency Recovery Reserve
MBASE	Machine MVA base
SBASE	System MVA base

Table of Contents

List of Figures

List of Tables

1 Introduction

1.1 Background

The stability of a power system is an important aspect for providing reliable and quality power supply to the consumers. As such, it is necessary to mitigate any disturbances that can occur. There are different ways of evaluating the stability of the system, which are rotor angle stability, frequency stability and voltage stability [8], of which, frequency stability is one of the more important issues in recent years.

The quality standards for frequency are agreed upon by the Nordic TSOs in the Nordic System Operation Agreement (SOA), according to which, the frequency has to be maintained within the normal frequency band of ± 100 mHz around the nominal frequency of 50 Hz. A goal has been set to limit the number of minutes outside the normal frequency band to 10000 min/year [9]. The rise in integration of power electronic converter-based energy resources is reducing the system inertia, causing an issue with the frequency stability of the system [10]. Low inertia makes the system agile, where even small disturbances lead to large frequency deviations which can go outside the frequency band. Frequency deviations can trigger under frequency load shedding (UFLS) and generator frequency protection, which lead to cascading outages and blackouts [9, 11]. As the frequency regulation is becoming more and more important and prices for it in the Nordic region reaches higher levels, there is a need for ancillary services to mitigate the problem.

One of the possible solutions to this issue is the Vehicle-to-Grid technology (V2G). There is a huge potential from EVs to provide V2G service for frequency regulation [12]. Smart chargers that support bidirectional power flow allow active power injection into the grid when needed. By controlling a large fleet of EVs, sufficient active power can be provided to regulate the system frequency [13]. The rapid response from the EV batteries make them a very attractive option [14]. In addition, EVs can act as a possible backup for renewable resources, allowing the integration of intermittent power production [15].

Utilization of large, distributed resources for active power injection, however, is complex due to various factors. Delays in communication to the EVs, various charging protocols, activation time of the chargers [16], ramp rate restrictions and more contribute to the complexity. Delay in providing the service can have a negative impact on the system. As demonstrated in [17], increase in the delay causes unnecessary oscillations in the system, leading to instability. It is therefore important to assess the impact of these complexities on the stability of the system and determine important factors that can improve the performance. The thesis will address some of the main issues and provide potential solutions.

RISE is a part of a consortium of 29-partner `SCALE` project [18] , co-funded by the new Horizon Europe programme [19], which aims to progress smart charging infrastructure and assist in mass deployment of electric vehicles. RISE has been tasked to study the Nordic synchronous area with regards to frequency stability, technical requirements and delays considering centralized or decentralized V2G services. The thesis will be a part of this project.

1.2 Aim

To study the role of V2G in contributing to the frequency stability of a low-inertia power system dominated with renewable generation. The analysis will be based on the Nordic synchronous power system, and consider power system inertia reductions, and system settings with future generation mixes.

1.3 Scope

The issue under investigation is the possibility of providing ancillary services with V2G in a stable manner. The goal is to model the power system in Simulink and PSS®E and using simulations to determine if:

- The service can abide by the grid codes and regulations.
- The EV model, created using either an existing load model or a user written model, behaves as intended.
- The power system is stable when V2G is provided by EVs, considering inertia reductions and various generation mixes.
- The power system is stable when local frequency measurement and centralized frequency measurement are compared.
- The EVs delivering V2G services can provide sufficient support to the system in case of disturbances created with the PSS®E framework.
- It can be improved by studying the impact of various parameters.
- The study will also discuss the practical limitations of providing large scale V2G services.

In addition, the project contributes to the societal aspect. Since electricity has become a core fundamental of today's society, it should be reliable and of good quality. The project deals with the reliability of the system by exploring new possibility of supporting the system stability.

1.4 Limitations

The scope of the project includes modelling and simulation of V2G whilst having some limitations due to certain assumptions:

- The EVs are lumped as a cluster which can deliver active power based on request. It is to simplify the modelling of the system and emphasise more on the analysis.
- The response of the chargers to deliver the power back to the grid from EVs is considered as a delay. As such, no detailed modelling of the chargers will be done.
- The economics of providing such a service will not be studied. The economic aspects deviate from the actual scope of the thesis and requires detailed analysis of the spot market.

- The forecast for available power from EVs will be excluded.
- The project is limited to simulation-based results. No real life experiments will be conducted on the power system or the charging infrastructure. Some references from literature review however will be based on actual experimental analysis.
- The available Nordic power system models are not detailed enough to represent the actual power system.
- The main emphasis is on the frequency stability of the system. Other stability aspects will be monitored but not emphasised.
- Different scenarios will be used in the system to test the frequency response. However, the selected few do not represent all the possible scenarios of the grid.

1.5 Structure of the thesis

The structure of the thesis is as follows:

Chapter 1 gives an introduction to the topic of the thesis and mentions the scope and limitations of the project.

Chapter 2 provides an insight of the theory necessary for understanding the studies performed in the thesis.

Chapter 3 consists of the detailed steps that were involved in the study and the models used.

Chapter 4 presents the results of the simulations from the case study.

Chapter 5 includes the conclusions of the report.

Chapter 6 contains the discussion on sustainable, ethical, societal aspects and further work.

2 Theory

2.1 Power System Dynamics

2.1.1 The Swing Equation

The swing equation describes the mechanics of motion of a rotating machine [3]. The energy of a rotating mass is given as

$$E_r = \frac{1}{2} J \omega_r^2 \tag{2.1}$$

where J is combined moment of inertia of the generator rotor and the turbine in $kg.m^2$ and ω_r is the angular velocity of the rotor in mech.rad/s. The rotor is in balance when the mechanical power from the turbine is equal to the electrical power output of the generator. In case of an unbalance, the change in the rotational energy is

$$\frac{dE_r}{dt} = P_m - P_e \tag{2.2}$$

where P_m is the mechanical power from the turbine and P_e is the electrical power of the generator. Substituting equation 2.1 in 2.2, we get

$$J\omega_r \frac{d\omega_r}{dt} = P_m - P_e \tag{2.3}$$

Now we define inertia constant H as the ratio between the kinetic energy at rated speed ω_0 in watt-sec and the VA base of the machine. The inertia constant is

$$H = \frac{\frac{1}{2} J \omega_0^2}{VA_{base}} \tag{2.4}$$

The moment of inertia J in terms of H is

$$J = \frac{2H}{\omega_0^2} VA_{base} \tag{2.5}$$

Substituting this in (2.3)

$$\frac{2H}{\omega_0^2} VA_{base} \omega_r \frac{d\omega_r}{dt} = P_m - P_e \tag{2.6}$$

Rearranging the equation gives

$$2H \frac{\omega_r}{\omega_0} \frac{d\frac{\omega_r}{\omega_0}}{dt} = \frac{P_m - P_e}{VA_{base}} \tag{2.7}$$

Since $\omega_{r,pu} = \omega/\omega_0$ and $P_{pu} = P/VA_{base}$, the equation in per unit form becomes

$$2H \frac{d\omega_{r,pu}}{dt} = \frac{P_{m,pu} - P_{e,pu}}{\omega_{r,pu}} \tag{2.8}$$

Torque is given as $T_{pu} = P_{pu}/\omega_{r,pu}$. Therefore, equation 2.8 changes to

$$2H \frac{d\omega_{r,pu}}{dt} = T_{m,pu} - T_{e,pu} \tag{2.9}$$

This is the swing equation in per unit. However, since power system deals with power instead of torque, equation 2.9 is linearized to get

$$2H\frac{d\Delta\omega_r}{dt} = \Delta P_m - \Delta P_e(p.u.) \tag{2.10}$$

Equation 2.10 is the small deviation linearized model of the Swing equation in p.u. It shows that an imbalance in active power causes a change in angular velocity ω_r of the machine.

In the event of a disturbance, the electrical power changes much faster than the mechanical power. Hence, ΔP_m is zero right after the disturbance. The equation 2.10 after rearranging becomes

$$ROCOF = \frac{d\Delta\omega_r}{dt} = \frac{-1}{2H}\Delta P_e(p.u.) \tag{2.11}$$

where ROCOF here is the initial Rate of Change of Frequency. This parameter shows the rate at which the frequency changes after a disturbance. ROCOF depends on the inertia constant H ,the size of the disturbance ΔP_e and also the location.

2.1.2 Inertia and Frequency

Frequency of a power system is one of the key indicators of system stability [8]. It is proportional to the angular velocity ω_r of the generator. As such, changes in speed reflect on the frequency. Whenever a disturbance occurs in the system, the speed of the machine varies according to the swing equation 2.10. Depending on the size and type of disturbance, the frequency can go out of the frequency band set by the Nordic SOA. The frequency needs to be within the frequency band of $\pm$100 mHz around the nominal frequency of 50 Hz [20]. The power system is a dynamic system with a constant variation of loads and occasional faults. Due to this, the frequency is also varying continuously and needs to be monitored.

The increase in penetration of power electronic converter-based renewable energy resources is causing a reduction in the inertia of the system [10]. Although wind power plants have rotating masses, they are indirectly coupled to the power system through power electronics. Other renewable sources do not have any rotating mass to contribute to the inertia of the system. This reduction in inertia decreases the stability of the system as the system ROCOF increases, which can be seen in equation 2.11. The increase in ROCOF leads to large frequency deviations, making it easier for the frequency to exceed the frequency band limits. To mitigate the issue, the Nordic power system has operational reserves which react to the changes in frequency.

2.2 Frequency Response Indicators

To evaluate the frequency response, it is important to define a set of parameters which can indicate the performance of the system. Using these indicators, comparisons can be made between different scenarios. A set of frequency response indicators are defined by ENTSO-E, which are used in this study [21].

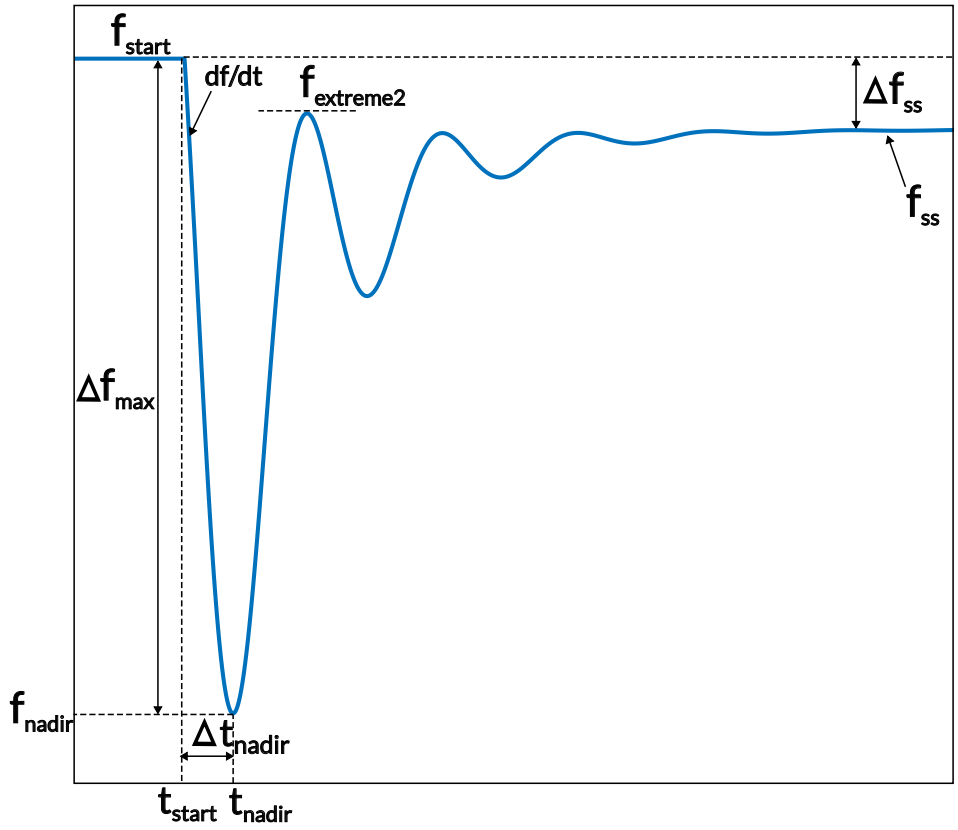

Figure 1: Frequency Response Indicators

- Starting frequency, $\mathbf{f_{start}}$:
  Starting frequency is the value of frequency right before the disturbance has occurred. Since the project is based on simulations, f_{start} will always be equal to 50 Hz.

- Starting of disturbance, $\mathbf{t_{start}}$:
  It is the time at which the absolute value of RoCoF exceeds 0.035 Hz/s.

- Frequency nadir, $\mathbf{f_{nadir}}$:
  Frequency nadir is defined as the lowest frequency when a disturbance has occurred.

- Time to nadir, $\mathbf{\Delta t_{nadir}}$:
  It is the time taken for the frequency to fall from f_{start} to f_{nadir}.

$$\Delta t_{nadir} = t_{nadir} - t_{start} \tag{2.12}$$

  where t_{nadir} and t_{start} are as shown in Figure 1.

- Rate of Change of Frequency, **RoCoF**:
  RoCoF is the time derivative of frequency df/dt. The average of the frequency derivative over 500 ms after the disturbance is presented as the RoCoF in this thesis, in accordance with [22].

- Maximum frequency deviation, $\mathbf{\Delta f_{max}}$:
  It is defined as the difference between the frequency nadir and the starting frequency.

$$\Delta f_{max} = |f_{nadir} - f_{start}| \tag{2.13}$$

- Steady state frequency, $\mathbf{f_{ss}}$:
  The steady state frequency is the final settling value of the frequency after a disturbance.

- Steady state frequency deviation, $\mathbf{\Delta f_{ss}}$:
  It is the absolute value of of frequency deviation after the frequency has reached the steady state.

$$\Delta f_{ss} = |f_{ss} - f_{start}| \tag{2.14}$$

- Frequency Bias Factor, **FBF**:
  Frequency Bias Factor or regulating strength is the ratio of total active power change at steady state to the steady state frequency deviation.

$$FBF = \frac{\Delta P}{\Delta f_{ss}} \tag{2.15}$$

- Frequency overshoot, f_{os}:
  Frequency overshoot is the maximum percentage of overshoot in the frequency from the steady state value, f_{ss}.

$$f_{os} = \frac{f_{extreme2} - f_{ss}}{f_{ss}} * 100 \tag{2.16}$$

- Decay rate, λ:
  The frequency of a power system after a disturbance behaves as a damped sinusoidal wave of the form:

$$y(t) = Ae^{-\lambda t} sin(\omega t - \Phi) \tag{2.17}$$

  where,
  y is the instantaneous magnitude of the function at time t,
  A is the amplitude of the initial peak of the wave,
  λ is the decay rate of the envelope,
  ω is the frequency of the signal, and
  Φ is the phase of the signal.

  To assess the damping of the system, the decay rate, λ is of particular interest, as it indicates the rate at which the frequency signal decays after the disturbance. High λ indicates high damping.

If $\lambda > 0$, the signal is damped.
If $\lambda < 0$, the signal is growing.
If $\lambda = 0$, the signal is un-damped.

2.3 Reserves in the Nordic Power System

The need for ancillary services grows every day as the penetration of renewable energy rises. These services are provided by different suppliers, who participate in the ancillary service market. The system operators procure the service through this market. In order for the supplier to participate in the market, they need to fulfill the requirements given in the Balance Responsibility Agreement [23]. There are different types of ancillary services based on the requirements for speed and endurance.

2.3.1 Fast Frequency Reserve (FFR)

Fast Frequency Reserve (FFR) is defined only for under frequency situations [6]. It aids in frequency containment process (FCP) during low inertia scenarios in the event of a sudden disturbance in the system such that the frequency can be stopped from reaching the maximum instantaneous frequency deviation [9].

To provide FFR service, automatic local control needs to be implemented [24]. The FFR service provider has three options to choose from based on the frequency level and activation time [6, 25].

Table 1: FFR alternatives

Alternative	Activation frequency (Hz)	Max full activation time (s)
A	49.7	1.30
B	49.6	1.00
C	49.5	0.70

Regardless of the above options, the service needs to deliver the full contracted power for either 5 s in case of short-term support or 30 s in case of long-term support.

2.3.2 Frequency Containment Reserve (FCR)

Frequency containment reserve (FCR) provides active power support to the grid in case of frequency deviations. It is controlled automatically based on the frequency deviation. It is divided into three services, which can be provided independently and regulate the frequency during normal operation and disturbances [26].

- Frequency Containment Reserve for Normal Operation (FCR-N): FCR-N provides frequency regulation within the frequency band of 49.90 Hz to 50.1 Hz. It facilitates both up and down regulation.
- Frequency Containment Reserve for Disturbances, Upwards (FCR-D up): FCR-D up provides upwards frequency regulation for under frequency conditions in the frequency range of 49.90 Hz to 49.50 Hz.
- Frequency Containment Reserve for Disturbances, Downwards (FCR-D down): FCR-D down provides the frequency regulation service for over frequency conditions in the frequency range of 50.10 Hz to 50.50 Hz.

2.3.3 Frequency Restoration Reserve (FRR)

FRR is aimed at bringing the frequency back to 50 Hz after the primary reserves have acted and the system has reached a steady state. FRR is of two types:

- Manual Frequency Restoration Reserve (mFRR): mFRR, as the name suggests, is manually controlled and is used to handle congestion in normal and disturbance conditions. It is a main prioritized balancing resource, which when activated replaces the remaining FCR and aFRR [9].
- Automatic Frequency Restoration Reserve (aFRR): aFRR is automatically activated through a control signal, whenever the frequency deviates from the nominal value [27]. The aFRR is a complement to mFRR in the frequency recovery process. The aFRR is different from FCR in the way that it is controlled by a centralised controller while FCR is locally controlled [9].

2.4 Vehicle-to-Grid

2.4.1 Overview

As the transition to Electric Vehicles (EVs) is increasing rapidly, the need for charging the vehicles is creating a challenge for the grid. Uncoordinated charging of EVs, where they charge at maximum power when connected to the grid till their batteries reach their full capacity, increases peak demand in the system. However, they are receiving great attention as a new alternative for frequency regulation due to their fast response. To utilize their potential, the use of smart chargers is essential [14]. Smart chargers provides control of EVs connected to the grid by the power utility or the EV aggregators. The EVs can be utilized to deliver ancillary services to the grid as and when required using this technology.

Unidirectional smart charging, also known as unidirectional V1G, provides controlled charging rate of the battery via communication [12]. The control of these chargers can be done in three ways: centralized, decentralized or local. The difference in these methods lies in the location of intelligence. Using V1G, the system load can be reduced during the peak hours by scheduling the charging to off-peak hours. This ensures system reliability and flexibility while also ensuring revenue to the EV owners. This technology is inexpensive compared to bidirectional smart charging as it utilizes the available infrastructure and avoids additional battery degradation.

Bidirectional smart charging or Vehicle-to-Grid (V2G) is a smart grid service that provides a means of communication and management of EV charging by the power utility or the aggregators [13]. Bidirectional V2G technology allows for bidirectional power flow between the EV and the grid to achieve benefits for different scenarios. This technology is more versatile than unidirectional smart charging in providing ancillary services. In addition to the benefits that unidirectional V1G provides, it can also provide frequency regulation, voltage regulation and reactive power support to the grid. A bidirectional V2G charger consists of two stages: a grid side AC/DC converter that provides active power factor correction, and an EV side DC/DC bidirectional converter that regulates the battery charging and discharging [28]. Though the technology may have numerous advantages, there are some setbacks for implementation which are discussed in the following sections.

2.4.2 Benefits

V2G is a flexible technology that can provide multiple services based on the requirement. EVs can provide V2G service when they are connected to the grid. Some advantages of this technology are discussed.

1. *Frequency and Voltage Regulation*
   Regulation services are important for maintaining the balance between the supply and demand during normal and disturbance scenarios. The frequency regulation can be provided by injecting active power into the grid, which relates to the equation 2.10. EVs have fast charging and discharging rates, which can provide frequency support quicker and cheaper than conventional regulation services [29]. Based on the frequency measurement, either centralized or local, the control signal is sent to

the EV whenever the frequency exceeds the limits set in the controller. The limits are set based on the type of service that the EV is providing, such as FCR or FFR. The voltage regulation deals with the reactive power balance between supply and demand. Using an embedded voltage control in the charger, the EVs can compensate inductive or capacitive reactive power by controlling the current phase angle [30].

2. *Demand Management*
   V2G can be used to control the charging schedules of the EVs. By discharging during peak demand hours and charging during low demand hours, the demand curve can be levelled. This avoids the peak loading capacity, which in turn avoids the need for increasing the peak power generation, thus reducing the cost of electricity [28]. The peak power generation is required for a short duration of the day. Therefore, it is more economical to provide this additional power from distributed resources. The EV owners profit from this service and are motivated to participate.

3. *Backup Storage*
   Renewable energy sources produce clean energy with zero emissions. However, their production is inconsistent and highly depend on environmental factors. There can be a lack of generation when the demand is high and excess generation when the demand is low. This drawback is a cause for concern as their penetration into the power system is increasing. To improve their reliability, energy storage systems are necessary. The integration of EVs can provide this service. EVs can act as energy storage backups to support the inconsistent renewable energy. EV fleets can provide the necessary power when there is a lack of generation from the renewable sources while also acting as energy storage when there is excessive production, which would otherwise be curtailed [31].

2.4.3 Challenges

As with every technology, there are challenges to overcome before the implementation of V2G technology.

1. *Investment Costs*
   EVs are connected to the grid via a charger. In order to participate in either V1G or V2G services, expensive charger hardware is necessary. Each EV owner that participates in V2G service needs to invest in a bidirectional charger. These chargers are equipped with complex controllers and software infrastructure, which are significantly more expensive than a traditional charger. The service can also increase the losses in the system due to multiple energy conversions in the EVs [32]. Depending on the penetration levels of EVs, they can overload the distribution equipment. When EVs provide active power support to the grid, the power flow reversal can cause large changes in the transformer flux and increase the losses, resulting in reduced transformer life [33]. New investments need to be made to increase the capacity of the transformers and cables to deal with the congestion and losses.

2. *Battery Degradation*
   Batteries have a limited cycle life due to the deterioration of different components

and irreversible chemical reactions that increase the battery internal resistance and reduce the usable capacity [34]. The age of the battery then becomes an important factor when participating in the V2G services. Older batteries with increased internal resistance will result in increased losses and heat. Also, the decrease in the usable capacity gives a very narrow operating window in which it can actively participate in V2G. Therefore, it is crucial to consider the battery health of EVs for an overall benefit for the grid operator and the EV owners.

3. *Participation*
   The whole idea of V2G services depends on the willingness of the EV owners to participate. However, due to concerns over battery health and range anxiety, the owners are discouraged to participate, even if the incentives are high. The technology is still in early stages of development.

2.4.4 Delays

To deliver the frequency regulation service with EVs, a good understanding of the available hardware is necessary. Testing the response of the charger and the EV battery is an important step to estimate its behaviour under various circumstances. Practical demonstrations are necessary in order to test the hardware. As the thesis only deals with simulations, a literature review has instead been conducted on the practical hardware tests that have been performed.

One interesting project is the Parker project, which is a Danish project to demonstrate the feasibility of existing EVs for providing frequency regulation services [35]. A number of EVs and bidirectional DC V2G chargers were utilized in the testing process at two different test sites. One test site consisted of a fleet of 10 EVs of same model and the other site consisted of 5 EVs of different make and models. All tested EVs had CHAdeMO standard charging ports as it was the only standard that could support V2G services during the project execution. The other advantages with the standard include the provision to test the reaction times, measure State-of-Charge (SOC) and identify the vehicle. The response times of these EVs were measured around 5-6 seconds (including communication delay) when using an EV aggregator [35].

A paper published in the World Electric Vehicle Journal provided a detailed testing of the response delays for locally and remotely controlled EVs [16]. The local control was carried out by providing the set-points manually on the hardware. The remote control utilized the infrastructure from the Parker project. The setup included communication, EV aggregator, a number of EVs and chargers. The local test is done to test the response of the hardware, which includes the charger and the EV battery while the remote test is to include the communication latencies. A Nuvve aggregator was used to monitor the grid frequency and remotely compute the control signal, which is then communicated to the controller present in the EV charger. The controller then sends a signal to the converter to provide the power from the battery. The local test resulted a maximum delay of 4 s and the remote test resulted in a maximum delay of 7 s. The 7 s delay is a comprehensive delay, which includes the response times of the charger, battery, communication latency and the processing delay of the aggregator.

An article published in Energies, MDPI [36] developed a V2G testing system with a Combined Charging Service (CCS) Type 2 together with the ISO 15118 communication protocol. The CCS Type 2 chargers are extensively used in Europe for a high power DC charging. Therefore, the article presents a potential scope of using the CCS Type 2 standard to deliver V2G services. Currently, the standard is not suitable to provide V2G services due to the lack of a communication unit to regulate the power flow. The test system includes a single EV equipped with a CCS Type 2 connector, ISO 15118-2 communication protocol and a vehicle control unit to enable V2G capability. An activation delay of 2 s was observed during the test. It should be noted that the delay is just the hardware response time without any remote communication delays. It can be seen that the CCS Type 2 hardware responds quicker than a CHAdeMO hardware. However, the test presented by [36] uses a highly modified EV and the test was performed just on a single vehicle. Therefore, it is difficult to compare the two standards.

The key takeaway is that there exists a delay in the response of EV hardware. And since the V2G service is provided by the EV aggregators, the communication latency needs to be considered.

2.5 Prequalification tests for FCR-D up and FFR in the Nordics

Prequalification tests are done to verify the compliance of the frequency regulation service providing entity with the requirements from the TSO [1]. It must be noted that there are multiple variations of these tests in different documents. Most of the documents are either in draft or pilot phase. Therefore, the latest finalized document available online is used as the main reference for the following tests [1], along with few other documents which have clearer description of the technical requirements [2, 5]. The main motivation is to demonstrate the evaluation process required by the TSOs and to assess the performance of the models in the prequalification tests. The different tests for the provision of FCR-D upwards and FFR are discussed in the upcoming sections.

2.5.1 Tests for FCR-D up

2.5.1.1 Step response sequence test

This test is conducted to check the compliance with the stationary performance requirements and to determine the capacity. The requirement is depicted in Figure 14. At 49.90 Hz, 0% of the FCR-D capacity should be activated and at 49.50 Hz and below, 100% of the capacity should be activated. A synthetic stepped frequency signal is provided as an input.

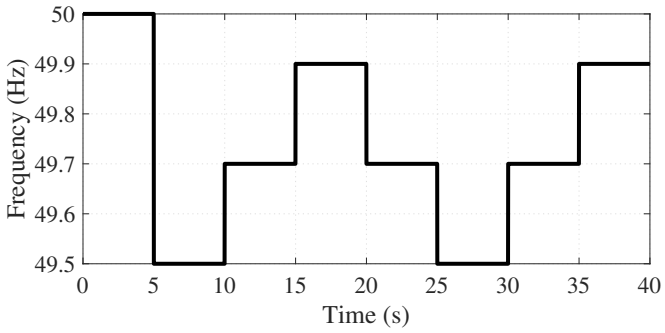

Figure 2: Frequency signal for step response test [1].

Figure 2 shows the input frequency signal for the test. The frequency is to be stepped only after the active power response has stabilized. The capacity of the FCR-D providing entity is calculated based on the active power response to the stepped frequency.

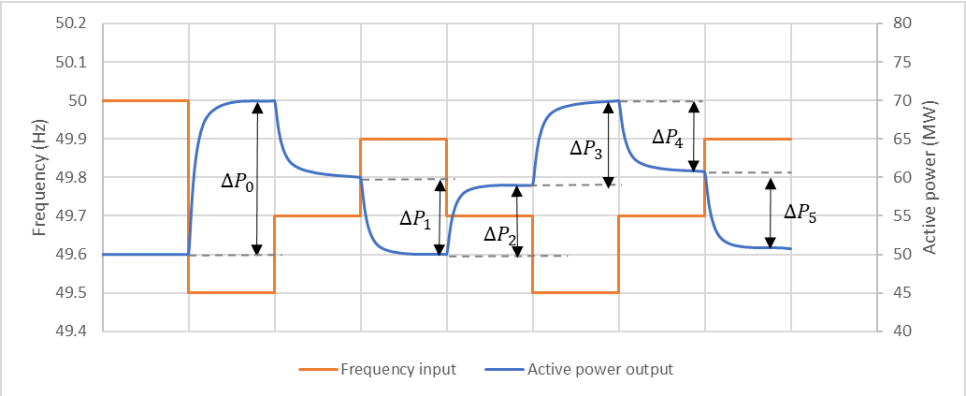

Figure 3: Step response test example from [1] showing the calculation of different power measurements.

The steady state activation is calculated as,

$$\Delta P_{ss} = |\Delta P_2 + \Delta P_3| \tag{2.18}$$

2.5.1.2 Ramp response test

The ramp response test is performed to determine the FCR-D dynamic performance. To perform ramp response test, the frequency signal input to the model is as shown in Figure 4.

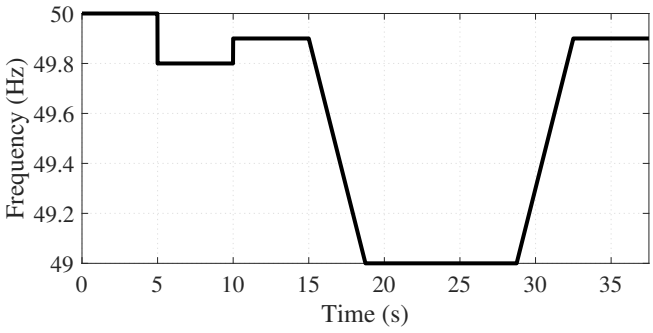

Figure 4: Frequency signal for ramp response test [1].

The frequency is first stepped to 49.80 Hz and back to 49.90 Hz. Then, a ramp signal is applied from 49.90 to 49.00 Hz with a slope of -0.24 Hz/s and back to 49.90 Hz with the same slope. Two quantities are obtained from the ramp test, $\Delta P_{7.5s}$ and $E_{7.5s}$, where $\Delta P_{7.5s}$ is the activated power in 7.5 s after the ramp and $E_{7.5s}$ is the activated energy from the start of the ramp to 7.5 s after the start of the ramp, given as:

$$E_{7.5s} = |\int_{t}^{t+7.5s} \Delta P(t)\, dt| \tag{2.19}$$

For the ramp test, the following requirements need to be fulfilled:

1. $\Delta P_{7.5s} \geq 0.93 \Delta P_{ss}$

2. $E_{7.5s} \geq 3.7\Delta P_{ss}$

The parameters 0.93 for power and 3.7 for energy are the performance goals in the open loop response for a good closed loop performance during a disturbance. Various KPIs were set up to evaluate the performance of the FCR contribution to keep the frequency above 49.0 Hz in the ENTSO-E report [37]. The system used has a rated apparent power of 23000 MVA, and 120 GWs of kinetic energy. The tests were conducted for a disturbance of 1450 MW. The KPIs showed that the power system needed at least 0.93 pu of active power and 1.8 pu s of energy activated in 5 seconds to ensure the power balance before the frequency drops down to 49.0 Hz. However, the newer reports indicated the possibility of relaxing the performance requirements to enable the qualification of more hydro FCR-D capacity [38], as they struggled to fulfill the dynamic requirements [39]. Hence, the parameters are slightly flexible, and change with every iteration of the report. More details on the tests are provided in the report [37].

In case the FCR-D entity fails to fulfill the requirements, it can provide partial support to the grid. This capacity, C_{FCR-D}, is the minimum of the three requirements from the steady state and ramp tests.

$$C_{FCR-D} = \min\left(\frac{\Delta P_{7.5s}}{0.93}, \Delta P_{ss}, \frac{E_{7.5s}}{3.7}\right) \tag{2.20}$$

2.5.1.3 Frequency domain stability test

To ensure that the FCR providing entity does not destabilize the system, the frequency domain stability requirement is tested through sine tests [2]. A number of sine waves with varying time periods, T, centered around 49.7 Hz with an amplitude of 0.1 Hz are applied. The time periods range between 10 s to 70 s. Figure 5 depicts one of the sine waves given as an input. The signal has a time period of 70 s.

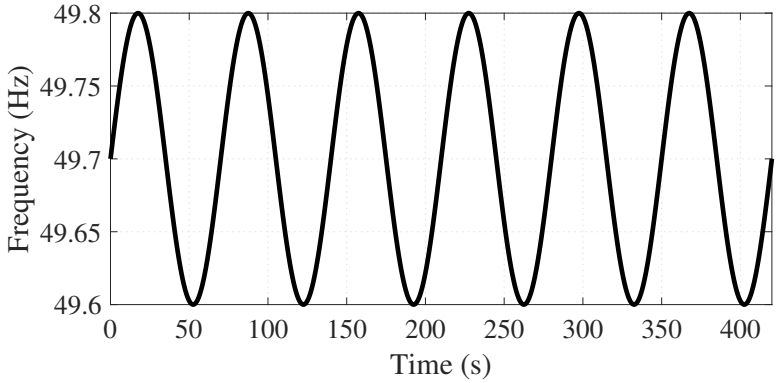

Figure 5: Sine wave input with an amplitude of 0.1 Hz, centered around 49.7 Hz for frequency domain stability test [2]. The curve in the figure has a time period of 70 s.

From the output power response, a transfer function of the system from the frequency input signal to the power output signal is constructed. The gain of the transfer function,

F(jω) is [2]:

$$|F(j\omega)| = \frac{A_p(\omega)}{A_f(\omega)} \frac{|\Delta f_{FCR}|}{|\Delta P_{ss}|} \tag{2.21}$$

where,
ω is the angular frequency of the sine wave,
$A_p(\omega)$ is the amplitude of the response power in MW,
$A_f(\omega)$ is the amplitude of the input frequency signal in Hz,
Δf_{FCR} is one-sided frequency band, equal to 0.4 Hz for FCR-D, and
ΔP_{ss} is the steady state activation in MW.

The phase of the transfer function in degrees is given as:

$$\Phi = \Delta t(\omega) \frac{360^\circ}{T} \tag{2.22}$$

where,
$\Delta t(\omega)$ is the time difference between the input and output signal, and
T is the time period of the sine wave.
To assess the performance of the FCR-D entity, a standardized power system model with a transfer function, G(jω), is considered to form an open loop system, $G_0(j\omega)$, given as:

$$G_0(j\omega) = F(j\omega)G(j\omega) \tag{2.23}$$

The transfer function of the power system model is:

$$G_(j\omega) = \frac{\Delta P_{FCR}}{\Delta f_{FCR}} \frac{f_0}{S_n} \frac{1}{2Hj\omega + K_f f_0} \tag{2.24}$$

The parameters for the power system model are presented in Table 2.

Table 2: Parameters for the power system model, G(jω) from [2].

Parameter	**Value**
FCR-D volume, ΔP_{FCR}	1450 MW
FCR-D one-sided frequency band, Δf_{FCR}	0.4 Hz
Nominal frequency, f_0	50 Hz
Nominal Power, S_n	23000 MW
Inertia constant, H	120000 MWs/S_n = 5.2174 s
Load frequency dependence, K_f	0.01

The Nyquist plot of the open loop system $G_0(j\omega)$ is plotted in the complex plane to evaluate the stability criteria. The system is considered stable if the Nyquist curve passes on the right side of and outside the stability margin circle with the center at (-1,j0) and radius 0.43.

2.5.1.4 Frequency domain performance test

The FCR-D entity must fulfill the frequency domain performance requirement for the

closed loop system, $G_c(s)$. The closed loop system transfer function of the system shown in Figure 6 is given as:

$$G_c(s) = K_{margin}\frac{G(s)}{1 + F(s)G(s)} \tag{2.25}$$

where K_{margin} is a scaling factor, which provides a margin of 95% on the requirement and F(s) and G(s) are the transfer functions of the FCR-D model and the power system model respectively from Section 2.5.1.3. The inertia constant, H, and the nominal power, S_n, for the power system model G(s) in this case are 4.5238 s and 42000 MW respectively.

The magnitude of the closed loop transfer function is required to be smaller than the typical disturbance profile of the system, D(s) = $\frac{1}{70s+1}$.

$$|G_c(s)| = |K_{margin}\frac{G(s)}{1 + F(s)G(s)}| < |\frac{1}{D(s)}| \tag{2.26}$$

The magnitude of the response of the closed loop transfer function and the disturbance profile for different time periods are plotted in a graph to assess the performance.

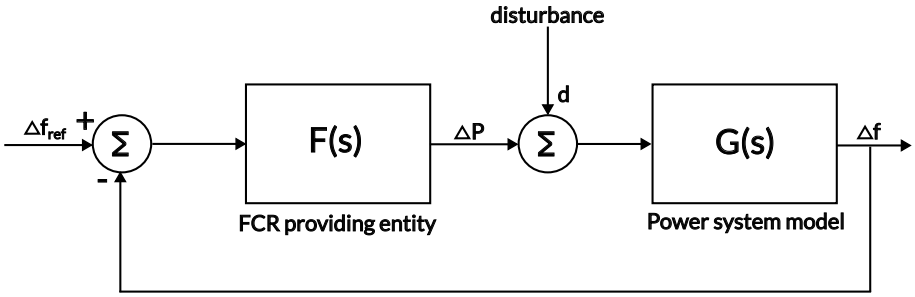

Figure 6: Closed loop system for frequency domain performance requirement from [2].

2.5.2 Tests for FFR

FFR is a fast acting active power support to the system, which responds to the frequency deviations. In order to provide the FFR service, the FFR providing entity must conform to the technical requirements laid out by ENTSO-E [6]. There are no specific tests to assess the performance of the FFR providing entity. However, the FFR capacity and overshoot need to be prequalified. A test is developed to assess the activation times of the FFR in the section below.

2.5.2.1 Activation

There are three different options for the FFR activation as mentioned in the Section 2.3.1. Any of the three alternatives can be chosen by the provider. To test the activation of the models built in simulink and PSS®E, a frequency pattern is developed to highlight the activation of the FFR models for each of the three alternatives. Figure 7 shows the frequency pattern for the test.

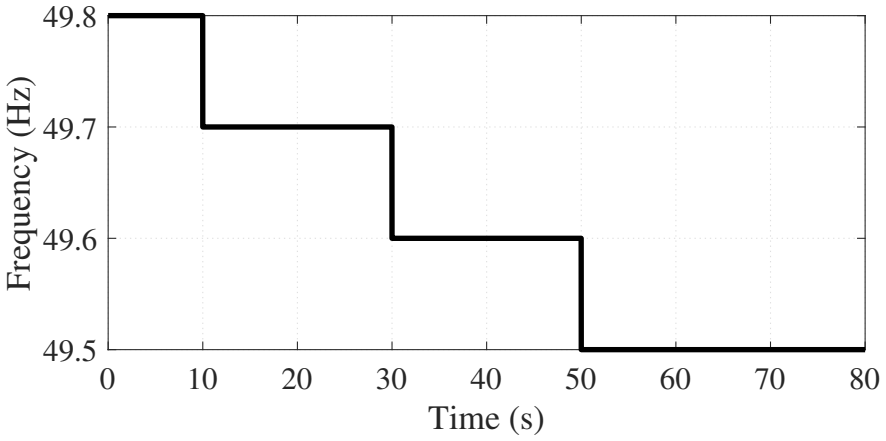

Figure 7: Frequency signal pattern to test the activation of FFR.

The prequalified FFR capacity is calculated as the minimum power from the entity during the support period, which is $t_2 - t_1$ in Figure 16. The capacity is calculated in per unit in this thesis.

$$C_{pre-qual} = min(|P(t) - P(0)|) \tag{2.27}$$

where,
$C_{pre-qual}$ is the prequalified capacity in pu,
P(t) is the power output of FFR entity in pu,
t is an arbitrary time in the interval $t_2 - t_1$ in Figure 16, and
P(0) is the power output of the FFR entity at activation instant t_1 in Figure 16.

The maximum acceptable overshoot over $C_{pre-qual}$ during the support duration is 35%.

$$FFR_{os} = \frac{max(|P(t) - C_{pre-qual}|)}{C_{pre-qual}} * 100 \tag{2.28}$$

where, FFR_{os} is the FFR overshoot in %.

2.5.2.2 Deactivation

After the support duration, the FFR should deactivate such that it does not exceed the maximum FFR capacity.

$$FFR_{deact,max} \leq FFR_{max} \tag{2.29}$$

where,
$FFR_{deact,max}$ is the maximum FFR during deactivation time in pu, and
FFR_{max} is the maximum FFR during the entire support duration in pu.

The rate of deactivation depends on the support duration. Long term support does not have any restrictions on the deactivation rate. However, the maximum deactivation rate is 20% of $C_{pre-qual}$ per second for short term support.

$$FFR_{deact,rate,max} = 0.2C_{pre-qual} \tag{2.30}$$

where, $FFR_{deact,rate,max}$ is in pu/s.

3 Modelling of V2G for frequency dynamic studies

3.1 Simulink Models

The preliminary model for simulation is developed in Simulink. The model consists of a generating unit with hydraulic turbine and an equivalent electrical battery model.

3.1.1 Hydro generating unit

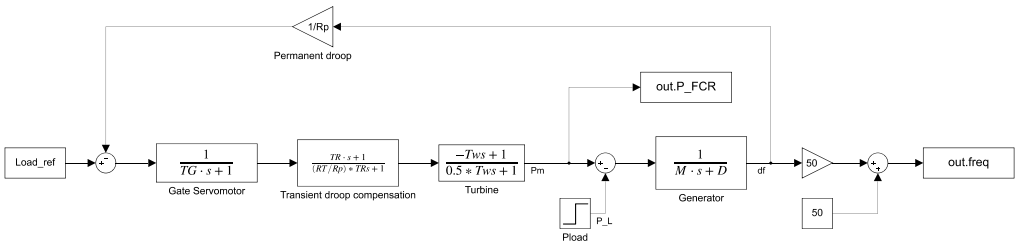

Figure 8: Block diagram of hydro generating unit implemented in simulink from [3].

The hydro generating unit depicted in Figure 8 is modelled according to the block diagram presented in [3] [1]. The governor includes a large transient droop, which compensates for the response of hydro turbines due to water inertia. When the water gate position is changed, the initial turbine power is the opposite to that sought. Therefore, a large transient droop R_T with a long resetting time T_R is included for a stable performance. The governor provides low gain for fast frequency deviations so that the water pressure level and output power can catch up, while it provides high gain for slower changes in frequency and during steady state.

Table 3: Typical values for hydro generating unit [3].

Parameter	Value
Permanent droop, R_P	0.05
Servo time constant, T_G	0.2 s
Inertia, M	6.0 s
Load-frequency dependence, D	1.0
Turbine time constant, T_W	1.0 s
Temporary droop, R_T	0.38
Resetting time constant, T_R	5.0 s

The model provides the speed deviation $\Delta\omega_r$ as an output. During steady state, the speed deviation is zero. The response of the system to a load step of 0.01 pu at 5 seconds is shown in Figure 9.

[1] chapter 11: Control of Active and Reactive Power, page 599.

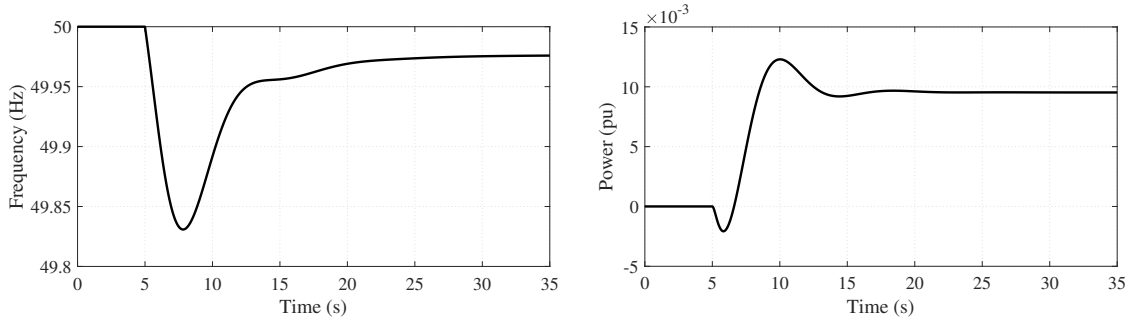

(a) Frequency. **(b)** Power output.

Figure 9: Hydro model response for a load step of 0.01 pu in simulink.

Figure 9a shows the frequency deviation. The increase in load causes a frequency reduction, which triggers the governor to open the gates to let in more water. This action initially causes a dip in the water pressure, resulting in a dip in the power output of the turbine at the 5 second mark as seen in Figure 9b. Once the water starts flowing, the output power starts to increase and consequently the frequency. This output power is the FCR provided by the hydro unit. The governor brings the system to a new steady state value, with the frequency settling at 49.976 Hz. The frequency settles at a lower value because of the frequency-dependent load factor, D. The steady state frequency deviation, Δf_{ss},is given as:

$$\Delta f_{ss} = \frac{-\Delta P_L}{\frac{1}{R_P} + D} \tag{3.1}$$

where, ΔP_L is the disturbance and R_P and D are the permanent droop and load-frequency dependence respectively, from Table 3.

3.1.2 Test scenarios for the Hydro generating unit

To analyze the effect of the simulink EV model on the system, various scenarios are selected based on the inertia of the hydro model. Table 4 shows the different inertia values for the tests. The high inertia is chosen from an ENTSO-E report [40]. The low inertia case is selected based on the damping of the system for the load step chosen.

Table 4: Test scenarios for the hydro generating unit with different inertia.

Scenario	Inertia, M (s)
Low inertia	4.0
High inertia	10.0

The hydro generator unit consists of a single droop characteristic for FCR-N as well as FCR-D. It provides 0.04 pu of power for FCR-N and the remaining for FCR-D. To limit the FCR-D up capacity, the dimensioning error is taken as the maximum deliverable FCR-D up for the hydro unit. The dimensioning error is set at 0.03 pu and the tests are executed on all the scenarios for a load step of $\Delta P_L = 0.03$ pu. Therefore, the total FCR capacity of the hydro unit is 0.07 pu. When the EV model provides the FCR-D up service, its

capacity is selected such that it provides 1/5 of the dimensioning error, which is 0.006 pu, and rest 0.024 pu is provided by the hydro unit.

3.1.3 V2G model

The V2G model consists of a battery with an SOC limiter. The battery model consists of a voltage source behind a series resistor, R_s, which is in series with a parallel RC network, denoted as R_t and C_t. The Thevenin equivalent of the model is presented in Figure 10.

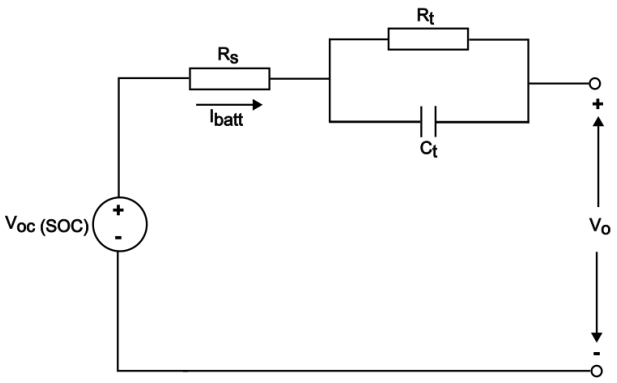

Figure 10: Thevenin equivalent model of the battery.

The voltage across the series resistor, V_{series} is given as:

$$V_{series} = IR_s \tag{3.2}$$

and the voltage across the parallel RC network is:

$$V_{trans} = I(\frac{R_t}{C_t R_t s + 1}) \tag{3.3}$$

The net battery output voltage then becomes:

$$V_0 = V_{OC} + V_{series} + V_{trans} \tag{3.4}$$

Now that we have the output voltage and current of the battery, the total power output is the product of V_0 and I.

$$P_0 = V_0 I \tag{3.5}$$

The block diagram in Figure 11 represents the equivalent electrical circuit, which is a Thevenin based electrical model [41] in simulink. It follows the design of the battery model presented in [4]. The input to the battery model is a power reference signal. The reference signal is calculated based on the type of service being provided. It depends on the trigger signal from the frequency measuring block. The battery is charging if the power signal is positive and discharging when the power signal is negative. The power signal is passed through a State-of-Charge (SOC) monitoring system, which limits the output of the battery based on the SOC limits provided. The SOC limiter represents the BMS of the battery. This signal is compared with the output power and the error is divided by the nominal voltage V_{nom} of the battery to convert it from error in power ΔP to error in

current ΔI. This current error signal is then fed to an integral controller, which provides the change in current to follow the reference power signal.

The SOC of the battery is calculated based on the current output from the model using Coulomb counting. The variation in charge ΔQ of the battery is then obtained. This charge is converted to per unit SOC value, with nominal capacity of the battery C_{nom} as the base. Given the initial SOC of the battery, the change in SOC is obtained. The open circuit voltage V_{OC} of the battery is generally modelled as a function of SOC. The function used in the proposed model follows the Nernst equation presented in [42], defined as:

$$V_{OC} = V_{nom} + s\frac{RT}{F}ln(\frac{SOC}{C_{nom} - SOC}) \tag{3.6}$$

where R, T and F are gas constant, battery temperature and Faraday constant respectively. s is a sensitivity factor between the SOC and V_{OC}.

The parameters of the battery model are presented in Table 5.

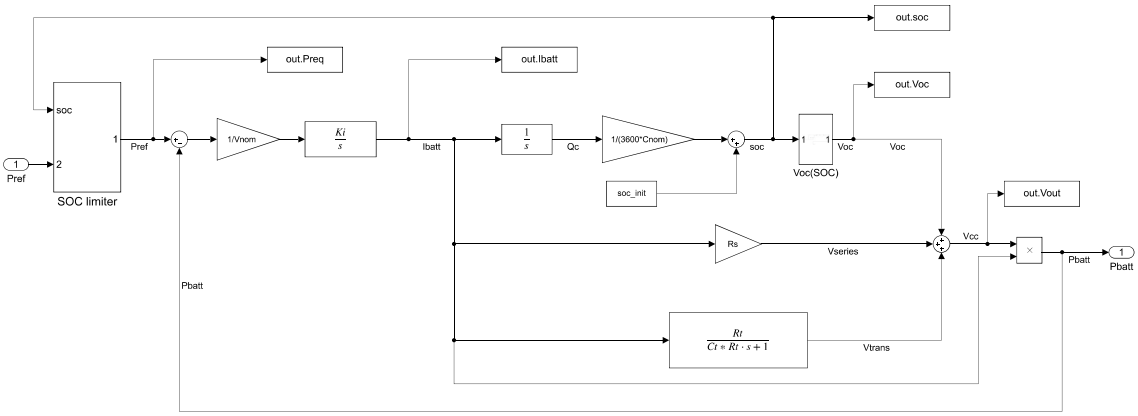

Figure 11: Equivalent electrical circuit model of the V2G model in Simulink following the battery design from [4].

Table 5: Parameters of the battery model from [4].

Parameter	Value
Nominal voltage, V_{nom}	364.8 V
Nominal capacity, C_{nom}	109.65 Ah
Battery size, C_{batt}	40 kWh
OCV sensitivity factor, s	60
RT/F	0.02612
Series resistance, R_{series}	0.074 Ω
Charge transfer resistance, R_{ct}	0.047 Ω
Double layer capacitance, C_t	703.6 F

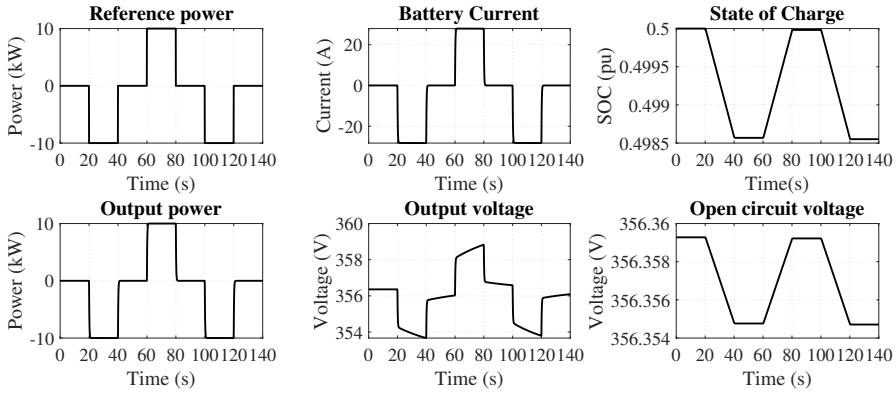

Figure 12: Response of the V2G model to stepped power reference in Simulink.

Figure 12 shows the response of the battery model in Simulink when subjected to a stepped reference power. A negative power reference indicates discharge, which results in a negative current, decrease in state of charge and the output voltage. The discharge instances can be seen at 20-40 second and 100-120 second periods. A positive power indicates charging, which increases the state of charge of the battery. The charging instance can be seen at 60-80 second period. The capacitive effect of the RC circuit can be seen in the output voltage. The instantaneous jumps in the voltage are due to the series resistance.

3.1.4 FCR-D Setup

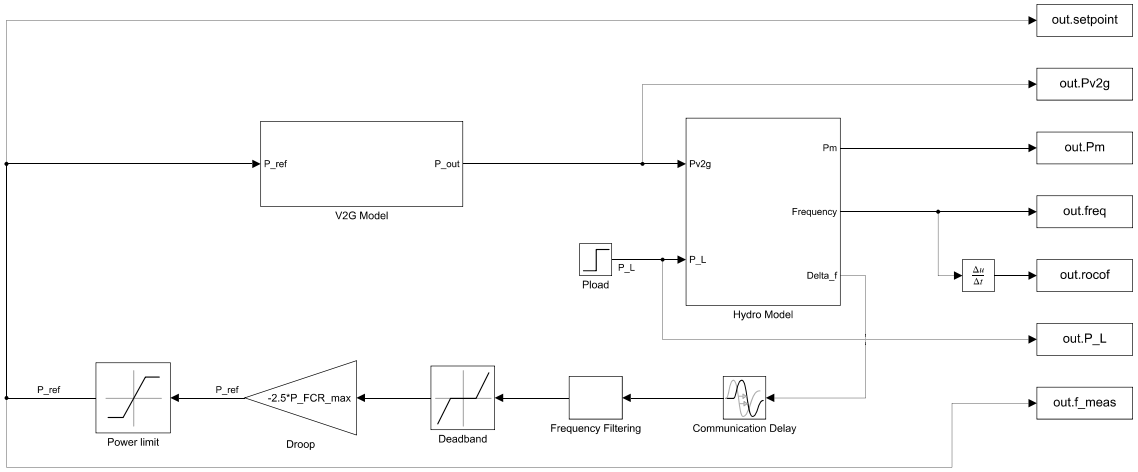

Figure 13: Complete Simulink model for studying FCR-D up response.

As mentioned in Section 2.3.2, FCR-D up is activated in the frequency range of 49.90-49.50 Hz. The activation is linear, ranging from 0% of the total power at 49.90 Hz to 100% of the total power at 49.50 Hz. The activation curve is shown in Figure 14. The slope of the curve defines the droop setting, which is equal to -2.5*P_{max}, where P_{max} is the maximum deliverable power for FCR-D. The frequency dead-band offsets the output such that the

signal starts from zero when the frequency deviation is outside the dead-band. The Δf from the model is the deviation of frequency from 50 Hz. Therefore, the dead-band is set in the range of (-0.1, ∞) Hz. The power limit sets the upper limit of the power demand signal to P_{max}. The net output from the droop, P_{ref}, is given as:

$$P_{ref} = -2.5P_{max}(\Delta f + 0.1) \tag{3.7}$$

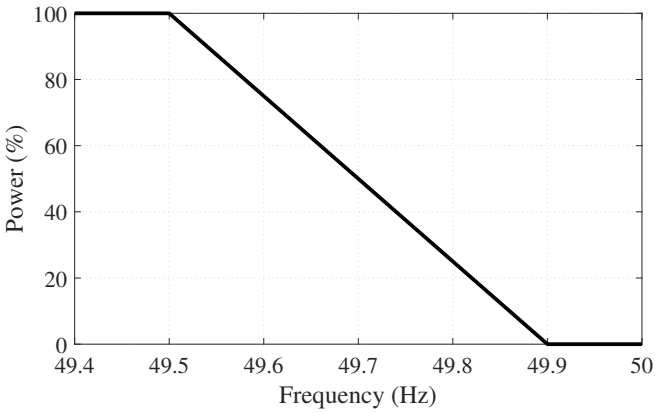

Figure 14: Linear activation of FCR-D up according to [5].

The EV charger communication is modelled as a delay. The delay is due to the activation time of the charger hardware. More details on the delays are provided in Section 2.4.4. The charger model sends the delayed reference signal to the battery. A power scaling factor converts the power reference signal from per unit to Watts on a base of 10 kW. The scaling is done to avoid conversion of the battery parameters to per unit. The 10 kW base is chosen based on the size of the available V2G chargers. The power output from the battery is converted to per unit before providing the necessary active power as FCR-D to the hydro generating unit.

3.1.5 FFR setup

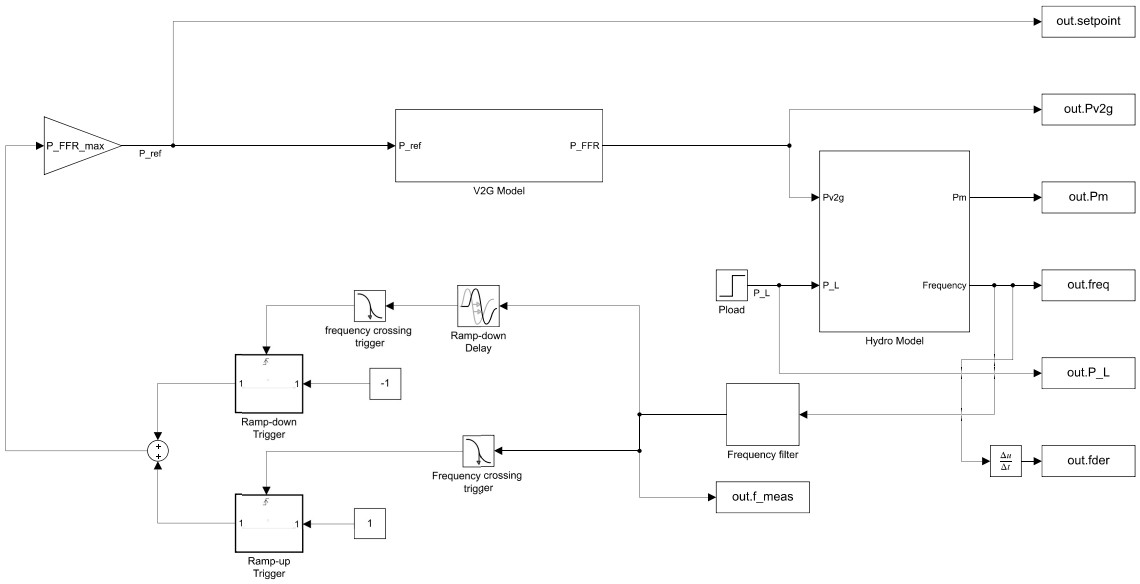

Figure 15: Complete Simulink model for studying FFR response.

The Simulink model for FFR simulation is shown in Figure 15. The V2G and the hydro model are identical to those used for FCR-D. To provide FFR service, the frequency measurement must be local according to the TSO requirements [24]. The local frequency measurement avoids the communication delays. Figure 16 shows the required output of FFR. It is triggered in different ways based on the frequency set-point, as discussed in Section 2.3.1. The activation time, t_1, must be less than or equal to the maximum full activation times. The duration of the support $(t_2 - t_1)$ can be 5 seconds for short duration support or 30 seconds for long duration support.

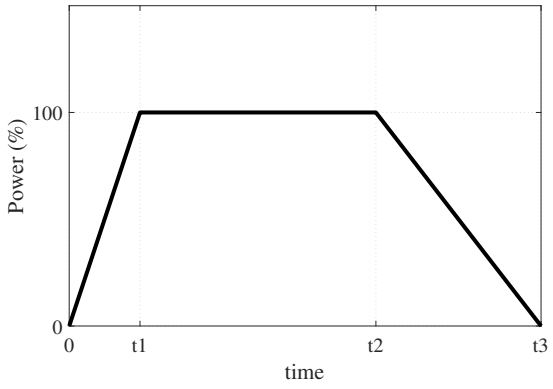

Figure 16: Activation of FFR according to [6].

To activate the FFR response, a hit crossing block is used, which sends a trigger signal when the frequency crosses the activation set-point. The power is then stepped up to 100%

of the capacity. The power is then ramped down after a certain duration. The duration of the signal is controlled by the ramp-down delay block. The ramp down rate is limited to 20% of the maximum FFR capacity per second in case of 5 second duration support, though no such limitation exists for the 30 second duration support.

3.2 PSS®E Models

3.2.1 Nordic 44 model

The Nordic power system is a large synchronous electrical grid, consisting of Swedish, Norwegian, Finnish and eastern part of Danish power system. The principles of system operation in the Nordic power system is based on the SOA between the Nordic TSOs [43]. This system is not synchronized with the rest of Europe. However, there are multiple non-synchronous HVDC connections with other European countries.

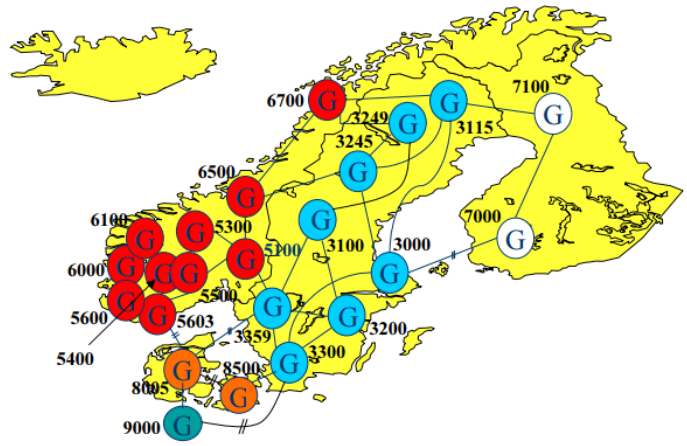

Figure 17: Geographical representation of the Nordic 44 Model from [7].

Nordic 44 is an aggregated 44-bus power system model, built for the analysis of dynamic behaviour of the Nordic power system [7]. The initial model was developed by STRI in collaboration with the Norwegian University of Science and Technology (NTNU) using the data from Statnett. The N44 model by NTNU is available in PSS®E and DIgSILENT Powerfactory. Figure 17 shows the geographical representation of the N44 model.

There are many variations of the N44 network model, each with different generation, loads, inertia, etc. Table 6 contains the details of the N44 model used in this thesis. The single line diagram of the model is provided in Appendix A.1.

Table 6: Nordic 44 base network parameters.

Parameter	Value
Buses	44
Generators	61
Load	25
Total Active Power Generation	51777.21 MW
Total Active Power load	50989.01 MW
Total production capacity	65763.05 MVA

3.2.2 Test Scenarios for Nordic 44 model

To analyze the impact of the PSS®E model introduced in Section 3.2.3, different test scenarios are created using the Nordic 44 model. The scenarios simulate the future, low-inertia grids due to increasing renewable energy resource penetration. To reduce the inertia of the Nordic 44 model, several conventional generators are replaced by renewable wind generators. The low inertia test scenario has a wind penetration level of 50%. Further increase in wind penetration created issues with the stability of the network and thus, not considered. The different scenarios are tabulated in Table 7.

Table 7: Test scenarios for different levels of wind penetration in PSS®E Nordic 44 network based on the active power generation.

Scenario	**Inertia constant M (s)**	**Kinetic Energy E_k (GWs)**	**Wind Power (MW)**
Base case	4.26	140.18	0
50% Wind	1.93	63.60	25978.31

The base network model is also modified in terms of the FCR provided by the conventional generators. The total reserve of the FCR providing units that is available in the base network model is 5462 MW. The network has an unrealistic high regulating power, which is reduced by removing the droop-based governors for many of the units. The total FCR from these units is calculated based on the dimensioning error of the network, ΔP_G, which is chosen as a single unit producing 1329 MW at Bus 6100. The unit is chosen since it is close to the dimensioning error of the Nordic region, which is 1450 MW. The total FCR requirement in the network then becomes 1329 MW for FCR-D and 600 MW for FCR-N, adding up to 1929 MW. Table 8 shows the conventional generation units which have a total FCR capacity of 2032.88 MW. These units are indicated in the single line diagram in Appendix A.2.

Table 8: FCR providing units in PSS®E N44 network model.

Bus Number	**Machine ID**	**Droop (pu)**	**Total FCR (MW)**
3115	1, 2, 3	0.04	391.68
5400	1, 2	0.05	290.07
6100	3, 4, 5	0.05	443.02
6700	1, 2	0.05	354
7100	1, 2, 3	0.04	554

The renewable wind generator consists of renewable plant control model REPCA1, renewable electric control model REECA1, renewable drive train model WTDTA1 and a renewable generator model REGCA1. The same models are used for all the wind generators at different buses. The wind model provides the necessary active and reactive power similar to the generator it replaces. However, it does not provide any FCR support during dynamic simulations. Table 9 provides the information about the generators that are replaced for the wind penetration scenario. The location of the wind generators are illustrated in Appendix A.4.

Table 9: Renewable wind generators for 50% wind penetration scenario in PSS®E N44 network.

Bus Number	Machine ID	Total Power(MW)
3000	1,2	2200
3300	1, 2, 3	1938.77
3359	1, 2, 3	3310
5100	1	972.44
5300	1, 2	2551.32
5600	1, 2	2492
7000	1, 2, 3, 4, 5, 6	6513
8500	1	994
3245	1	1000
3249	1	1042
5500	1	900
6000	1	735.73
6100	1	1329.06

Seven EV models for the V2G service provision are located at different locations in the network. These locations are chosen such that the EVs are spread evenly throughout the network. Each EV model represents an aggregate of EVs at each location, and have a peak output power of 40 MW each. The rating of the EV models are chosen such that they provide 1/5 of the dimensioning error capacity. When the EVs provide FCR-D service, the generator units with machine IDs 1 and 2 at Bus 6700, that provide FCR, are disconnected. Therefore, the total contribution for FCR from conventional generators reduces to 1678.772 MW and 280 MW from the EVs for a total FCR capacity of 1958.772 MW. The locations and capacities of the aggregated EV models are tabulated in Table 10 and also indicated on the single line diagram in Appendix A.2.

Table 10: Aggregated EV models in PSS®E N44 network model.

Bus Number	Machine ID	FCR-D up capacity (MW)	FFR capacity (MW)
3100	1	40	14.286
3115	4	40	14.286
5300	3	40	14.286
6100	6	40	14.286
6500	5	40	14.286
7100	4	40	14.286
8500	7	40	14.286

For FFR provision from the EVs, the models are located at the same buses as in Table 10. However, the capacity is reduced to 14.286 MW each, which gives a total FFR capacity of 100 MW.

The loads in the N44 network are modelled as 40% active power and 9% reactive power for the constant admittance characteristic, while the rest is constant power characteristic. This load profile is chosen due to stability issues with the N44 model in dynamic

simulations when wind penetration is introduced.

3.2.3 PSS®E Dynamic Models for V2G

Dynamic simulations are required to study the dynamic behaviour of the system during an event. Events such as line to ground faults, generator tripping, load variations etc. cause a disturbance in the system. It is necessary to understand the response of the system when subjected to such disturbances to determine the stiffness of the system. Precautionary measures can then be taken to avoid complete failure of the system. In order to simulate the dynamics of the system, the use of dynamic models is necessary. PSS®E has two types of dynamic models that can be implemented:

- Defined models within PSS®E
- User written models

Defined models within PSS®E are built-in models, ready to use. Models for generators, loads, stabilizers, excitation systems, etc. are defined in the PSS®E dynamics model library. The model library document provided with the software contains the details of all the defined models. On the other hand, user written models can be built by anyone using FORTRAN programming language. PSS®E has this provision for users who need a customized model that is not available in the model library.

3.2.3.1 User-written Models

To build a basic user written model, the preliminary step is to have a detailed block diagram with a good knowledge of each stage of the system. The block diagram can utilize the dynamic simulation arrays present in the PSS®E dynamic simulation data structure as an input to the model or to enter values into the arrays. The different dynamic simulation arrays are listed in the program operational manual[2]. PSS®E runs through different modes at different stages in the dynamic simulation process. A MODE flag, present in the PSS®E common memory, is set by the PSS®E activities before calling the equipment models. The value of the flag determines the action that the model must take. A short description of the different states of the MODE flag are provided below.

1. MODE = 1: The model must initialize all the state variables and algebraic variables.
2. MODE = 2: The model must compute the derivatives of each state.
3. MODE = 3: The model must compute the current value of the output signal and update the appropriate dynamic simulation array.
4. MODE = 4: The model must update the variable NINTEG, which keeps track of the highest indexed state under use.
5. MODE = 5 to 7: These modes are used for documenting and creating data report for the model.
6. MODE = 8: The mode is used to give a description of the constants used in the model.

[2]chapter 25: Dynamic simulation setup and procedures, page 1191.

More details on the MODE flag are available in the program operation manual[3].The FORTRAN code contains the necessary computations for each mode. The code is written in Visual Studio. The derivatives of each state of the model need to be described in MODE 2 in the code. To make it easier, PSS®E provides functions for elementary blocks, which can be used in modes 1, 2 and 3. The elementary block functions are provided in the program application guide volume 2[4]. After the code is written, it is compiled using the PSS®E environment manager. The file is then converted to a .dll file using the environment manager, which can be imported directly into PSS®E.

To use the written model, it needs to be implemented in the .dyr file. The format to be used for different types of models, including the user-written models and their details are provided in the program operational manual[5]. The general format for a user-written model is:

BUSID 'USRMDL' ID 'model name' IC IT NI NC NS NV data list /

where,
BUSID - bus number.
ID - sequence number of the model.
IC - user model type code.
IT - for user models that are called from CONEC and/or CONET.
NI - Number of ICONS used by the model.
NC - Number of CONS used by the model.
NS - Number of STATES used by the model.
NV - Number of VARS used by the model.
data list - ICONs followed by CONs values in sequence.

The parameters ICON, CON, STATE and VAR are large general purpose storage arrays. These arrays contain the constants and variables used by various models in contiguous block of locations. The details about these arrays are provided in the program operation manual[6].

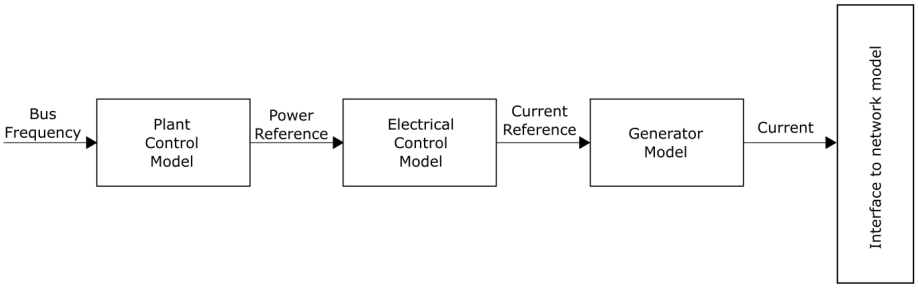

Figure 18: General structure of a Renewable Generator Model in PSS®E.

A user written renewable generator model is built for the thesis to represent an EV model

[3]chapter 27: Model writing, page 1229.
[4]chapter 24: elementary blocks for handling transfer functions in dynamic models, page 521
[5]chapter 18: dynamic simulation activity descriptions, page 1001.
[6]chapter 25: dynamic simulation setup and procedures, page 1191.

in the power system. The general structure of the model is shown in Figure 18. It is to be noted that the term 'Renewable' is an important detail for the modelling. Renewable models in PSS®E use a completely different set of dynamic simulation arrays, which are grouped as wind related models in the PSS®E documents. The 'renewable' term is implied whenever user-written models are mentioned in this report. It is possible to build generic user-written models, but are not covered under the scope of the work. The model consists of a plant control model, electrical control model and a generator model. The plant control model is similar to a governor model. It monitors the bus frequency and provides the power reference signal based on the logic used. It can be modified to provide either FCR or FFR service. The electrical control model takes the reference power and calculates the required power into a reference current signal. It contains the battery model described in Section 3.1.3. The generator model is a current injecting model and provides the connection point to the network. The three models are written separately, following the sequence shown in Figure 18.

3.2.3.2 Renewable Plant Control Model

The renewable plant control model makes the distinction between FCR and FFR service. The models follow similar principles used in the simulink models in Section 3.1.4 and 3.1.5.

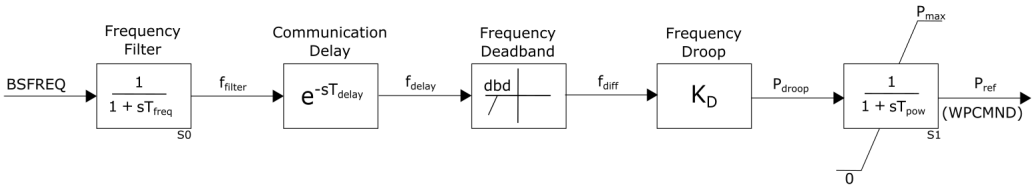

Figure 19: User-written Renewable Plant Control Model for FCR-D up (USPMDL) in PSS®E.

The renewable plant model in Figure 19 shows the block diagram of the user written plant model for providing FCR-D up service. The name of the model 'USPMDL' is arbitrarily chosen. The input to the model is the bus frequency array, BSFREQ. The BSFREQ array contains the per unit frequency deviation of all the buses in the network. The bus sequence number of the bus to which the generator model is connected is used to find the right index of the BSFREQ array. The frequency signal is passed through a low pass filter to filter out noise. This filtered signal, f_{filter}, is sent to a delay block, which represents the communication delay in the frequency measurement signal when centralized measurements are used.

The delay block is coded as a circular buffer and uses multiple VARS to simulate act as communication delay. The delayed signal f_{delay} then passes through a frequency dead-band, that gives an output when the frequency deviation exceeds the set threshold. Since FCR-D up is provided in the range of 49.90-49.50 Hz or 0.998-0.990 pu, the dead-band passes the signal through when the frequency deviation exceeds -0.002 pu. The model takes the frequency trigger (49.90 Hz) as the input and calculates the dead-band as:

$$dbd = 1 - f_{trigg} \tag{3.8}$$

The output of the dead-band is shifted such that it begins from zero. The frequency droop is calculated in a similar way as presented in Section 3.1.4 but in per unit instead. The

droop is calculated to be -125*P_{max}, where P_{max} is the maximum available capacity in the V2G model in per unit on MBASE. The output of the frequency droop, P_{droop} is an unbounded active power reference signal.

The power filter limits the active power reference signal to P_{max}. This power reference signal is stored in the WPCMND array, which contains the active power command from wind plant control models in per unit on the base of machine MVA rating (MBASE). Reactive power support is not in the scope of this thesis and thus not implemented in the model. In the background, the reactive power reference signal is explicitly equated to zero in WQCMND array.

The model details for the CONS, STATES and VARS are listed in Tables 11, 12 and 13 respectively. The FORTRAN code for the model is provided in Appendix B.1.

Table 11: CONS for user-written plant model for FCR-D up (USPMDL).

CONS			
Number	**Name**	**Unit**	**Description**
J	T_{freq}	s	Frequency filter time constant
J+1	T_{del}	s	Measurement delay
J+2	f_{trigg}	pu	Frequency trigger
J+3	K_D	pu/pu	Droop constant
J+4	T_{pow}	s	Power filter time constant
J+5	P_{max}	pu	Max output power in pu on MBASE

Table 12: STATES for user-written plant model for FCR-D up (USPMDL).

STATES		
Number	**Name**	**Description**
K	f_{filt}	Filtered frequency
K+1	P_{ref}	Reference power output (WPCMND)

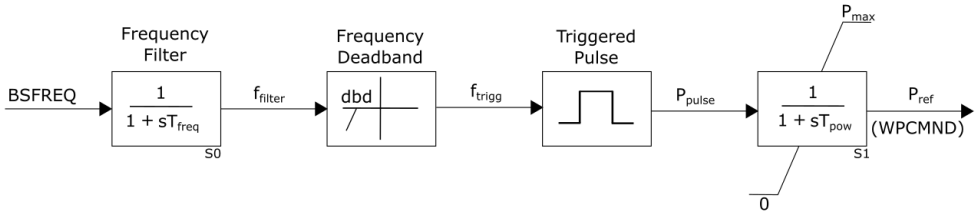

Figure 20: User-written Renewable Plant Control Model for FFR (USPFFR) in PSS®E.

Table 13: VARS for user-written plant model for FCR-D up (USPMDL).

VARS		
Number	**Name**	**Description**
L	f_{diff}	Frequency error signal
L+1	P_{droop}	Ulimited reference power
L+2	dbd	Frequency deadband
L+3	f_{delay}	Delayed frequency signal
L+4	ind	Index tracker for circular buffer
L+5	status	status flag for circular buffer
L+6 to L+505		storage locations for circular buffer

The renewable plant control model for providing FFR (USPFFR) is shown in Figure 20. The principle of operation is different from the method in Section 3.1.5. The input to the model is the frequency deviation array BSFREQ, which is filtered and passed through the dead-band. The dead-band is calculated as given in (3.8). The different options for triggering frequency and activation times are provided in Section 2.3.1. Based on the option specified, the dead-band adjusts the threshold.

When the frequency exceeds the threshold, a trigger signal is sent to the triggered pulse block. The block generates a 5 second long pulse. The 5 second duration is selected as it is the minimum support duration. This pulse is similar to the curve shown in Figure 16. The pulse is bounded by the limiter and stored in WPCMND array. The signal is provided as an input to the electrical control model. The model details of CONS, STATES and VARS for USPFFR model are provided in Tables 14, 15 and 16. The FORTRAN code for the model is provided in Appendix B.2.

Table 14: CONS for user written plant model for FFR (USPFFR).

CONS			
Number	**Name**	**Unit**	**Description**
J	T_{freq}	s	Frequency filter time constant
J+1	f_{trigg}	pu	Trigger frequency
J+2	P_{max}	pu	Max output power in pu on MBASE
J+3	T_{pow}	s	Power filter time constant
J+4	t_{act}	s	Activation time of FFR

Table 15: STATES for user-written plant model for FFR (USPFFR).

STATES		
Number	**Name**	**Description**
K	f_{filter}	Filtered frequency
K+1	P_{ref}	Reference power output (WPCMND)

Table 16: VARS for user-written plant model for FFR (USPFFR).

VARS		
Number	**Name**	**Description**
L	*dbd*	Frequency deadband
L+1	P_{pulse}	Power pulse signal
L+2	t_0	Time of trigger
L+3	*status*	trigger flag
L+4	t_{deact}	deactivation instant
L+5		deactivation flag

3.2.3.3 Renewable Electrical Control Model

The renewable electrical control model consists of the battery model discussed in Section 3.1.3.

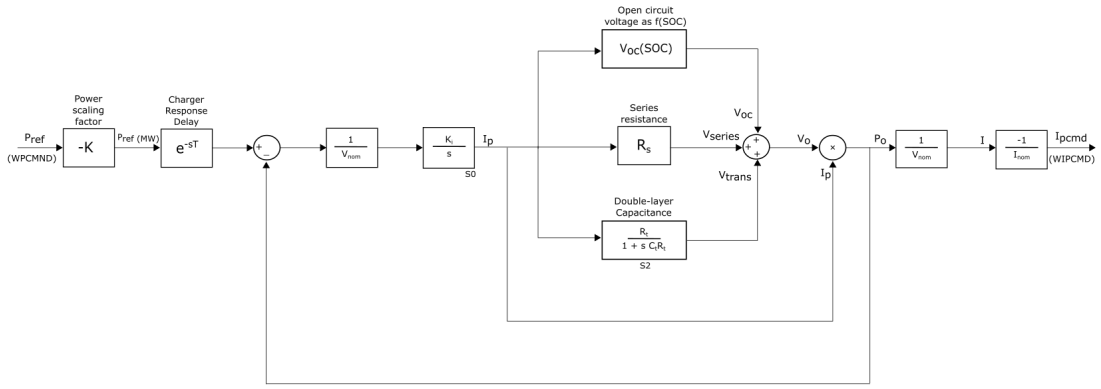

Figure 21: User-written Renewable Electrical Control Model (USEMDL) in PSS®E.

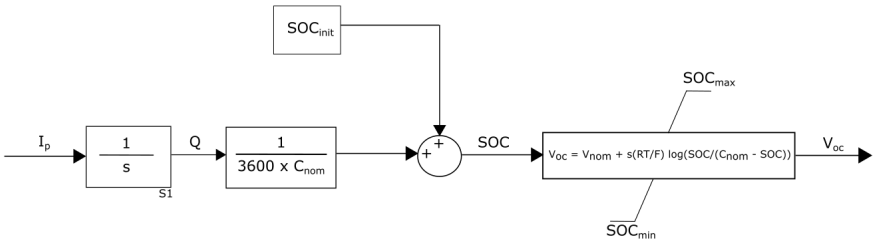

Figure 22: V_{oc} of the user-written battery model (USEMDL) as a function of SOC.

The block diagram of the battery model is shown in Figure 21 and follows the same model and principle described in Section 3.1.3. The active power reference signal from the plant control model, P_{ref} (WPCMND) is provided as the input to the model. As mentioned during the battery model description in Section 3.1.4, the battery parameters are in actual units in PSS®E as well. This is to make it easier to relate to the parameters in actual units. Hence, P_{ref} is provided in MW to the model. The charger response delay is also included within the model. Figure 22 shows the open circuit voltage dependence on SOC, defined by the equation 3.6. The output power P_0 is converted to output current I_{pcmd} in per unit, which is provided as an input to the generator model. This value is stored in the WIPCMD dynamic simulation array. As with the plant model in Section 3.2.3.2, the reactive current is explicitly equated to zero in the WIQCMD array since reactive power support is not provided. The CONs, STATEs and VARs description are provided in Tables 17, 18 and 19. The FORTRAN code for the model is provided in Appendix B.3.

Table 17: CONS for user-written electrical model (USEMDL).

CONS			
Number	**Name**	**Unit**	**Description**
J	K		Power scaling factor
J+1	n		Alternate scaling factor
J+2	V_{nom}	V	Nominal battery voltage
J+3	$C_t * R_t$	s	Double layer capacitance time constant
J+4	R_s	Ω	Series resistance
J+5	SOC_{init}	pu	Initial SOC value
J+6	SOC_{max}	pu	Max SOC value
J+7	SOC_{min}	pu	Min SOC value
J+8	s		OCV sensitivity factor on SOC
J+9	RT/F		RT/F constant
J+10	C_{nom}	Ah	Nominal battery capacity
J+11	R_t	Ω	Charge transfer resistance
J+12	K_i		Current integrator gain
J+13	I_{nom}	A	Nominal battery current
J+14	K_e		Energy integrator gain
J+15	T_{del}	s	Charger activation delay time

Table 18: STATES for user-written electrical model (USEMDL).

STATES		
Number	**Name**	**Description**
K	I_p	Active current
K+1	Q_p	Charge
K+2	V_{trans}	Voltage across double layer capacitance
K+3	E	Energy utilized

Table 19: VARS for user-written electrical model (USEMDL).

VARS		
Number	**Name**	**Description**
L	V_{oc}	Open circuit voltage of battery
L+1	V_{series}	series voltage of battery
L+2	SOC	State of charge
L+3	V_0	battery output voltage
L+4	P_0	battery output power
L+5	I_{pcmd}	Active current output
L+6	P_{ref}	Reference power in MW
L+7	ind	Index tracker for circular buffer
L+8	status	status flag for circular buffer
L+9 to L+508		storage locations for circular buffer

3.2.3.4 Renewable Generator Model

The renewable generator model is presented in Figure 23. PSS®E converts the generator models to a Norton equivalent circuit during the dynamic simulation process. Therefore, the input to the model are the active and reactive currents I_{pcmd} (from WIPCMD array) and I_{qcmd} (from WIQCMD array) respectively, which are provided by the electrical control model. The currents are stored as a complex vector in the ISORCE, which is the Norton current source array.

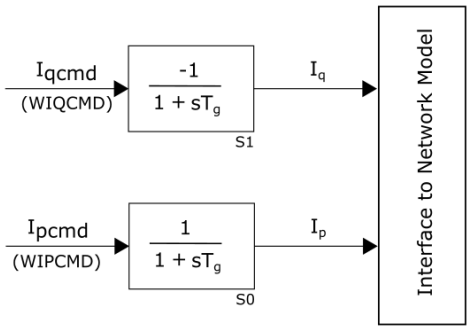

Figure 23: User-written Renewable Generator Model (WT4GU) in PSS®E.

Tables 20 and 21 list the CONs and STATEs of the model. No VARs are utilized by the model.

Table 20: CONS for user-written generator model (WT4GU).

CONS			
Number	**Name**	**Unit**	**Description**
J	T_g	s	Current filter time constant
J+1	$RateL$		reactive current rate limiter

Table 21: STATES for user-written generator model (WT4GU).

STATES		
Number	**Name**	**Description**
K	I_p	Active current
K+1	I_q	Reactive current

The models USPMDL/USPFFR, USEMDL and WT4GU make up the overall structure of the renewable generator model, which represents an EV cluster. To use these models together, a renewable generator needs to be connected at a bus. Then, the model parameters are specified in the .dyr file along with the bus number and machine ID.

3.3 Sample results of prequalification tests for FCR-D up in Simulink

3.3.1 Step response test

Figure 24 presents the frequency signal for prequalification testing for FCR-D up (top) and the power output of the V2G model presented in Section 3.1.4. The test is performed on the model without considering any delays. As the active power varies linearly in the frequency range of 49.90-49.50 Hz, when the frequency is at 49.70 Hz, the power output must be 50% and at 49.5 Hz, 100% of the active power must be delivered. The total available FCR-D capacity for the model is 0.01 pu. At 5 s, when the frequency is stepped from 50.00 Hz to 49.50 Hz, the output power steps up to 0.01 pu. Similarly, when the frequency steps up to 49.70 Hz at 10 s, the output power steps down to 0.005 pu and to 0.0 pu at 15 s as the frequency steps up to 49.90 Hz. This pattern shows that the power output of the model follows the frequency linearly and therefore fulfills the first requirement.

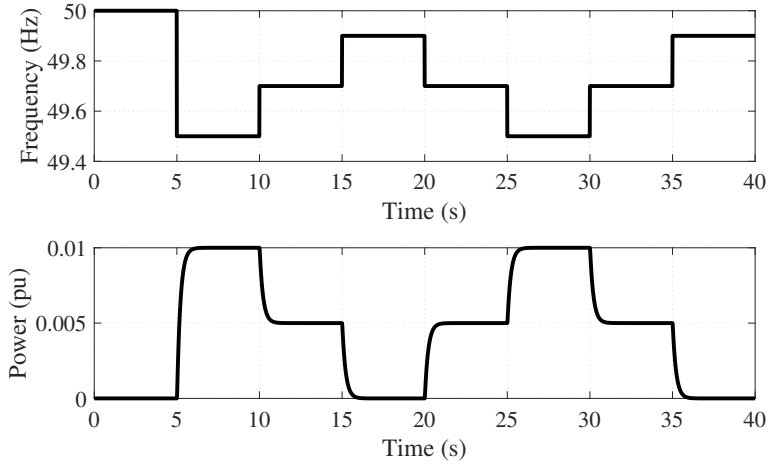

Figure 24: Step response test frequency signal (top) for FCR-D up and the output power of the V2G model (bottom) in Simulink.

3.3.2 Ramp response test

The output power of the V2G model in response to the ramp test is shown in Figure 25. The power (bottom) steps up to 0.0025 pu when the frequency (top) drops to 49.80 Hz at 5 s and ramps up linearly when the frequency ramps down from 49.90-49.00 Hz at 15 s, saturating at 49.50 Hz.

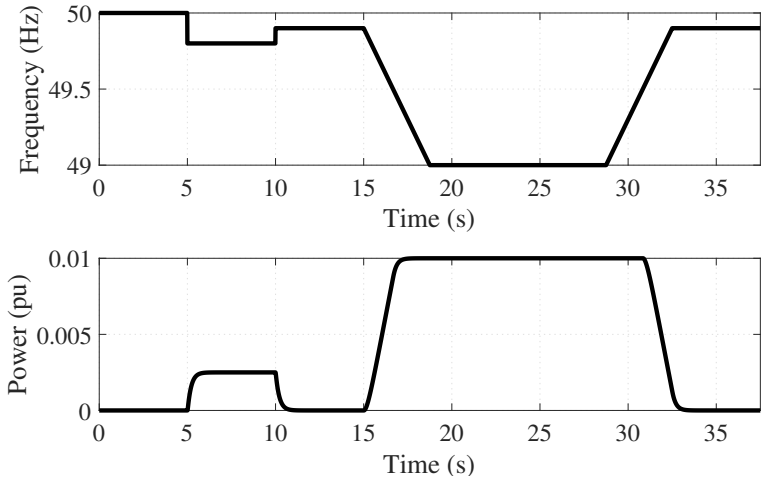

Figure 25: Ramp response test frequency signal (top) for FCR-D up and the output power of the V2G model (bottom) in Simulink.

The parameter values from the step and ramp tests are tabulated in Table 22. To clear the ramp response test requirements, the criteria mentioned in Section 2.5.1.2 must be fulfilled. Table 23 shows the status of clearance of the model.

Table 22: Test parameter values for the Simulink V2G model.

Parameter	Value
ΔP_{ss}	0.01 pu
$\Delta P_{7.5s}$	0.01 pu
$E_{7.5s}$	0.0644 pu
C_{FCR-D}	0.01 pu

Table 23: Ramp response test clearance status of the Simulink V2G model.

Requirement	Status
$\Delta P_{7.5s} \geq 0.93 \Delta P_{ss}$	✓
$E_{7.5s} \geq 3.7 \Delta P_{ss}$	✓

3.4 Sample results of prequalification tests for FCR-D up in PSS®E

3.4.1 Step response test

As with the Simulink model, the step response test for FCR-D up is performed to test the steady state activation of the user-written model. The models USPMDL, USEMDL and WT4GU are used in the EV model for the provision of FCR-D up.

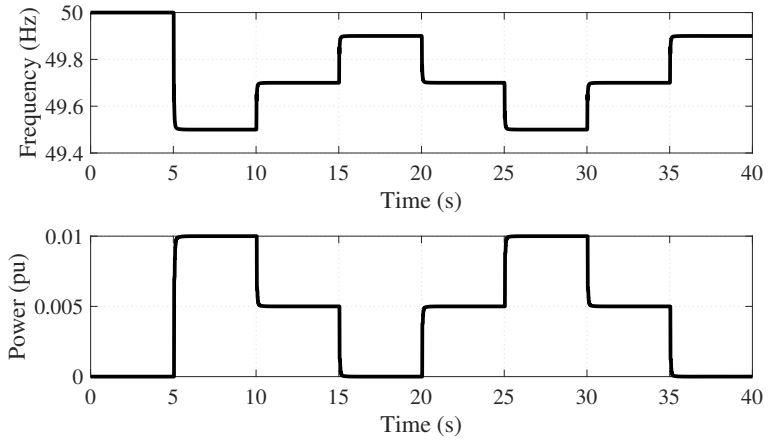

Figure 26: Step response test frequency signal (top) and the reference signal P_{ref} (bottom) from the PSS®E user-written plant model (USPMDL) in per unit on SBASE (100 MVA).

The response of the plant model USPMDL, P_{ref}, in per unit on SBASE to the stepped frequency is plotted in Figure 26. It can be seen that P_{ref} steps up to 0.01 pu when the frequency drops to 49.50 Hz at 5 s and to 0.005 pu when the frequency then steps up to 49.70 Hz at 10 s. The response of the model is similar to the response of the Simulink model in Figure 24. Therefore, the plant model complies with the linear activation requirements.

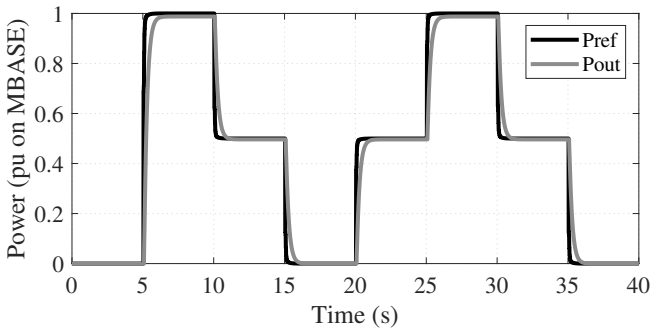

Figure 27: Reference power P_{ref} from the PSS®E user-written plant model, USPMDL, vs the net output power of the user-written generator model in pu on MBASE.

The plot of the reference power from the user-written plant model, P_{ref} and the total output power of the model, P_{out} in Figure 27 shows that the output of the model follows the plant reference power. This indicates that the model works as intended. It can also be observed that the output power takes certain time to settle to the new value. This is due to the capacitive behaviour of the electrical model, USEMDL, on the output voltage, V_0.

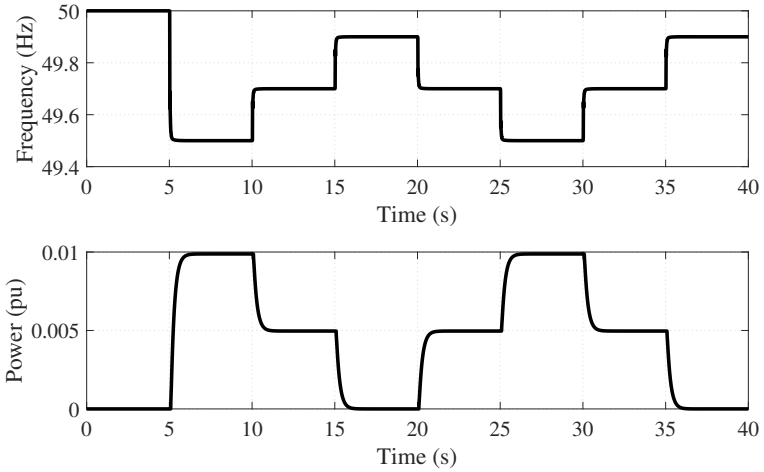

Figure 28: Step test frequency signal (top) and the net output of the PSS®E user-written generator model (bottom) in per unit on SBASE.

In Figure 28, the output of the total user-written generator model follows a similar pattern as the reference power signal, P_{ref} as expected. Thus, the complete user-written generator model complies with the linear activation.

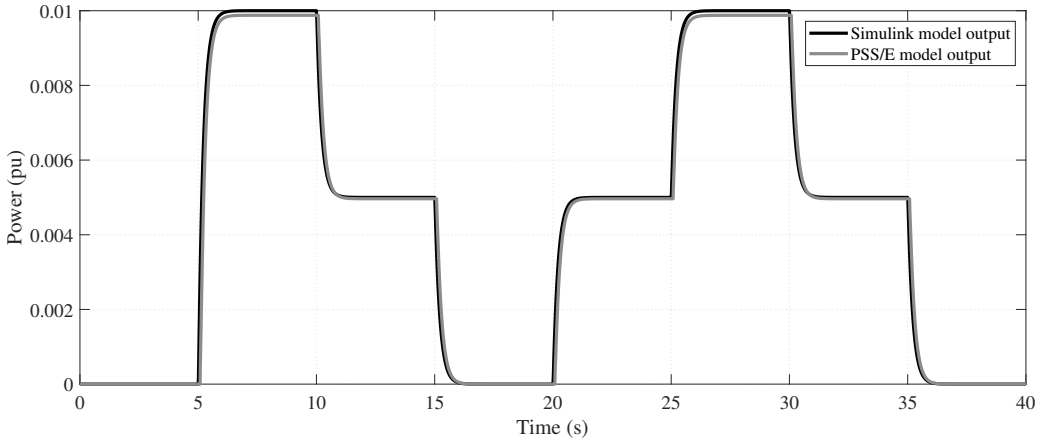

Figure 29: Output of the V2G model in Simulink vs output of the V2G model in PSS®E when subjected to the same stepped frequency signal.

In order to compare the Simulink model with the PSS®E model, their response is plotted together in the Figure 29. Both models are subjected to the same step test frequency signal. It is interesting to see that their responses are almost identical. The slight deviations in the PSS®E model output is due to the filter time constants present in the plant model, electrical control model, and the generator model. The time constants have been set as low as possible to minimize their effect. The peak output power of the PSS®E model is also lower than the Simulink model. This is due to the drop in bus voltage when the frequency drops in the test setup used.

3.4.2 Ramp response test

The ramp test is performed for the PSS®E model and the response of the plant model, USPMDL, is plotted in the Figure 30.

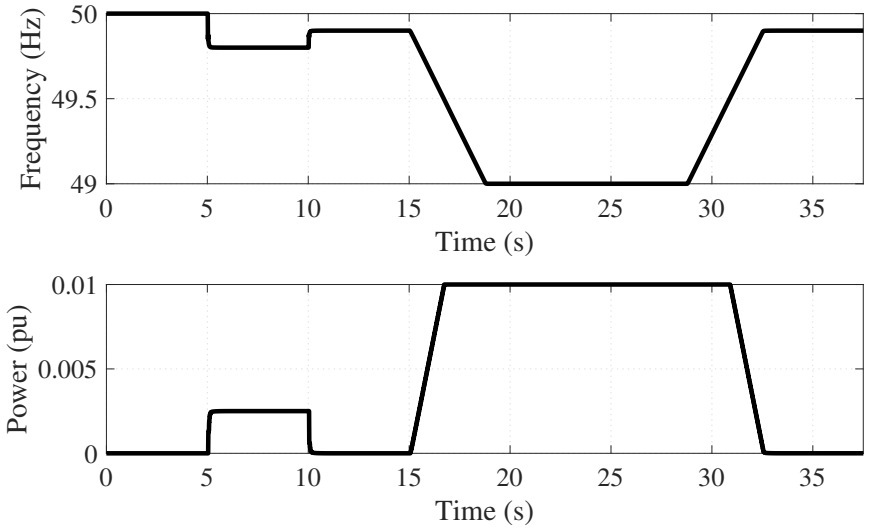

Figure 30: Ramp test frequency signal (top) and the reference signal P_{ref} (bottom) from the PSS®E user-written plant model USPMDL in per unit on SBASE (100 MVA).

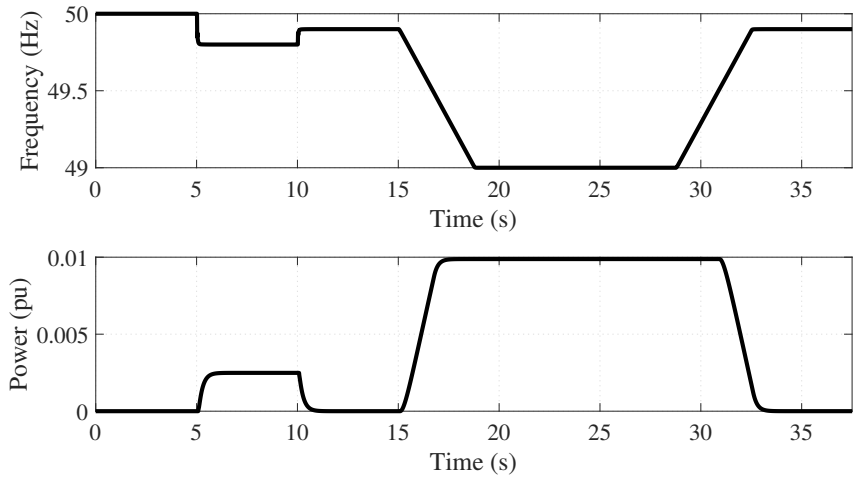

Figure 31: Ramp test frequency signal (top) and the net output from the PSS®E user-written generator model (bottom) in per unit on SBASE.

Figure 30 and 31 show the response of the plant model and the total V2G model respectively to the ramp response test. In order to clear the test, the criteria mentioned in Section 2.5.1.2 must be fulfilled. The prequalification test parameter values are presented in Table 24. The clearance status of the user-written generator model is tabulated in Table 25. It is observed that the model fulfills the criteria for FCR-D up dynamic performance.

Table 24: Test parameter values for the PSS®E V2G model.

Parameter	Value
ΔP_{ss}	0.0099 pu
$\Delta P_{7.5s}$	0.0099 pu
$E_{7.5s}$	0.0629 pu

Table 25: Ramp response test clearance status for the PSS®E V2G model.

Requirement	Status
$\Delta P_{7.5s} \geq 0.93\Delta P_{ss}$	✓
$E_{7.5s} \geq 3.7\Delta P_{ss}$	✓

3.5 Prequalification test results of the Simulink V2G model for FCR-D up

The prequalification tests described in Section 2.5 are performed on the Simulink model considering the delays due to communication and the hardware. The maximum delay considered is 4 s as the maximum time to nadir in the simulations is 2.51 s. More details on the delays are presented in Section 2.4.4.

Table 26: Prequalification test results of the Simulink V2G model for dynamic performance with different delays.

Delay (s)	ΔP_{ss} **(pu)**	$\Delta P_{7.5s}$ **(pu)**	$E_{7.5s}$ **(pu)**	**status**	C_{FCR-D} **(pu)**	**capacity (%)**
0.0	0.01	0.01	0.064	✓	0.01	100
1.0	0.01	0.01	0.054	✓	0.01	100
2.0	0.01	0.01	0.044	✓	0.01	100
3.0	0.01	0.01	0.034	**x**	0.0093	93.04
4.0	0.01	0.009	0.024	**x**	0.0066	66.01

Table 26 shows the prequalification test results of Simulink model for different delays. The steady state activation, ΔP_{ss}, remains the same regardless of the delay as the activation is not affected by it. The results from ramp response test on the other hand, $\Delta P_{7.5s}$ and $E_{7.5s}$, vary with the delay as they are time-based values. The status indicates if they fulfill the dynamic performance requirements described in Section 2.5.1.2. The FCR-D capacity, C_{FCR-D}, is calculated using (2.20). This is the capacity that the FCR-D providing entity is qualified to provide. The percentage of capacity is based on the maximum power output of the model, which in this case, is 0.01 pu. It can be observed that the qualified capacity is 100% up to 2 s delay, after which it starts to decrease. This indicates that, though the V2G service has sufficient capacity, the delays prevent it from being qualified to provide 100% of its capacity, thus failing to monetize the total available resources.

3.6 Prequalification test results of the PSS®E V2G model for FCR-D up

The prequalification tests are performed on the PSS®E V2G model, considering the various delays and the results are tabulated in Table 27. A maximum delay of 7 s is considered as

the system takes longer to reach the frequency nadir. The 7 s delay is also the maximum delay to come across during the literature review [16]. As seen in Figure 29, the output of the PSS®E V2G model is similar to the Simulink model. Hence, the results are also the same for different delays. The V2G model qualifies to provide 100% of its capacity up to 2 s of delay. The qualified capacity then continues to reduce with the increase in delay. At 7 s delay, the model can only provide about 1% of its total capacity.

Table 27: Prequalification test results of the PSS®E V2G model for dynamic performance with different delays.

Delay (s)	ΔP_{ss} **(pu)**	$\Delta P_{7.5s}$ **(pu)**	$E_{7.5s}$ **(pu)**	**status**	C_{FCR-D} **(pu)**	**capacity** (%)
0.0	0.0099	0.0099	0.0640	✓	0.0099	100
1.0	0.0099	0.0099	0.0540	✓	0.0099	100
2.0	0.0099	0.0099	0.0440	✓	0.0099	100
3.0	0.0099	0.0099	0.0340	**x**	0.0093	93.7
4.0	0.0099	0.0099	0.0240	**x**	0.0066	66.7
5.0	0.0099	0.0099	0.0150	**x**	0.0039	39.7
6.0	0.0099	0.0078	0.0050	**x**	0.0014	14.5
7.0	0.0099	0.0019	0.0004	**x**	0.0001	1.1

3.7 Prequalification test results of the Simulink V2G model for FFR

The activation requirements for FFR are specifically defined, as mentioned in Section 2.3.1.

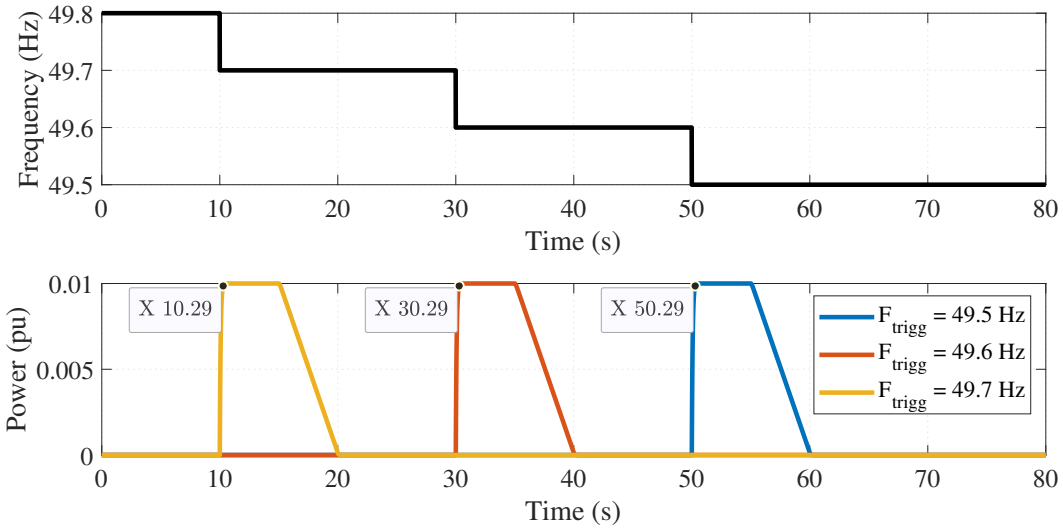

Figure 32: Frequency signal pattern to test the activation of FFR (top) and the FFR output of the Simulink V2G model (bottom).

Figure 32 shows the response of the model to the input frequency signal with no delays. The model is tested thrice with different trigger frequencies. It can be seen that the FFR is triggered at the 10 second mark when the frequency drops to 49.70 Hz at the same time instant. The activation time for the trigger frequency of 49.70 Hz is 0.29 s, which is much faster than the requirements mentioned in Section 2.3.1. Similarly, the FFR is triggered for the other two cases when the frequency drops to their respective trigger frequencies. The activation times and the prequalification results are presented Table 28. The model satisfies all the requirements for the provision of FFR service.

Table 28: Prequalification test results of the Simulink V2G model for dynamic performance with different delays.

Parameter	F_{trigg} **= 49.70 Hz**	F_{trigg} **= 49.60 Hz**	F_{trigg} **= 49.50 Hz**
Activation time	0.29 s	0.29 s	0.29 s
$C_{pre-qual}$	0.01 pu	0.01 pu	0.01 pu
FFR_{os}	0%	0%	0%
$FFR_{deact,max} \leq FFR_{max}$	✓	✓	✓
$FFR_{deact,rate,max} = 0.2C_{pre-qual}$	✓	✓	✓

When the delays mentioned in Section 2.4.4 are considered, the longest delay that the model can have is 1.01 s for a trigger frequency of 49.70 Hz. Delays longer than 1.01 s result in disqualification for not fulfilling the activation time requirements. The leeway is more constricted for the remaining trigger frequencies as the activation time requirement reduces, with only 0.4 s of acceptable lag for the 49.50 Hz option.

3.8 Prequalification test results of the PSS®E V2G model for FFR

The prequalification tests for FFR are performed on the PSS®E V2G model similar to the Simulink model. The FFR output of the V2G model is illustrated in Figure 33. It can be seen that the FFR triggers at the right times corresponding to their trigger frequencies.

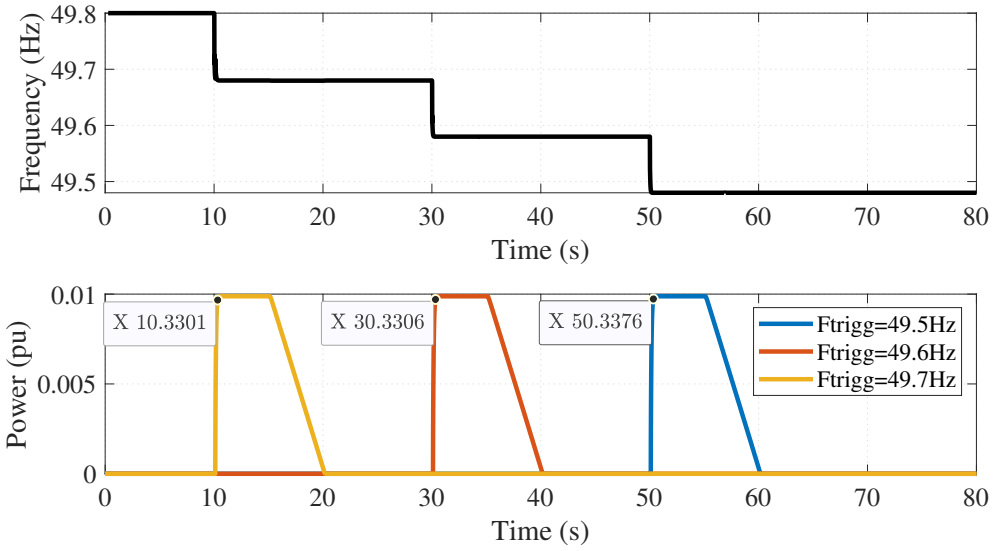

Figure 33: Frequency signal pattern to test the activation of FFR (top) and the FFR output of the PSS®E V2G model (bottom).

The activation times and the prequalification test results are tabulated in Table 29. The activation times are slightly longer in comparison to the Simulink results. This can be due to the additional time constant of the renewable generator model, WT4GU. The model clears the all the necessary requirements to provide FFR service.

Table 29: Prequalification test results of the PSS®E V2G model for dynamic performance with different delays.

Parameter	F_{trigg} **= 49.70 Hz**	F_{trigg} **= 49.60 Hz**	F_{trigg} **= 49.50 Hz**
Activation time	0.33 s	0.33 s	0.33 s
$C_{pre-qual}$	0.0099 pu	0.0099 pu	0.0099 pu
FFR_{os}	0%	0%	0%
$FFR_{deact,max} \leq FFR_{max}$	✓	✓	✓
$FFR_{deact,rate,max} = 0.2C_{pre-qual}$	✓	✓	✓

When the delays are introduced, the model can have a maximum delay of 0.97 s for the 49.70 Hz trigger frequency case. As with the Simulink model in Section 3.7, delays longer than 0.97 s fail to fulfill the activation time requirement.

4 FCR-D and FFR simulations in Simulink and PSS®E

4.1 FCR-D up simulation results in Simulink

4.1.1 Comparison of the test scenarios

The scenarios in Simulink, which are mentioned in Section 3.1.2, are tested for a load step of $\Delta P_L = 0.03$ pu. The frequency response of the test scenarios, with no support from the V2G model, can be visualized in Figure 34. The FCR is entirely provided by the hydro generating unit. The load is stepped at the 5 s mark.

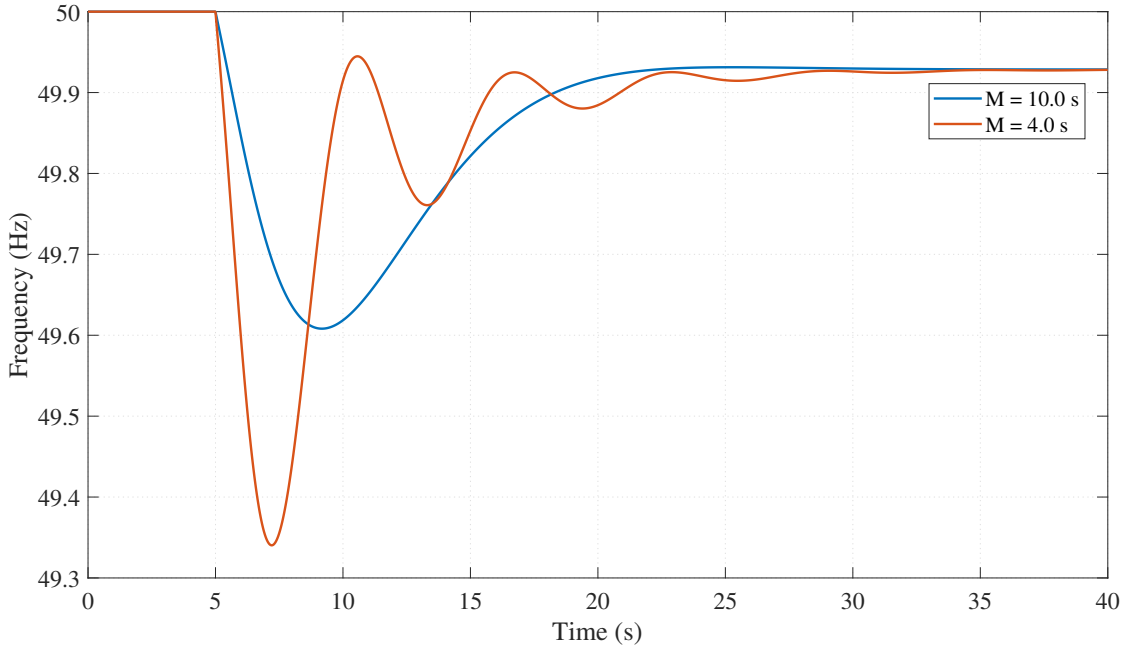

Figure 34: Frequency response of the different test scenarios for a load step of $\Delta P_L = 0.03$ pu without any contribution from the V2G model in Simulink.

The frequency response indicators for the different scenarios are presented in Table 30. Comparing the different frequencies, it can be seen that the RoCoF of the system increases as the inertia reduces. The RoCoF depends on the load step and the inertia of the system, according to (2.11). Since the load step is the same for all cases, it only depends on the inertia of the system. The frequency nadir depends on the system inertia, load-frequency dependence and the load step. As the load-frequency dependence and load step are same throughout, it depends only on the inertia as well. The same can be observed in Table 30. The frequency nadir decreases with decrease in inertia. The steady state frequency is the same for all cases, as it depends on the droop constant, load-frequency dependence and the load step according to (4.1).

$$\Delta f_{ss} = \frac{-\Delta P_L}{\frac{1}{R} + D} = \frac{-0.03}{\frac{1}{0.05} + 1} = -0.0014285\ pu\ (or)\ -0.0714\ Hz \tag{4.1}$$

From Table 30, it can be seen that the time to frequency nadir, Δt_{nadir}, is observed to reduce with a reduction in inertia. Furthermore, it can be observed that the frequency overshoot, f_{os}, increases with decrease in inertia and the same can be observed in the Figure 34. In the upcoming results, a selected few indicators will be compared as most indicators remain quite similar for all the cases.

Table 30: Frequency response indicators for the test scenarios for a load step of $\Delta P_L = 0.03$ pu in Simulink.

Scenario	**RoCoF** (Hz/s)	f_{nadir} (Hz)	Δf_{max} (Hz)	Δt_{nadir} (s)	Δf_{ss} (Hz)	**FBF** (MW/Hz)	f_{os} (%)
M = 10.0 s	-0.150	49.61	0.391	4.17	0.0714	20.948	0.0
M = 4.0 s	-0.386	49.34	0.659	2.21	0.0714	20.993	0.033

4.1.2 Impact of V2G delays on the frequency

To assess the impact of the delays when providing FCR-D up using V2G, the frequency response of the system is plotted with varying delays, ranging from 0 s to 4 s. The response for longer delays are not included as the frequency nadir of the system is reached in a short duration. The disturbance is the same load step of $\Delta P_L = 0.03$ pu at 5 s mark. In the 'Base' scenario, the FCR is only provided by the hydro generating unit.

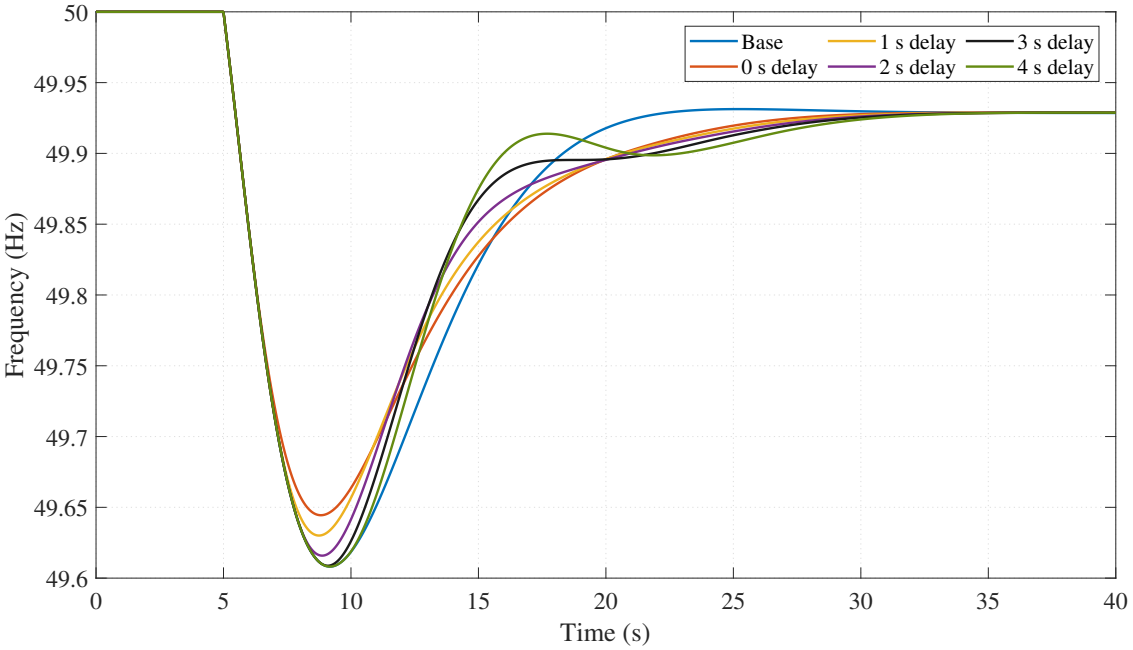

Figure 35: Frequency response of the FCR-D Simulink model with M = 10.0 s for a load step of $\Delta P_L = 0.03$ pu considering various delays in V2G support.

Figure 35 illustrates the frequency response of the M = 10.0 s scenario in Simulink for different delays in FCR from V2G. The frequency nadir is improved when the delay of the V2G model is below 4 s. This is due to the frequency reaching the nadir in 4.17 s (from Table 30). FCR with delays close to or greater than the time to nadir do not improve the frequency nadir. The frequency nadir values are presented in Table 31. The decay rate λ, described in Section 2.2, and the frequency overshoot are not included for this scenario, as there are no oscillations in the frequency, nor any overshoots.

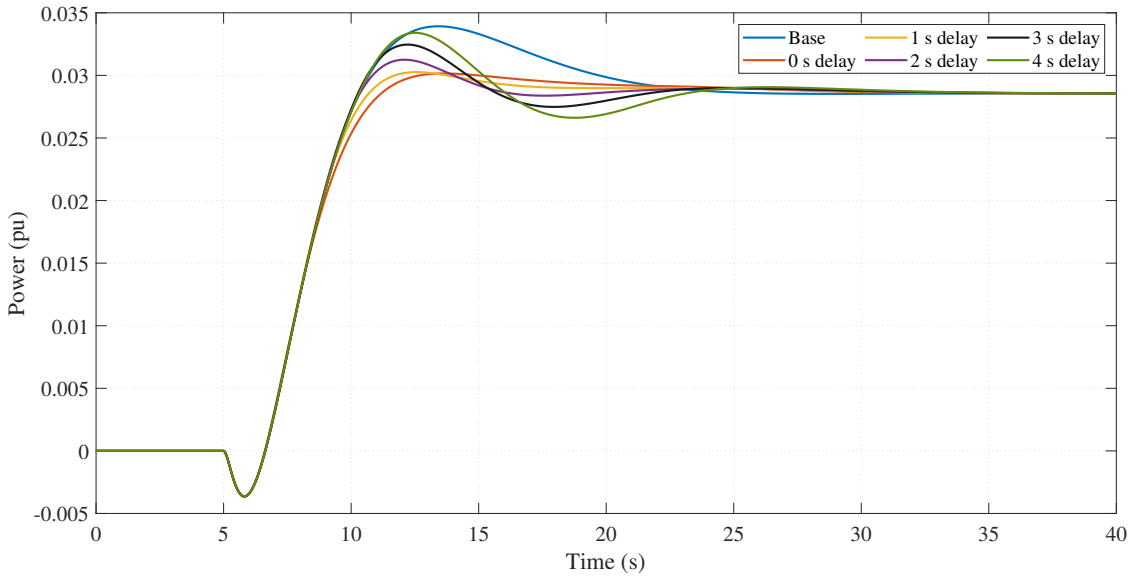

(a) FCR from the hydro generating unit.

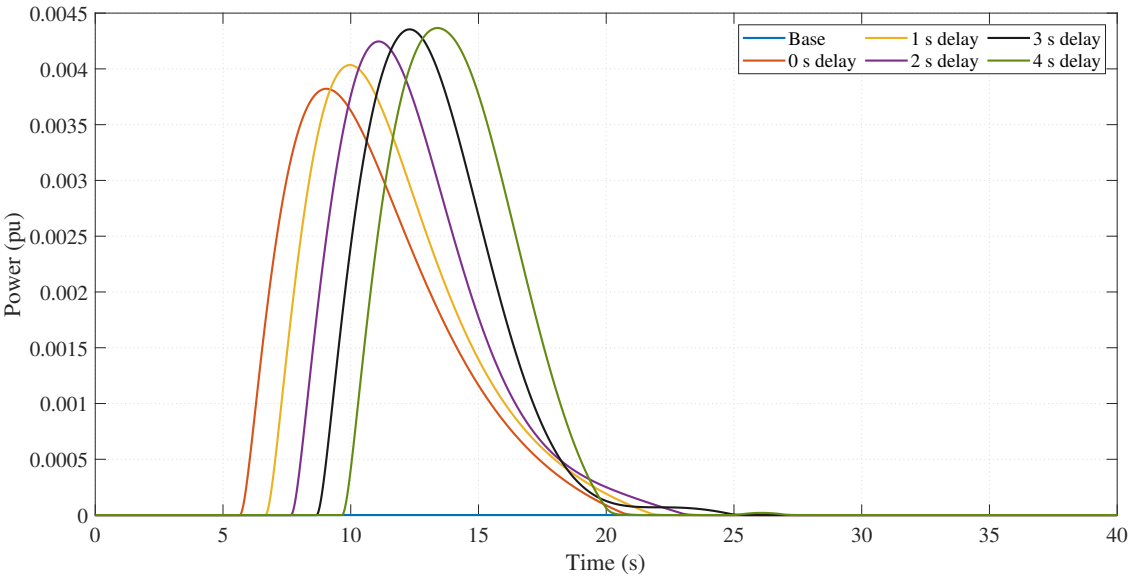

(b) FCR output of the V2G model.

Figure 36: FCR from the hydro generating unit and the V2G model for a load step of $\Delta P_L = 0.03$ pu in Simulink with M = 10.0 s for varying delays.

The FCR from the hydro unit and the V2G are illustrated in Figure 36. It can be seen that the peak output of the V2G model increases with the increase in delay. This is due to the decreasing frequency nadir, as seen in Table 31. The hydro model provides the total FCR till the V2G model starts to contribute. As the delay in V2G support increases, the hydro model provides more power, which can be observed in Figure 36a for delays 2, 3 and 4 s. When the FCR from V2G activates, it provides the power when the frequency starts to recover. The total instantaneous FCR is excessive, which speeds up the frequency recovery, and can be noticed in Figure 35. This response is magnified when the inertia of the system decreases.

Table 31: Frequency nadir for the M = 10.0 s test scenario for a load step of $\Delta P_L = 0.03$ pu in Simulink considering delays.

Delay	f_{nadir} (Hz)
Base	49.608
0 s	49.644
1 s	49.630
2 s	49.616
3 s	49.609
4 s	49.608

The frequency response of the Simulink model with inertia M = 4.0 s for the same disturbance is shown in Figure 37. The figure only consists of 2 s and 4 s delays, as they are of particular interest. Table 32 presents the frequency response indicators for the different delays. It can be observed that the improvement in frequency nadir is up to 1 s of delay. The frequency overshoot increases as the delay increases to 2 s, but starts to reduce as the delays increase further. The decay rate λ is the lowest for the 2 s delay, and starts to increase with further increase in the delays.

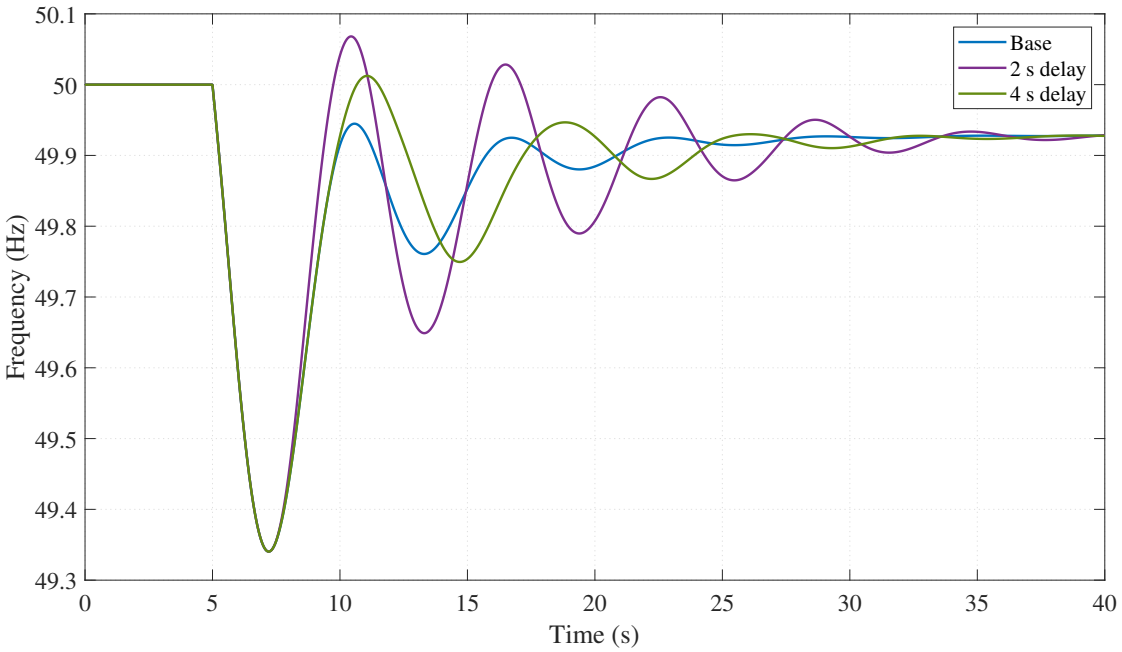

Figure 37: Frequency response of the FCR-D Simulink model with M = 4.0 s for a load step of $\Delta P_L = 0.03$ pu considering various delays in V2G support.

Table 32: Frequency response indicators for the M = 4.0 s test scenario for a load step of $\Delta P_L = 0.03$ pu in Simulink considering delays.

Delay	f_{nadir} (Hz)	f_{os} (%)	λ
Base	49.34	0.033	0.223
0 s	49.43	0.0	0.250
1s	49.36	0.140	0.197
2s	49.34	0.279	0.178
3s	49.34	0.269	0.180
4s	49.34	0.168	0.194

The high frequency overshoot for a delay of 2 s can be visualised in Figure 38. It can be seen that the FCR from V2G reaches its peak output along with the hydro FCR. The surplus power results in an increase in frequency overshoot. Since the second frequency nadir is not as low as the first, the FCR output is reduced, which allows the frequency to eventually settle. If the system inertia is reduced enough, the FCR can sustain these oscillations. The opposite is observed for 4 s delay. The FCR from V2G reaches its peak output when the hydro FCR is decreasing. This action reduces the successive frequency dips, thus damping the frequency oscillations. However, it does not always hold true since it is situational.

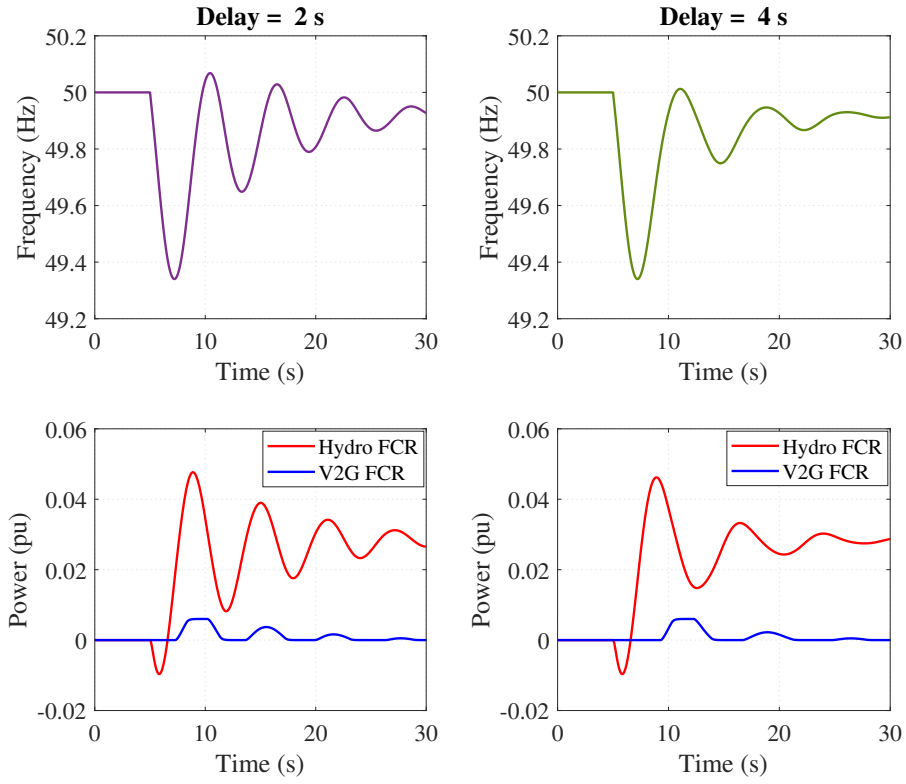

Figure 38: Comparison of FCR output from V2G model and hydro FCR in Simulink with M = 4.0 s, for 2 s and 4 s delay in V2G support when a load step of $\Delta P_L = 0.03$ pu in applied.

4.2 FFR simulation results in Simulink

Similar to FCR-D up, the different scenarios are tested for a load step of $\Delta P_L = 0.03$ pu, with FFR provision from the V2G model.

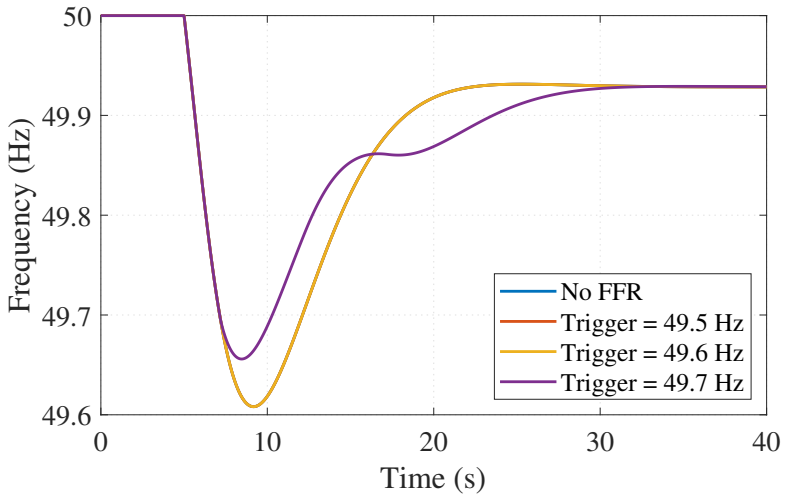

Figure 39: Frequency response of M = 10.0 s scenario in Simulink for a load step of $\Delta P_L = 0.03$ pu with 5 s FFR provision from V2G.

Figure 39 shows the frequency response of the M = 10.0 s scenario with 5 s FFR provision from V2G model for different trigger frequencies. It can be observed that the frequency nadir is improved with FFR support to the system for 49.7 Hz trigger frequency, when compared to the No FFR case. Since the frequency nadir is 49.61 Hz, the output of the V2G model in Figure 40 activates only for the 49.7 Hz trigger frequency case.

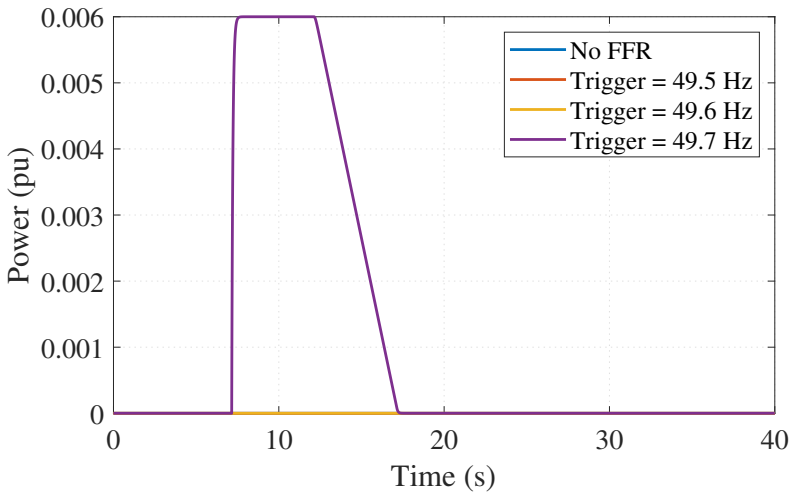

Figure 40: FFR output of the V2G model in M = 10.0 s scenario in Simulink for a load step of $\Delta P_L = 0.03$ pu with 5 s FFR provision from V2G.

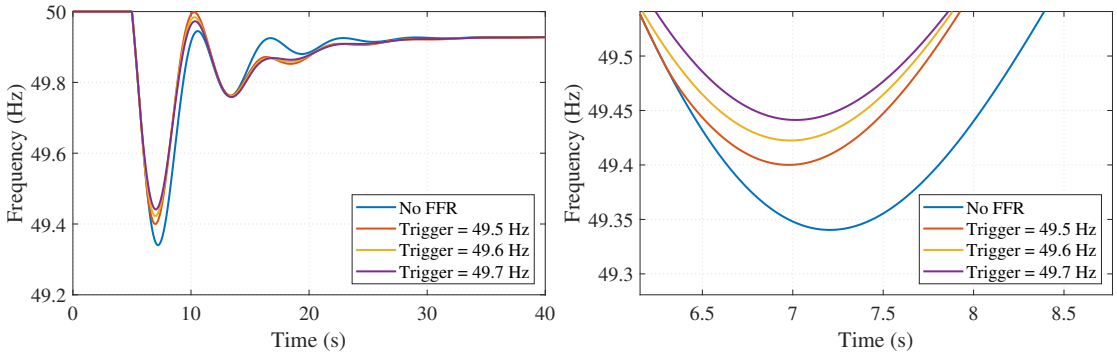

(a) Frequency response. **(b)** Frequency nadir.

Figure 41: Frequency response and the frequency nadir of M = 4.0 s scenario for a load step of $\Delta P_L = 0.03$ pu in Simulink.

The frequency response and the frequency nadir of the M = 4.0 s test scenario is shown in Figure 41. It can be seen that the FFR is activated for all three trigger frequencies, since the nadir reaches 49.34 Hz. From Table 33, it can be observed that the frequency nadir is slightly improved between the three FFR cases for M = 4.0 s inertia case. This is because the high RoCoF reduces the activation times between the three triggers. Comparing the two inertia cases, the frequency is improved better for the M = 4.0 s scenario over the No FFR case.

Table 33: Frequency nadir of the test scenarios in Simulink with a 5 s FFR support from EV models for a load step of $\Delta P_L = 0.03$ pu.

Scenario	**No FFR**	$f_{trigger}$ **= 49.5 Hz**	$f_{trigger}$ **= 49.6 Hz**	$f_{trigger}$ **= 49.7 Hz**
M = 10.0 s	49.61	49.61	49.61	49.66
M = 4.0 s	49.34	49.40	49.42	49.44

4.3 Nordic 44 scenarios in PSS®E

The test scenarios in PSS®E are conducted for a single generator trip (N-1) of 1329 MW (ΔP_G) at Bus 6100. This generator is chosen since its generation is closest to the dimensioning error of 1450 MW in the Nordic region.

4.3.1 Frequency response of the test scenarios

To assess the performance of the system without any contribution from the user-written model, the frequency response of the different test scenarios are presented. The frequency responses shown in the upcoming figures are the average frequencies of all the buses in the system. Figure 42 shows the frequency response of the basecase to the generation trip ΔP_G. The disturbance occurs at the 10 s mark. The frequency has a nadir of 49.55 Hz and reaches it in 14.75 s. The reason for the long time to nadir is due to the load profile of the N44 model, as described in Section 3.2.2. The 40% constant impedance load characteristic is dependent on the bus voltage. This load sheds about 1000 MW of active power when the voltage drops due to the generation trip at 10 s. This compensates for the decrease in active power generation and as a result, the RoCoF reduces. The oscillations in the frequency when the disturbance occurs is the inter-area oscillations between the different generators. The ROCOF is calculated as -0.293 Hz/s and has a regulating power or frequency bias factor of 9776 MW/Hz.

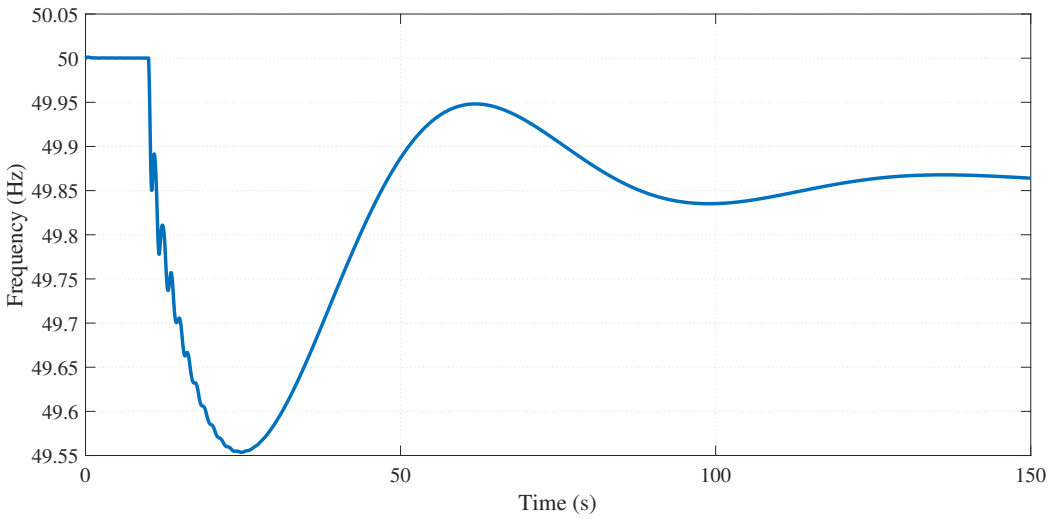

Figure 42: Frequency response of the Base (M = 4.26 s) N44 model to a single generator trip of ΔP_G = 1329 MW (Bus 6100) in PSS®E.

Similarly, the disturbance is simulated in the other test scenarios and are presented in Figure 43. The detailed description of the different scenarios are given in Section 3.2.2. It can be seen that for the same disturbance, the frequency nadir decreases with the inertia. The frequency response indicators give a better comparison of the different frequencies, which are given in Table 34. The RoCoF increases with the reduction in inertia, and the

time taken to reach the frequency nadir reduces with inertia. The frequency overshoot increases as the inertia reduces.

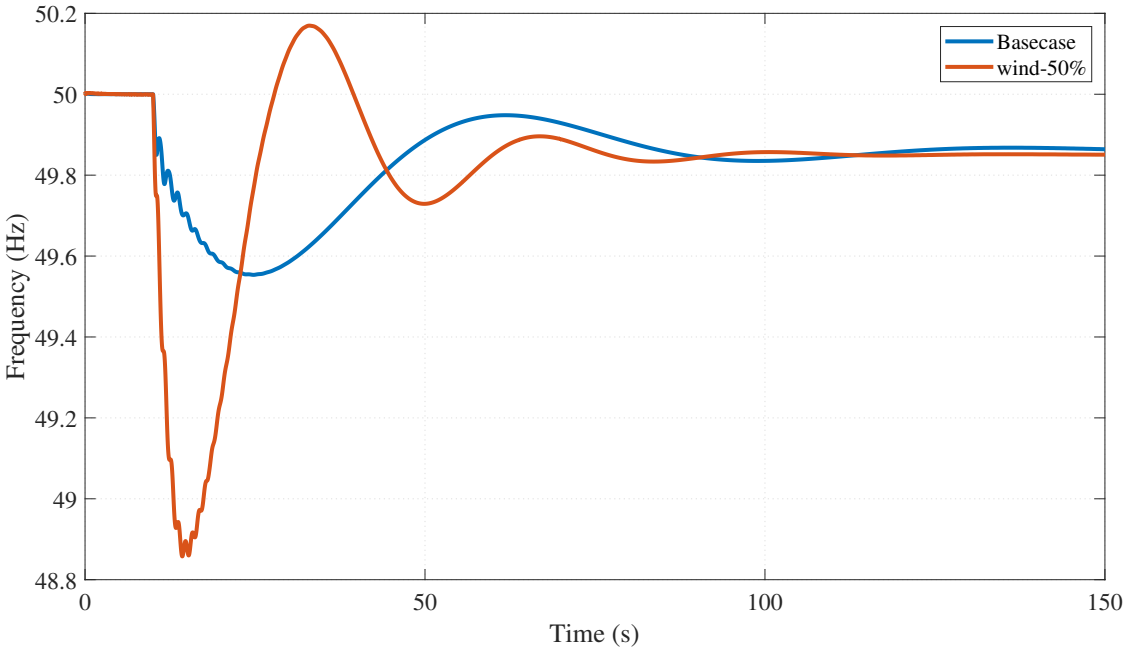

Figure 43: Frequency response of the test scenarios of N44 model to a single generator trip of $\Delta P_G = 1329$ MW (Bus 6100) in PSS®E.

Table 34: Frequency response indicators for the PSS®E N44 network for different test scenarios when a generator of $\Delta P_G = 1329$ MW is tripped.

Scenario	**RoCoF** (Hz/s)	f_{nadir} (Hz)	Δf_{max} (Hz)	Δt_{nadir} (s)	Δf_{ss} (Hz)	**FBF** (MW/Hz)	f_{os} (%)
Base case (M = 4.26 s)	-0.293	49.55	0.442	14.75	0.13	10186	0.167
50% Wind (M = 1.93 s)	-0.494	48.86	1.136	4.28	0.143	9287	0.639

4.4 FCR-D up simulation results in PSS®E

Simulation results of the test scenarios with FCR-D support from the V2G model in PSS®E are presented in this section. Each scenario is tested with varying delay in the response of the V2G model. The 'Base' scenario indicates that the FCR is provided completely by the conventional generation units. The delays are considered in the range of 0 s to 7 s. Longer delays are included as compared with the Simulink results as the system takes a longer duration to reach the frequency nadir.

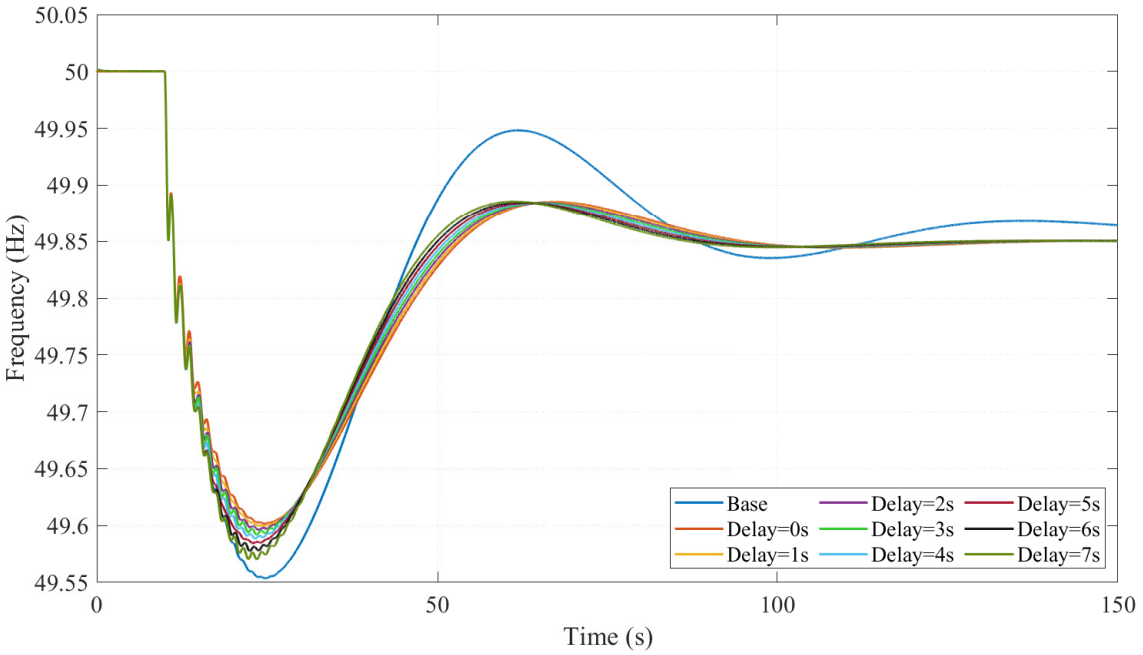

Figure 44: Frequency response of the N44 model base case test scenario (M = 4.26 s) for a generator trip of 1329 MW with varying delay of FCR-D provision from V2G in PSS®E.

Figure 44 illustrates the frequency response of the basecase. The frequency nadir improves when V2G contributes to the FCR when compared to the base scenario, which can be observed in Figure 45. This is due to the fast acting V2G support. Though the delays extend up to 7 s, it is quicker than the FCR from the conventional generators, as noticed in Figure 46. Since every V2G model is identical, the V2G output is shown for a single model located at Bus 8500. The slow FCR from the conventional generators also results in a higher overshoot in frequency.

The FCR output from the conventional generators as seen in Figure 46 (right) has a sharp increase at 10 s. This is the inertial response to the sudden decrease in frequency. This response dies out quickly. The oscillations after the sharp increase are due to the swinging action between the generators.

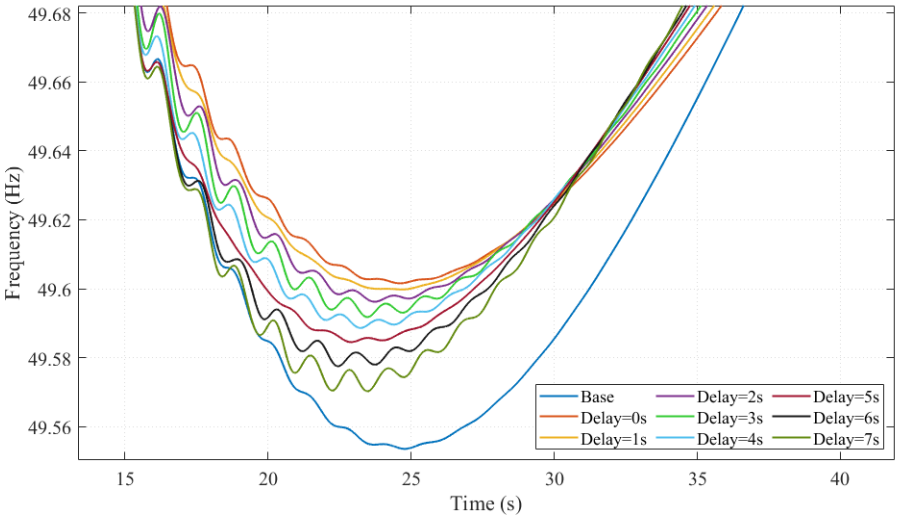

Figure 45: Frequency nadir of the N44 model base case test scenario (M = 4.26 s) for a generation trip of 1329 MW with varying delay of FCR-D provision from V2G in PSS®E.

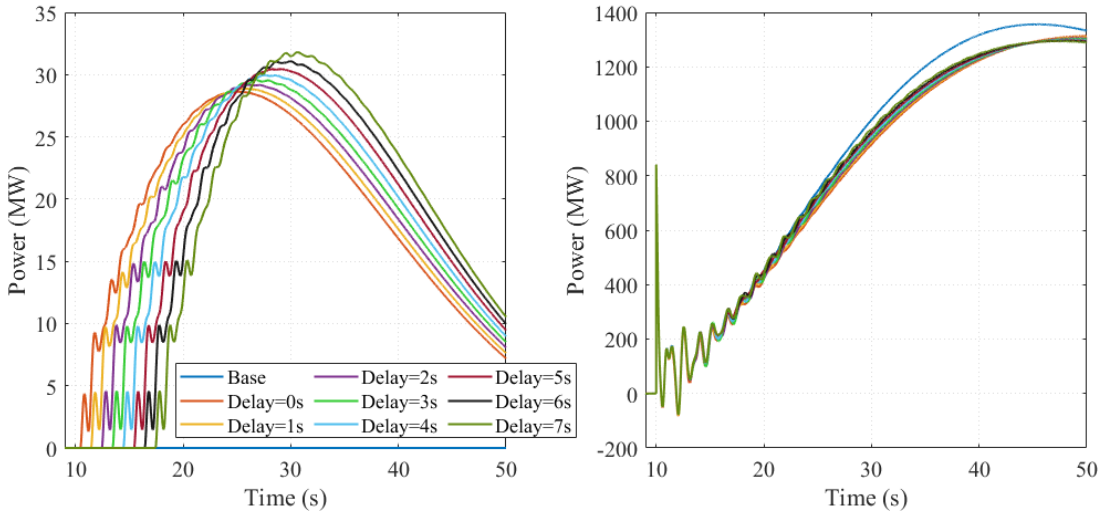

Figure 46: FCR output of the V2G model located at Bus 8500 for different delays (left) and the FCR from the conventional generation units (right) in the basecase test scenario (M = 4.26 s) for a generation trip of 1329 MW in PSS®E.

The frequency response of the different test cases are presented in Figure 47. It can be observed that the impact of the delays increases with the reduction in system inertia. For the base case in Figure 47a, the frequency nadir is improved for all the delays, since the time it takes to reach the nadir is longer than 7 s. However, for the 50% wind penetration case in Figure 47b, the V2G support with longer delays delivers the FCR after the nadir, aiding in frequency recovery instead. This leads to an overshoot in frequency.

Looking at the frequency response indicators for the basecase in Table 35, the frequency overshoot is higher for the Base scenario, while it is similar with V2G support regardless

of the delays. The decay rate λ also indicates higher damping with V2G support, and the same can be visually confirmed from Figure 47a.

Table 35: Frequency response indicators for the PSS®E N44 network for base case test scenario (M = 4.26 s) when generation of $\Delta P_G = 1329$ MW is tripped.

Delay	f_{nadir} (Hz)	f_{os} (%)	λ
Base	49.55	0.167	0.035
0 s	49.60	0.07	0.051
1s	49.60	0.069	0.051
2s	49.596	0.068	0.050
3s	49.592	0.068	0.051
4s	49.589	0.067	0.051
5s	49.585	0.068	0.051
6s	49.578	0.069	0.050
7s	49.57	0.07	0.051

The frequency response indicators for the 50% wind case are tabulated in Table 36. It can be observed that the frequency nadir is improved up to 3 s of delay in V2G support, as the time to nadir for this scenario is 4.28 s as shown in Table 34. It is the same as the Base scenario for 4 s delay. The slightly lower nadir for greater than 4 s delay cases is due to the lower FCR from the conventional units as compared to the Base scenario, which ramps up at the same instant regardless of the delays in V2G. The frequency overshoot is similar up to 3 s of delay, after which, it gradually increases. The Base scenario, however, has the highest overshoot due to the slow acting FCR of the conventional units.

Table 36: Frequency response indicators for the PSS®E N44 network for 50% Wind test scenario (M = 1.93 s) when generation of $\Delta P_G = 1329$ MW is tripped.

Delay	f_{nadir} (Hz)	f_{os} (%)	λ
Base	48.86	0.639	0.06
0 s	49.10	0.171	0.079
1s	49.06	0.160	0.073
2s	48.98	0.160	0.070
3s	48.90	0.161	0.081
4s	48.86	0.256	0.077
5s	48.85	0.367	0.084
6s	48.85	0.478	0.074
7s	48.85	0.595	0.05

The decay rate λ is the lowest for 7 s delay, followed by the Base scenario. This indicates that it takes longer for the large frequency oscillations to subside. This can be observed in Figure 47b, where the oscillations sustain for a long time after the frequency overshoot. In case of lower delays, these oscillations are comparatively well damped.

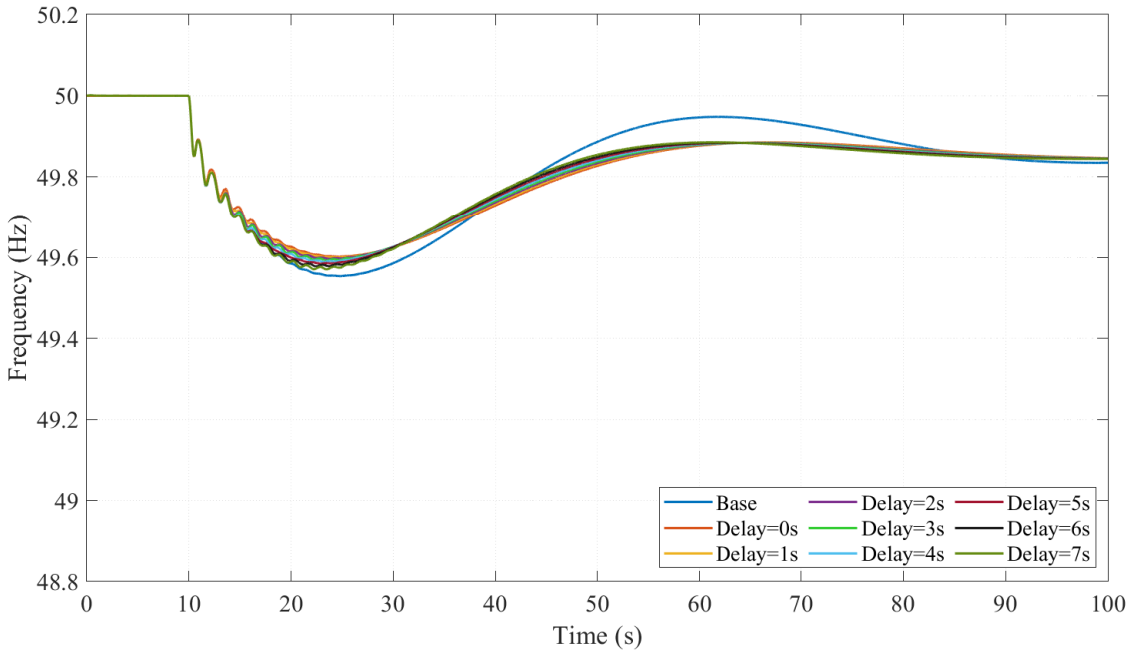

(a) Frequency response of base case test scenario (M = 4.26 s).

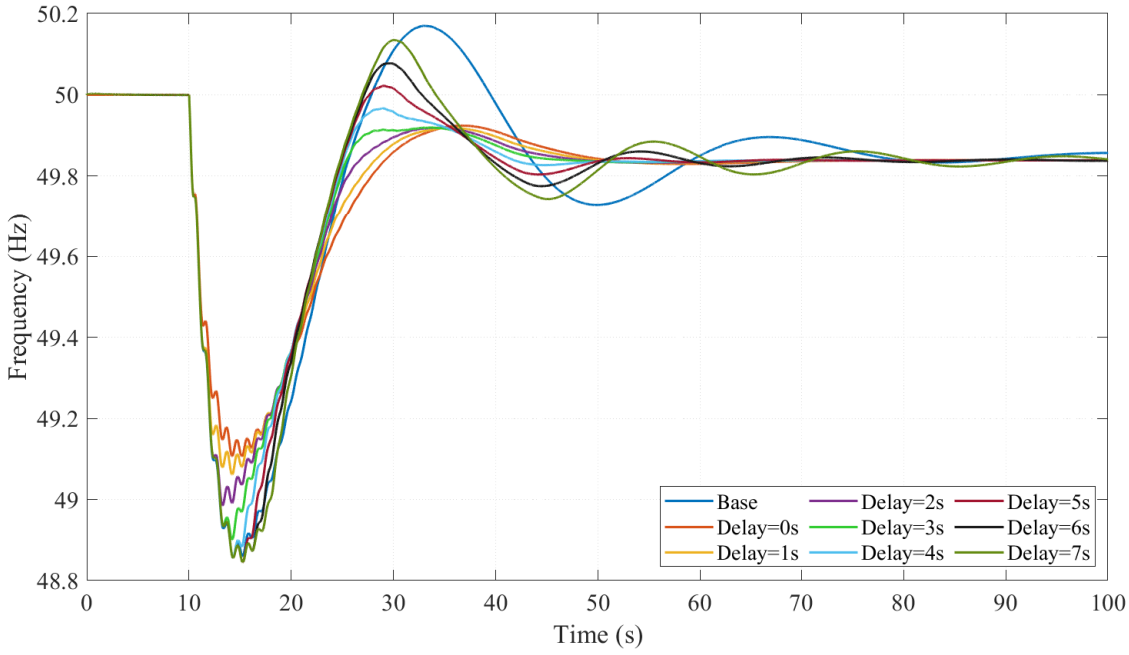

(b) Frequency response of 50% wind test scenario (M = 1.93 s).

Figure 47: Frequency response of different test scenarios for a a generator trip of 1329 MW with varying delay of FCR-D provision from EVs in PSS®E.

4.5 FFR simulation results in PSS®E

To study the impact of FFR provision by V2G, the V2G models in the network are equipped with the plant model for FFR, USPFFR. As mentioned in Section 3.7, no delays are considered for the analysis of FFR. The frequency response for a generator trip with 5 s FFR support and varying trigger frequencies are plotted in Figure 48. The disturbance is the same as for FCR-D, a generator trip of 1329 MW at 10 s mark.

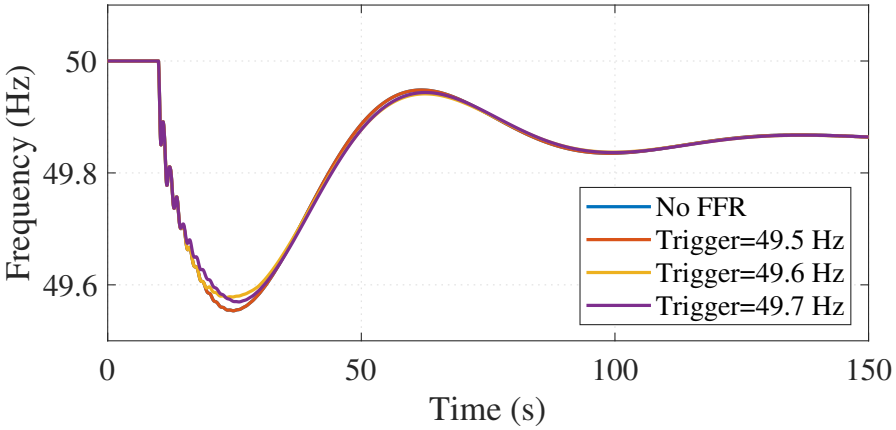

Figure 48: Frequency response of the Nordic 44 system in the basecase scenario (M = 4.26 s) to a generation trip of 1329 MW with 5 s FFR support from V2G in PSS®E.

The FFR output of the V2G model is shown in Figure 49. The FFR is activated for 49.60 Hz and 49.70 Hz trigger cases but not for 49.50 Hz, as the frequency does not drop below 49.50 Hz.

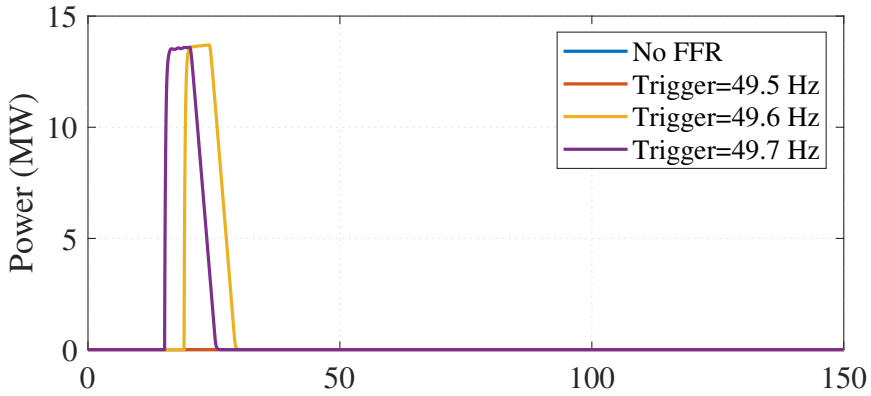

Figure 49: FFR output of the V2G model in the basecase scenario (M = 4.26 s) for a generation trip of 1329 MW in PSS®E.

Figure 50 shows the frequency nadir of all the test scenarios with FFR support at different trigger frequencies. The frequency nadir for each scenario are tabulated in Table 37. It is observed that for the same FFR capacity, the frequency nadir is most improved in the 50% wind case with an improvement of +0.093 Hz over the No FFR case for 49.70 Hz trigger frequency.

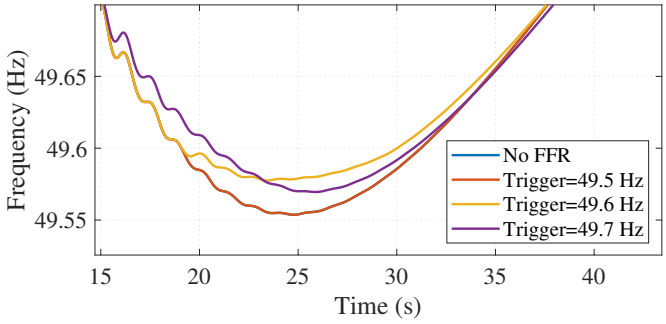

(a) Frequency nadir of base case (M = 4.26 s) test scenario.

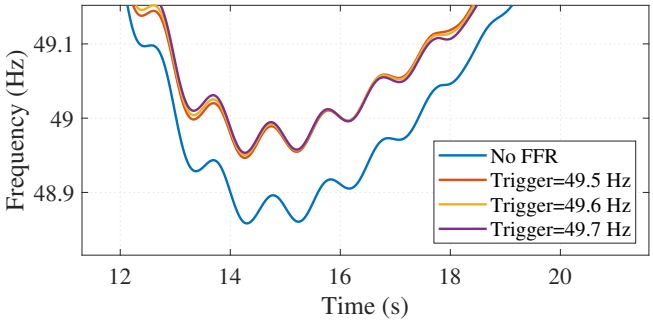

(b) Frequency nadir of 50% wind (M = 1.93 s) test scenario.

Figure 50: Frequency nadir of different test scenarios for a generation trip of 1329 MW with varying delay of FCR-D provision from V2G in PSS®E.

In Figure 50a, the frequency nadir of the base case is the highest for 49.60 Hz trigger case, followed 49.70 Hz. This is because for 49.60 Hz case, the FFR is activated closer to the nadir while in the 49.70 Hz case, the FFR support deactivates before reaching the nadir. However, the difference in these cases diminishes for the 50% wind penetration case, as shown in Figure 50b. The high RoCoF means that the frequency crosses all the trigger frequencies quite rapidly, which activates the FFR in quick succession.

Table 37: Frequency nadir (in Hz) of the test scenarios in PSS®E with a 5 s FFR support from EV models for a generation trip of ΔP_G = 1329 MW.

Scenario	**No FFR**	$f_{trigger}$ **= 49.5 Hz**	$f_{trigger}$ **= 49.6 Hz**	$f_{trigger}$ **= 49.7 Hz**
Base case (M = 4.26 s)	49.55	49.554	49.576	49.573
50% Wind (M = 1.93 s)	48.86	48.946	48.950	48.953

4.6 Centralized and Decentralized frequency measurements

The idea of centralized frequency measurements is to measure the frequency at a single bus and communicate the signal to the different EV aggregators. In an actual power system, the local frequency differs at each bus during the initial stages of a large disturbance. Therefore, it is necessary to understand the impact of the V2G service when the measured frequency differs from the local frequency at the location of the EV aggregators. The user-written model in PSS®E is designed to measure the frequency locally, which gives similar results as decentralized measurements. This is because, in the Nordic 44 power system model, the local frequencies have similar trends and identical frequency nadir, as observed in Figure 51.

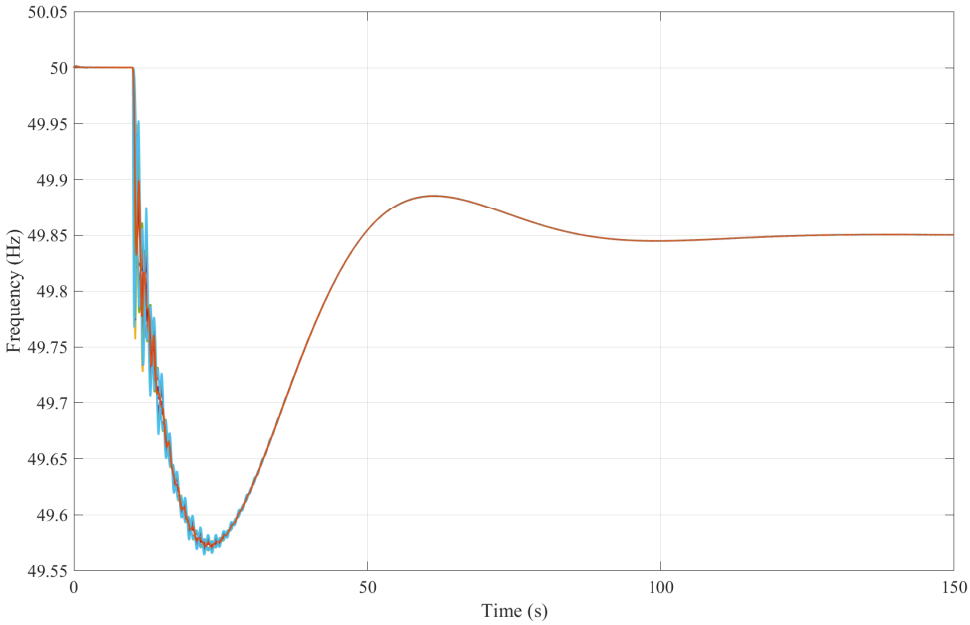

Figure 51: Frequency at all buses in PSS®E Nordic 44 model.

The oscillations in the frequencies differ, which can be noticed right after the disturbance and up to the frequency nadir. These oscillations activate the V2G models at different instances. This does not have a significant impact for FCR-D provision, since the time taken for the power to ramp up is much longer in comparison to the difference in activation times. Another aspect is the delays in communication in case of centralized frequency measurement, which is included in the analysis in previous sections.

If we take a look at the activation of FFR in Figure 52, the trigger frequency in this case is 49.60 Hz. It can be noticed that the FFR is activated at different instances due to distinct frequency oscillations at each bus. However, no significant difference was observed in the local frequencies when compared to the average frequency of all buses. This can be due to the output of the individual V2G models not being significant enough to impact their local frequencies. Further analysis is needed to setup a suitable test case and assess the impact of the different activation times.

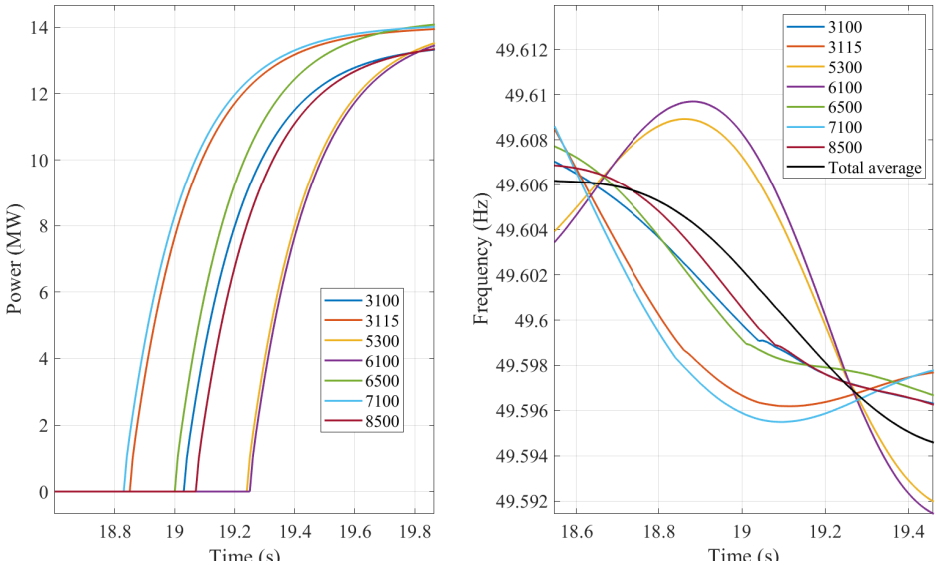

Figure 52: FFR output from the V2G models at different buses (left) with trigger frequency at 49.60 Hz and the corresponding local frequencies (right) in PSS®E.

5 Conclusions

V2G models were developed, tested and simulated in Simulink and PSS®E to provide two types of frequency support - FCR-D up and FFR. The Simulink models allowed for validation of PSS®E user-written V2G models. The simulations in Simulink were performed with a single hydro generating unit representing the power system, while the Nordic 44 system was used for PSS®E simulations.

To provide frequency ancillary service, the models are required to undergo prequalification testing laid out by ENTSO-E [1]. The step and ramp response tests for FCR-D up were performed on the Simulink V2G model first, to verify the linear activation based on the system frequency. The results confirmed that the model worked as intended. The tests were then performed on the PSS®E user-written model and the results conformed to the requirements. A comparison between the output of the two models indicated that their responses were in good agreement. When delays in the V2G service were introduced, it was observed that the models with longer delays failed to qualify to provide their full capacity, thus losing out on the revenue for the services. The frequency domain stability and performance tests were skipped due to time constraints, which is a good further work for the thesis. The prequalification tests for FFR showed that the models fulfilled all the requirements and were qualified to provide FFR service. The delays were not included for FFR, as the activation times are predefined.

The simulations were conducted to implement the model for frequency support. In Simulink, a load was stepped to create a disturbance and in PSS®E, a generating unit was tripped. The same disturbances were used for analyzing the impact of FCR-D and FFR services. Two inertia scenarios were considered both, in Simulink and PSS®E. For the higher inertia case in Simulink when the V2G model provided FCR-D support, the frequency nadir improved for shorter delays. But as the delays approached closer to the time to frequency nadir value, the improvement reduced. Similar findings were made in the PSS®E higher inertia case. The delays did not affect the frequency stability of the system in these cases. However, When the inertia of the system was reduced, the effect of the delays were pronounced. The longer delays led to an increased overshoot in frequency after the nadir, which resulted in frequency oscillations. Though the oscillations in the simulations are well damped, this may not always be the case in an actual power system.

In case of FFR simulations, results from both Simulink and PSS®E indicated an improvement in frequency nadir for higher and lower inertia scenarios. In the lower inertia case, it was observed that the difference in the frequency nadir improvement for the three trigger frequencies diminished due to high RoCoF. Also, for the same FFR quantity and disturbance, the frequency nadir improved better for the lower inertia case.

The possibility of studying the effect of centralized frequency measurements in PSS®E Nordic 44 model was looked into. A similar trend in the local frequencies at all buses was observed and thus, it was not possible to entirely simulate the effect of centralized measurements with different frequency profiles. The communication delay was taken into consideration when providing FCR-D support with the V2G models. In case of FFR,

since it requires local frequency measurements due to the short activation times, there was no question of centralized measurements. It was seen that the frequency oscillations at different buses were distinct, which activated the FFR at different instances. This, however, did not have any significant impact on the frequency.

6 Discussion

6.1 Sustainable, societal, and ethical aspects

The increasing trend in the sales of EVs has paved a way for a sustainable future. EVs help in reducing the emission levels from the transport sector. In addition to this, they can also provide many services to the power system that are discussed in this report, that can accelerate the transition to a more sustainable power production. It is a crucial benefit for the advancement of the society. The discussion of the topic and the methods used for the study do not have any ethical issues.

Renewable energy sources are the sustainable alternative for the future power system. The rapid integration of these renewable energy sources, however, is causing a decrease in the power system inertia. Low inertia power systems are prone to large instabilities due to the disturbances that commonly occur. To maintain a stable power system, and a secure supply of electricity, there is an increasing demand for ancillary services now more than ever.

The concept of V2X is a huge aspect of utilizing the EVs for various purposes like Vehicle-to-Home, Vehicle-to-Load, Vehicle-to-Grid, etc. Using the Vehicle-to-Grid technology, EVs can participate in the ancillary service market, which can aid in the advancement of renewable energy integration. V2G is a flexible technology, that can benefit both the EV owners and the power system. This report deals with the frequency support aspect; However, it can also provide other ancillary services such as demand response, backup storage, energy arbitrage and many more. The results in this report highlight the issues with the current V2G technology, that need to be addressed before it can be implemented on a large scale.

6.2 Further work

The thesis poses as an introduction to power system simulations implementing V2G services. As the possibilities with V2G are endless, the scope of research is huge and requires experimentation and rigorous testing. Few recommendations for further work in this thesis include:

- **Frequency domain stability and performance tests** -
  The step response and ramp response prequalification tests for FCR-D up were performed on the Simulink and PSS®E V2G models and the results were included in this thesis. The frequency domain stability and performance tests were also performed, but they required deeper analysis on the estimated transfer function of the V2G model from the sine tests, and also the Nyquist plots to determine the stability of a test power system defined by ENTSO-E. These tests provide extensive information about the performance of the V2G models, which will enhance the prequalification results.
- **Testing different combinations of delays** -
  In this thesis, the various scenarios based on delays in V2G support were tested.

However, the delays were considered the same for all the models in these scenarios. In reality, having multiple EV aggregators at different locations with EVs from various manufacturers would mean that they can have mismatched delays in their support. The impact of different delays in the models is an interesting work for the future.

- **Improvement in the user-written models** -
  The user-written models in PSS®E were validated by thorough testing, and they provide the necessary support to the system. However, the parameters used in these models, especially the electrical control model, need further tuning to match the performance characteristics currently available in the industry. The scaling factor needs testing to provide accurate SOC level of the battery model, corresponding to the power output to the power system. The output from the EVs have granularity and varying levels of accuracy, which have to be taken into account for a precise representation of the V2G service. To simulate the centralized frequency measurements with different frequency profiles, the model can be altered to read the frequency from an external source.

- **Improvement in the Nordic 44 model** -
  The Nordic 44 model provides a good representation of the Nordic power system. However, there are large differences in the available models and they often need modifications before they can be used for dynamic simulations. There is a need for an improvement in these available models to portray the frequency response of the actual Nordic power system, few of which are the frequency bias factor, FCR support from the hydro units and load models.

References

[1] "Supporting Document on Technical Requirements for Frequency Containment Reserve Provision in the Nordic Synchronous Area," Tech. Rep., 2021. [Online]. Available: https://www.svk.se/contentassets/8eb69c35106a4bdaa3aa5aeb6b4f346a/fcr-supporting-document_2021_draft.pdf

[2] "Technical Requirements for Frequency Containment Reserve Provision in the Nordic Synchronous Area," Tech. Rep., 2022. [Online]. Available: https://www.svk.se/contentassets/969e2290a9144454885f4ed753bb80f9/fcr-technical-requirements-2022-06-27_.pdf?siteid:40c776fe-7e5c-4838-841c-63d91e5a03c9,andquerymatch

[3] P. Kundur, *Power System Stability and Control*. EPRI power system engineering series, 1994. [Online]. Available: https://search.ebscohost.com/login.aspx?direct=true&db=cat09075a&AN=clpc.oai.edge.chalmers.folio.ebsco.com.fs00001000.d81a574b.0d61.4f0a.8e57.51996459786a&site=eds-live&scope=site

[4] X. Luo, S. Xia, and K. W. Chan, "A decentralized charging control strategy for plug-in electric vehicles to mitigate wind farm intermittency and enhance frequency regulation," *Journal of Power Sources*, vol. 248, pp. 604–614, 2014.

[5] "Technical Requirements for Frequency Containment Reserve Provision in the Nordic Synchronous Area," Tech. Rep., 2017.

[6] N. Modig, R. Eriksson, . Svenska, L. Haarla, P. Ruokolainen, M. Kuivaniemi, F. Knut, S. Hornnes, A. Vada, S. Soroush, A. Meybodi, . Energinet, D. Karlsson, and D. Gl, "Technical Requirements for Fast Frequency Reserve Provision in the Nordic Synchronous Area," Tech. Rep., 2019.

[7] S. Hofsmo, J. Lester, K. Espen, and H. Solvang, "The Nordic 44 test network," Tech. Rep., 2018.

[8] Jan Machowski, *Power System Dynamics: Stability and Control*. John Wiley & Sons, Incorporated, 2008.

[9] "Nordic Balancing Philosophy," Tech. Rep., 2021. [Online]. Available: https://eepublicdownloads.azureedge.net/clean-documents/Publications/SOC/Nordic/2022/Nordic%20Balancing%20Philosophy%20updated%202021%20for%20publication.pdf

[10] A. Shrestha and F. Gonzalez-Longatt, "Frequency stability issues and research opportunities in converter dominated power system," *Energies*, vol. 14, no. 14, 7 2021.

[11] W. Ju, K. Sun, and R. Yao, "Simulation of cascading outages using a power-flow model considering frequency," *IEEE Access*, vol. 6, pp. 37 784–37 795, 6 2018.

[12] K. Sevdari, L. Calearo, P. B. Andersen, and M. Marinelli, "Ancillary services and electric vehicles: An overview from charging clusters and chargers technology perspectives," 10 2022.

[13] K. M. Tan, V. K. Ramachandaramurthy, and J. Y. Yong, "Integration of electric vehicles in smart grid: A review on vehicle to grid technologies and optimization techniques," pp. 720–732, 1 2016.

[14] J. Hu, H. Morais, T. Sousa, and M. Lind, "Electric vehicle fleet management in smart grids: A review of services, optimization and control aspects," pp. 1207–1226, 4 2016.

[15] M. Yilmaz and P. T. Krein, "Review of benefits and challenges of vehicle-to-grid technology," in *2012 IEEE Energy Conversion Congress and Exposition, ECCE 2012*, 2012, pp. 3082–3089.

[16] A. Zecchino, A. Thingvad, P. B. Andersen, and M. Marinelli, "Test and modelling of commercial V2G CHAdeMO chargers to assess the suitability for grid services," *World Electric Vehicle Journal*, vol. 10, no. 2, 6 2019.

[17] A. Zecchino, A. M. Prostejovsky, C. Ziras, and M. Marinelli, "Large-scale provision of frequency control via V2G: The Bornholm power system case," *Electric Power Systems Research*, vol. 170, pp. 25–34, 5 2019.

[18] "Smart Charging ALignment for Europe." [Online]. Available: https://scale-horizon.eu/

[19] "Horizon Europe." [Online]. Available: https://research-and-innovation.ec.europa.eu/funding/funding-opportunities/funding-programmes-and-open-calls/horizon-europe_en

[20] "Requirement for minimum inertia in the Nordic power system," Tech. Rep., 2021.

[21] E. Ørum, L. Haarla, M. Kuivaniemi, M. Laasonen, A. Jerkø, I. Stenkløv, F. Wik, K. Elkington, R. Eriksson, N. Modig, and P. Schavemaker, "Future System Inertia 2," Tech. Rep. [Online]. Available: https://eepublicdownloads.entsoe.eu/clean-documents/Publications/SOC/Nordic/Nordic_report_Future_System_Inertia.pdf

[22] "Rate of Change of Frequency (RoCoF) withstand capability ENTSO-E guidance document for national implementation for network codes on grid connection," Tech. Rep., 2017. [Online]. Available: https://docstore.entsoe.eu/Documents/Network%20codes%20documents/Implementation/CNC/IGD-RoCoF_withstand_capability.pdf

[23] Svenska kraftnät, "Information about ancillary services." [Online]. Available: https://www.svk.se/en/stakeholders-portal/electricity-market/information-about-ancillary-services/

[24] "Frequency measurements for the provision of FFR." [Online]. Available: https://www.svk.se/aktorsportalen/bidra-med-reserver/fragor-och-svar-om-stodtjanster/

[25] "Fast Frequency Reserve SVK." [Online]. Available: https://www.svk.se/aktorsportalen/bidra-med-reserver/om-olika-reserver/ffr/

[26] "Frequency Containment Reserve, Fingrid." [Online]. Available: https://www.fingrid.fi/en/electricity-market/reserves_and_balancing/frequency-containment-reserves/

[27] "Automatic Frequency Recovery Reserve (aFRR), SVK." [Online]. Available: https://www.svk.se/aktorsportalen/bidra-med-reserver/om-olika-reserver/afrr/

[28] M. Yilmaz and P. T. Krein, "Review of the impact of vehicle-to-grid technologies on distribution systems and utility interfaces," pp. 5673–5689, 2013.

[29] W. Kempton and J. Tomić, "Vehicle-to-grid power fundamentals: Calculating capacity and net revenue," *Journal of Power Sources*, vol. 144, no. 1, pp. 268–279, 6 2005.

[30] C. Wu, H. Mohsenian-Rad, J. Huang, and J. Jatskevich, "PEV-based combined frequency and voltage regulation for smart grid," in *2012 IEEE PES Innovative Smart Grid Technologies, ISGT 2012*, 2012.

[31] Y. Tu, C. Li, L. Cheng, and L. Le, "Research on vehicle-to-grid technology," in *Proceedings - International Conference on Computer Distributed Control and Intelligent Environmental Monitoring, CDCIEM 2011*, 2011, pp. 1013–1016.

[32] E. S. Dehaghani and S. S. Williamson, "On the inefficiency of vehicle-to-grid (V2G) power flow: Potential barriers and possible research directions," in *2012 IEEE Transportation Electrification Conference and Expo, ITEC 2012*, 2012.

[33] R. Frotscher, M. Rave, E. Tenyenhuis, and P. Upadhyay, "IEEE PES Transformers Committee Reverse Power Flow Impact on Transformers-Technical Presentation," Tech. Rep., 2021.

[34] J. D. Dogger, B. Roossien, and F. D. Nieuwenhout, "Characterization of li-ion batteries for intelligent management of distributed grid-connected storage," *IEEE Transactions on Energy Conversion*, vol. 26, no. 1, pp. 256–263, 3 2011.

[35] P. Bach, H. Toghroljerdi, T. Meier, B. Eske, and J. Christian Morell Lodberg, "The Parker Project: Final Report," Tech. Rep., 2023. [Online]. Available: https://parker-project.com/introducing-parker/

[36] S. Jaman, B. Verbrugge, O. H. Garcia, M. Abdel-Monem, B. Oliver, T. Geury, and O. Hegazy, "Development and Validation of V2G Technology for Electric Vehicle Chargers Using Combo CCS Type 2 Connector Standards," *Energies*, vol. 15, no. 19, 10 2022.

[37] N. Modig, R. Eriksson, F. Svenska, and S. Kraftnät, "FCR-D design of requirements," Tech. Rep., 2017. [Online]. Available: www.entsoe.eu

[38] A. Evert, A. Soroush, A. Meybodi, M. Kuivaniemi, P. Ruokolainen, J. N. Ødegård, N. Modig, R. Eriksson, D. Gl, E. Fingrid, F. Statnett, and S. Kraftnät Svenska, "FCR-Design Project Summary report v 1.0," Tech. Rep., 2019.

[39] E. Agneholm, . Dnv-Gl, and E. A. Jansson, "FCP Project Summary report," Tech. Rep., 2017.

[40] E. Ørum, M. Kuivaniemi, M. Laasonen, A. I. Bruseth, E. A. Jansson, A. Danell, K. Elkington, and N. Modig, "Future system inertia," Tech. Rep. [Online]. Available: https://eepublicdownloads.entsoe.eu/clean-documents/Publications/SOC/Nordic/Nordic_report_Future_System_Inertia.pdf

[41] M. Chen and G. A. Rincón-Mora, "Accurate electrical battery model capable of predicting runtime and I-V performance," *IEEE Transactions on Energy Conversion*, vol. 21, no. 2, pp. 504–511, 6 2006.

[42] Y. Ota, H. Taniguchi, T. Nakajima, K. M. Liyanage, J. Baba, and A. Yokoyama, "Autonomous distributed V2G (vehicle-to-grid) satisfying scheduled charging," *IEEE Transactions on Smart Grid*, vol. 3, no. 1, pp. 559–564, 3 2012.

[43] "System Operation Agreement between the Nordic Transmission System Operators (Nordic SOA)," Tech. Rep. [Online]. Available: https://eepublicdownloads.entsoe.eu/clean-documents/SOC%20documents/Nordic/Nordic%20SOA_Main%20Agreement.pdf

Appendix

A Nordic 44 model

A.1 SLD of the N44 model

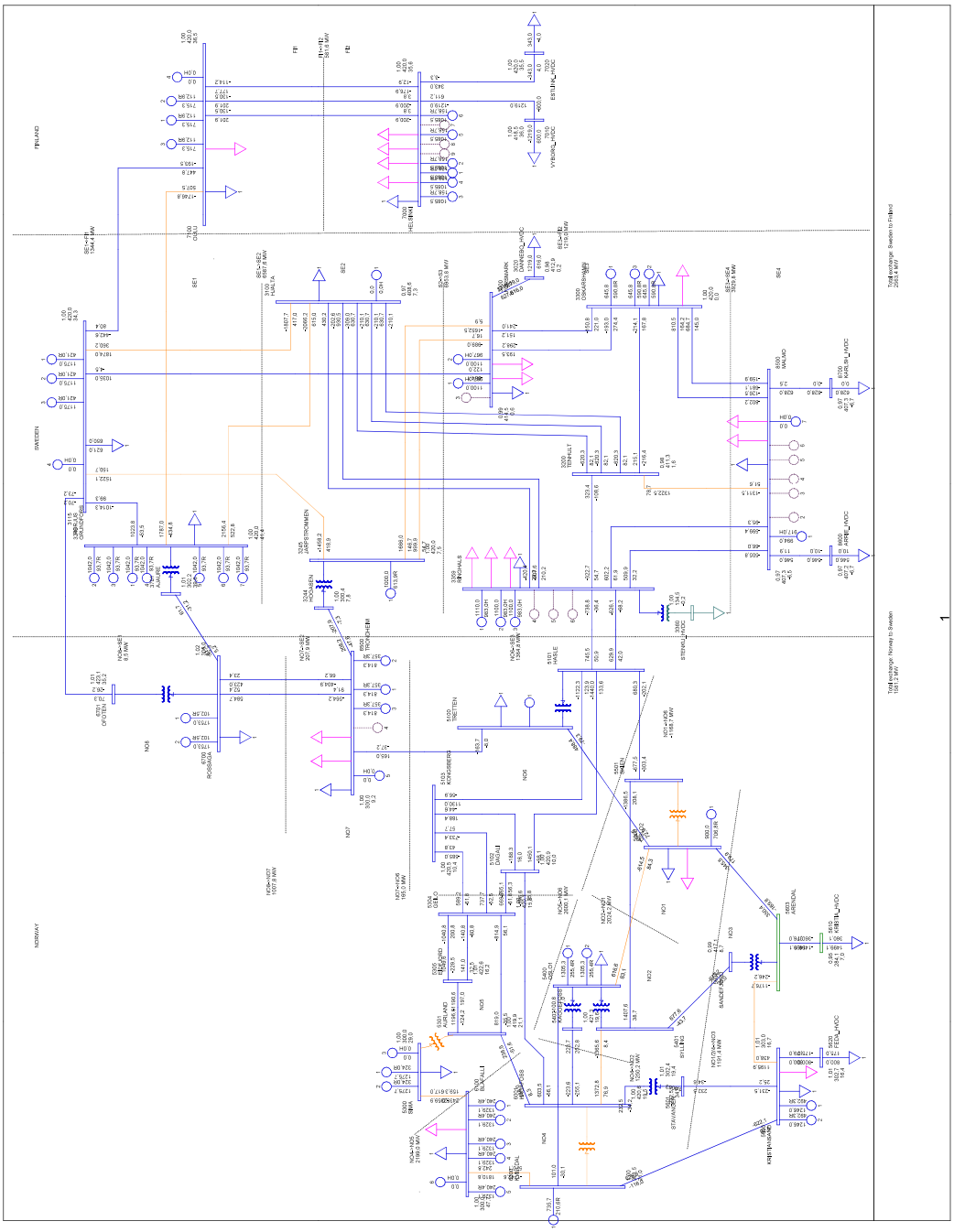

A.2 Location of FCR units and V2G models

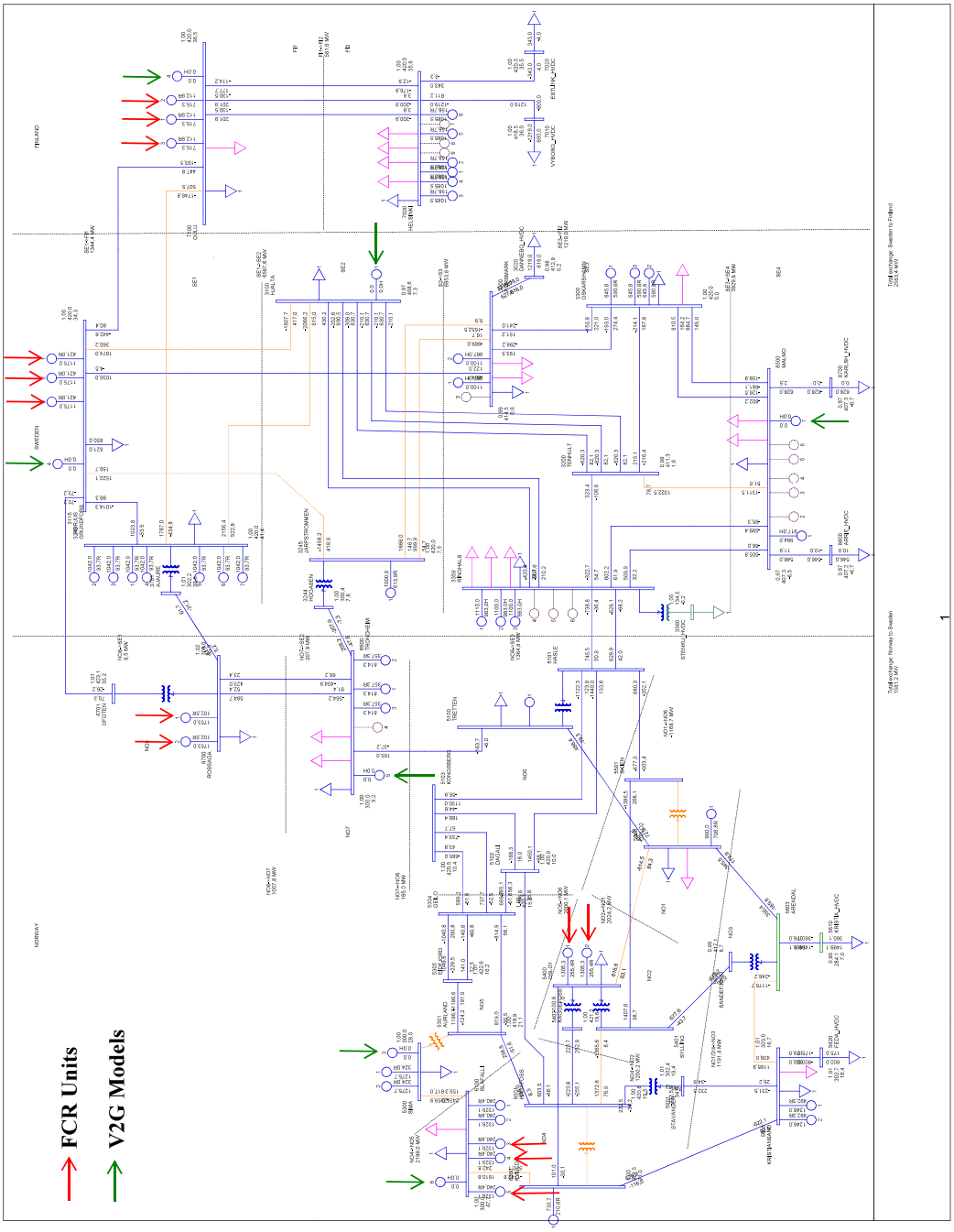

A.3 Location of Generator trip

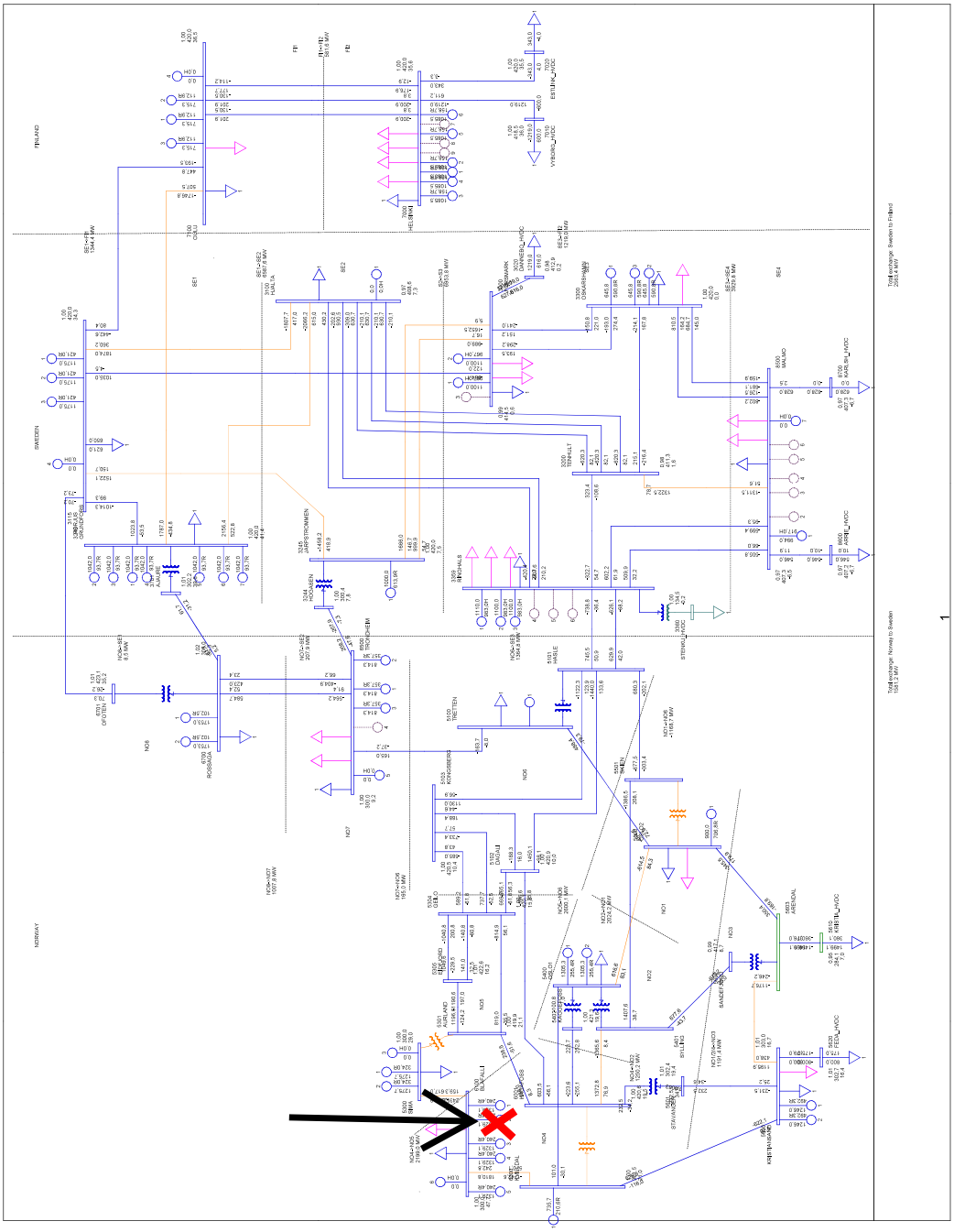

A.4 Location of Wind generators

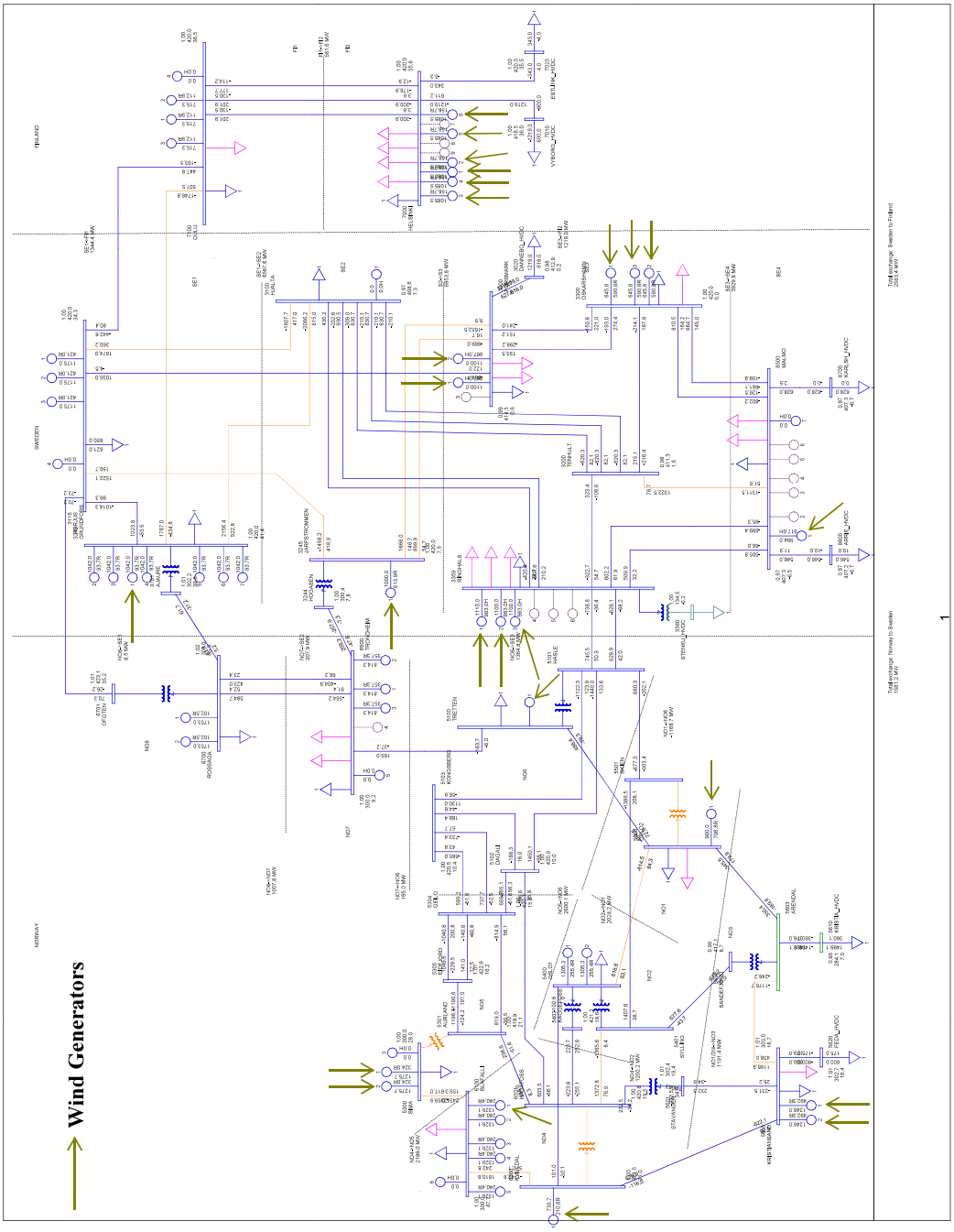

B Code for user-written models

B.1 Code for plant control model - USPMDL

...PSSE models\Nordic44_SE_battery_model\Plant_Model.for 1

```
C[USPMDL] Generic Renewable Plant Model
C
      SUBROUTINE USPMDL(MC,SLOT)
C
C
      INCLUDE 'COMON4.INS'
C
      IMPLICIT NONE
C
      INTEGER J          ! starting CON index
      INTEGER K          ! starting STATE index
      INTEGER L          ! starting VAR index
      INTEGER M          ! starting ICON index
      INTEGER MC         ! machine index
      INTEGER SLOT       ! index into STRT array allocation
      INTEGER IBUS       ! bus index
      INTEGER index
C
      REAL Pdroop        ! local variables
      REAL VINP          ! Elementary block variable
      REAL VOUT          ! Elementary block variable
      REAL freq
      REAL dbd
      REAL length
      REAL Fdelay
      EXTERNAL  NOTMID
C
C++
C     MODE 8 - GET DATA DESCRIPTIONS
C--
      IF (MODE.EQ.8) THEN
C++
C     Add CON_DSCRPT here
      CON_DSCRPT(1) = 'Tfreq (s)'     ! Frequency filter time constant
      CON_DSCRPT(2) = 'Tdel (s)'      ! Frequency measurement delay
      CON_DSCRPT(3) = 'f_trigg (s)'   ! FCR trigger frequency
      CON_DSCRPT(4) = 'KD'            ! Droop constant
      CON_DSCRPT(5) = 'Tpow (s)'      ! Power output filter time constant
      CON_DSCRPT(6) = 'Pmax (pu)'     ! Max power output


C     Add ICON_DSCRPT here
C--
         RETURN
      ENDIF
C
      J=WSTRTIN(1,SLOT)                          ! STARTING 'CON'
      K=WSTRTIN(2,SLOT)                          ! STARTING 'STATE'
      L=WSTRTIN(3,SLOT)                          ! STARTING 'VAR'
```

...PSSE models\Nordic44_SE_battery_model\Plant_Model.for 2

```
50        M=WSTRTIN(4,SLOT)                          ! STARTING 'ICON'
51        IBUS = ABS(NUMTRM(MC))                  ! BUS INTERNAL INDEX NUMBER
52        freq = BSFREQ(IBUS)
53        length = L+6+(CON(J+1)/(DELT))-1
54  C
55  C++
56  C     MODE 2 - CALCULATE DERIVATIVES
57  C--
58        IF (MODE.EQ.2) THEN
59  C
60  C++
61  C        MODE 2 code portion is inserted here
62
63  C     STATE K derivative
64        VINP = freq
65        VOUT = LAG_MODE2( 1.0,CON(J),VINP,K )
66
67  C     STATE L+3 calculation
68        IF (KPAUSE == 1) THEN
69            CONTINUE
70        ELSE
71
72            IF (VAR(L+4) > length) THEN
73                VAR(L+4) = L+6
74                VAR(L+5) = 1
75            ELSE
76                index = INT(VAR(L+4))
77                VAR(index) = freq
78                VAR(L+4) = VAR(L+4)+1
79            ENDIF
80
81            IF (VAR(L+4) > length) THEN
82                CONTINUE
83            ELSE
84
85                IF (VAR(L+5) >= 1) THEN
86                    index = INT(VAR(L+4))
87                    VAR(L+3) = VAR(index)
88                ELSE
89                    VAR(L+3) = 0.0
90                ENDIF
91            ENDIF
92        ENDIF
93
94
95  C     VAR L calculation
96        IF(VAR(L+3) < VAR(L+2)) THEN
97            VAR(L) = VAR(L+3)-VAR(L+2)
98        ELSE
```

```
...PSSE models\Nordic44_SE_battery_model\Plant_Model.for                    3
 99            VAR(L) = 0.0
100         ENDIF
101
102 C       VAR L+1 calculation
103         Pdroop = VAR(L)*CON(J+3)
104         VAR(L+1) = Pdroop
105
106 C       STATE K+1 derivative
107         VINP = VAR(L+1)
108         VOUT = NWLAG_MODE2(1.0,CON(J+4),CON(J+5),0.0,VINP,K+1 )
109
110
111
112 C--
113            RETURN
114         ENDIF
115 C
116 C++
117 C       MODE 3 - SET Model output
118 C--
119         IF (MODE.EQ.3) THEN
120 C
121 C++
122 C          MODE 3 code portion is inserted here
123             WPCMND(WNDNUM(MC)) = STATE(K+1)
124 C--
125            RETURN
126         ENDIF
127 C
128 C++
129 C       MODE 1 - INITIALIZATION
130 C--
131         IF (MODE.EQ.1) THEN
132 C
133 C++
134 C       MODE 1 code portion is inserted here
135
136 C       Frequency filter
137         STATE(K) = freq
138
139 C       Frequency delay
140         Fdelay = STATE(K)
141         VAR(L+3) = Fdelay
142
143 C       VAR(L) initialization
144         dbd = CON(J+2)-1
145         VAR(L+2) = dbd
146
147         IF(VAR(L+3) < VAR(L+2)) THEN
```

```
...PSSE models\Nordic44_SE_battery_model\Plant_Model.for                    4
148           VAR(L) = VAR(L+3)-VAR(L+2)
149         ELSE
150           VAR(L) = 0.0
151         ENDIF
152
153   C     VAR(L+1) initialization
154         Pdroop = CON(J+3)*VAR(L)
155         VAR(L+1) = Pdroop
156
157   C     STATE(K+1) initialization
158         STATE(K+1) = VAR(L+1)
159         WPCMND(WNDNUM(MC)) = STATE(K+1)
160
161   C     Delay initialization
162         VAR(L+4) = L+6
163         VAR(L+5) = 0
164
165         IF (CON(J+1) > 5) THEN
166           CON(J+1) = 5
167           WRITE(LPDEV, *) 'ERROR: USPMDL: Time delay should be <= 5 s'
168         ELSE
169           VAR(L+6:length) = 1.0;
170         ENDIF
171
172
173   C--
174            RETURN
175         ENDIF
176   C
177   C++
178   C     MODE 4 - set NINTEG
179   C--
180         IF (MODE.EQ.4) THEN
181            IF (MIDTRM) THEN
182               CALL NOTMID
183            ELSE
184   C++
185   C        Set NINTEG
186            IF(NINTEG < K+1) NINTEG = K+1
187   C--
188            ENDIF
189   C
190            RETURN
191         ENDIF
192   C
193   C++
194   C        MODE 6 - DYDA
195   C--
196         IF (MODE.EQ.6) THEN
```

...PSSE models\Nordic44_SE_battery_model\Plant_Model.for 5

```
197 C++
198 C        MODE 6 code portion is inserted here
199 C--
200          RETURN
201       ENDIF
202 C
203 C++
204 C        MODE 5 OR 7 - ACTIVITY DOCU
205 C--
206       IF (MODE==5 .OR. MODE==7) THEN
207          IF (MODE==5) THEN
208             CALL DOCUHEADING
209          ELSE
210 C++
211 C        If you don't have MODE 7 checks, just RETURN
212 C--
213             RETURN
214 C ============================================================================
215
216          ENDIF
217 C++
218 C     This portion of code is common to both MODE 5 and MODE 7
219 C--
220 C     Add code to output the model variables
221 C
222          RETURN
223       ENDIF
224 C
225       RETURN
226 C++
227 C     FORMAT STATEMENTS
228 C--
229       END SUBROUTINE USPMDL
230
```

B.2 Code for plant control model - USPFFR

```
... models\Nordic44_SE_battery_model\Plant_Model_FFR.for                    1
C[USPMDL] Generic Renewable Plant Model
C
      SUBROUTINE USPFFR(MC,SLOT)
C


C
      INCLUDE 'COMON4.INS'
C
      IMPLICIT NONE
C
      INTEGER J          ! starting CON index
      INTEGER K          ! starting STATE index
      INTEGER L          ! starting VAR index
      INTEGER M          ! starting ICON index
      INTEGER MC         ! machine index
      INTEGER SLOT       ! index into STRT array allocation
      INTEGER IBUS       ! bus index
C
      REAL VINP          ! Elementary block variable
      REAL VOUT          ! Elementary block variable
      REAL freq
      REAL dbd
      EXTERNAL  NOTMID
C
C++
C     MODE 8 - GET DATA DESCRIPTIONS
C--
      IF (MODE.EQ.8) THEN
C++
C     Add CON_DSCRPT here
      CON_DSCRPT(1) = 'Tfreq (s)'     ! Frequency filter time constant
      CON_DSCRPT(2) = 'f_trigg (s)'   ! FFR trigger frequency
      CON_DSCRPT(3) = 'Pmax (pu)'     ! Max power output
      CON_DSCRPT(4) = 'Tpow (s)'      ! Power output filter time constant

      CON_DSCRPT(5) = 'Tactivate (s)' ! Activation time of FFR

C     Add ICON_DSCRPT here
C--
         RETURN
      ENDIF
C
      J=WSTRTIN(1,SLOT)                          ! STARTING 'CON'
      K=WSTRTIN(2,SLOT)                          ! STARTING 'STATE'
      L=WSTRTIN(3,SLOT)                          ! STARTING 'VAR'
      M=WSTRTIN(4,SLOT)                          ! STARTING 'ICON'
      IBUS = ABS(NUMTRM(MC))                  ! BUS INTERNAL INDEX NUMBER
      freq = BSFREQ(IBUS)
C
```

```
... models\Nordic44_SE_battery_model\Plant_Model_FFR.for                    2
 49 C++
 50 C     MODE 2 - CALCULATE DERIVATIVES
 51 C--
 52       IF (MODE.EQ.2) THEN
 53 C
 54 C++
 55 C        MODE 2 code portion is inserted here
 56
 57 C     STATE K derivative
 58       VINP = freq
 59       VOUT = LAG_MODE2( 1.0,CON(J),VINP,K )
 60
 61 C     VAR L+2 calculation
 62       IF ((STATE(K) < VAR(L)) .AND. (VAR(L+3) == 0.0)) THEN
 63           VAR(L+2) = TIME
 64           VAR(L+3) = 1.0
 65       ENDIF
 66
 67 C     VAR(L+1) calculation
 68       IF (VAR(L+3)  > 0.0) THEN
 69           VAR(L+1) = (CON(J+2)/CON(J+4))*(TIME-VAR(L+2))
 70       ELSE
 71           VAR(L+1) = 0.0
 72       ENDIF
 73
 74       IF ((VAR(L+1)>=CON(J+2)) .AND. (TIME>=VAR(L+2)+CON(J+4)+5.0)) THEN
 75           IF (VAR(L+5) == 0.0) THEN
 76               VAR(L+4) = TIME
 77               VAR(L+5) = 1.0
 78           ENDIF
 79
 80       ENDIF
 81
 82       IF (VAR(L+5) >= 1.0) THEN
 83           VAR(L+1) = CON(J+2)-(CON(J+2)/5)*(TIME-VAR(L+4))
 84       ENDIF
 85
 86
 87 C     STATE K+1 derivative
 88       VINP = VAR(L+1)
 89       VOUT = NWLAG_MODE2(1.0,CON(J+3),CON(J+2),0.0,VINP,K+1 )
 90
 91
 92
 93 C--
 94          RETURN
 95       ENDIF
 96 C
 97 C++
```

```
... models\Nordic44_SE_battery_model\Plant_Model_FFR.for                    3
 98 C     MODE 3 - SET Model output
 99 C--
100       IF (MODE.EQ.3) THEN
101 C
102 C++
103 C        MODE 3 code portion is inserted here
104           WPCMND(WNDNUM(MC)) = STATE(K+1)
105 C--
106          RETURN
107       ENDIF
108 C
109 C++
110 C     MODE 1 - INITIALIZATION
111 C--
112       IF (MODE.EQ.1) THEN
113 C
114 C++
115 C     MODE 1 code portion is inserted here
116
117 C     Frequency filter
118       STATE(K) = freq
119
120 C     VAR(L) initialization
121       dbd = CON(J+1)-1.0
122       VAR(L) = dbd
123
124 C     VAR(L+1) initialization
125       VAR(L+1) = 0.0
126
127 C     VAR(L+2) initialization
128       VAR(L+2) = 0.0
129
130 C     VAR(L+3) initialization
131       VAR(L+3) = 0.0
132
133 C     VAR(L+4) initialization
134       VAR(L+4) = 0.0
135
136 C     VAR(L+5) initialization
137       VAR(L+5) = 0.0
138
139 C     STATE(K+1) initialization
140       STATE(K+1) = VAR(L+1)
141       WPCMND(WNDNUM(MC)) = STATE(K+1)
142
143
144 C--
145          RETURN
146       ENDIF
```

```
... models\Nordic44_SE_battery_model\Plant_Model_FFR.for                    4
147 C
148 C++
149 C     MODE 4 - set NINTEG
150 C--
151       IF (MODE.EQ.4) THEN
152          IF (MIDTRM) THEN
153             CALL NOTMID
154          ELSE
155 C++
156 C     Set NINTEG
157       IF(NINTEG < K+1) NINTEG = K+1
158 C--
159          ENDIF
160 C
161          RETURN
162       ENDIF
163 C
164 C++
165 C        MODE 6 - DYDA
166 C--
167       IF (MODE.EQ.6) THEN
168 C++
169 C        MODE 6 code portion is inserted here
170 C--
171          RETURN
172       ENDIF
173 C
174 C++
175 C        MODE 5 OR 7 - ACTIVITY DOCU
176 C--
177       IF (MODE==5 .OR. MODE==7) THEN
178          IF (MODE==5) THEN
179             CALL DOCUHEADING
180          ELSE
181 C++
182 C        If you don't have MODE 7 checks, just RETURN
183 C--
184             RETURN
185 C ======================================================================
186
187          ENDIF
188 C++
189 C     This portion of code is common to both MODE 5 and MODE 7
190 C--
191 C     Add code to output the model variables
192 C
193          RETURN
194       ENDIF
195 C
```

```
... models\Nordic44_SE_battery_model\Plant_Model_FFR.for                    5
196         RETURN
197  C++
198  C      FORMAT STATEMENTS
199  C--
200         END SUBROUTINE USPFFR
201
```

B.3 Code for electrical control model - USEMDL

...E models\Nordic44_SE_battery_model\Electric_Model.for 1

```
C[USEMDL]         RENEWABLE ELECTRICAL CONTROLLER MODEL
C
C
C
C
C
C
      SUBROUTINE USEMDL(MC,SLOT)
C
C
C
      INCLUDE 'COMON4.INS'
C
      IMPLICIT NONE
C
      INTEGER J          ! starting CON index
      INTEGER K          ! starting STATE index
      INTEGER L          ! starting VAR index
      INTEGER M          ! starting ICON index
      INTEGER MC         ! machine index
      INTEGER SLOT       ! index into STRT array allocation
      INTEGER WMC        ! Wind machine index
      INTEGER index

      REAL VINP
      REAL VOUT
      REAL dP
      REAL Vsense
      REAL Ti
      REAL length

C

      EXTERNAL  NOTMID
C
C++
C     MODE 8 - GET DATA DESCRIPTIONS
C--
      IF (MODE.EQ.8) THEN
C++
C     Add CON_DSCRPT here
      CON_DSCRPT(1) = 'Power scaling factor K'
      CON_DSCRPT(2) = 'Number of EVs n'
      CON_DSCRPT(3) = 'Battery nominal voltage Vnom (V)'
      CON_DSCRPT(4) = 'Double layer capacitance time constant Ct*Rt (s)'
      CON_DSCRPT(5) = 'Series resistance Rs (Ohms)'
      CON_DSCRPT(6) = 'Initial SOC (pu)'
      CON_DSCRPT(7) = 'Max SOC (pu)'
      CON_DSCRPT(8) = 'Min SOC (pu)'
```

```
50        CON_DSCRPT(9) = 'Sensitivity parameter of OCV to the SOC s'
51        CON_DSCRPT(10) = 'RT/F constant'
52        CON_DSCRPT(11) = 'Nominal battery capacity Cnom (Ah)'
53        CON_DSCRPT(12) = 'Charge transfer resistance Rt (Ohms)'
54        CON_DSCRPT(13) = 'Current integrator gain Ki'
55        CON_DSCRPT(14) = 'Nominal current (A)'
56        CON_DSCRPT(15) = 'Energy gain Ke'
57        CON_DSCRPT(16) = 'Time delay in sec'
58
59  C     Add ICON_DSCRPT here
60  C--
61           RETURN
62        ENDIF
63  C
64        J=WSTRTIN(1,SLOT)                          ! STARTING 'CON'
65        K=WSTRTIN(2,SLOT)                          ! STARTING 'STATE'
66        L=WSTRTIN(3,SLOT)                          ! STARTING 'VAR'
67        M=WSTRTIN(4,SLOT)                          ! STARTING 'ICON'
68        WMC = WNDNUM(MC)                           ! Wind machine index
69        length = L+9+(CON(J+15)/(DELT))-1          ! length of delay
70
71  C
72
73  C++
74  C     MODE 2 - CALCULATE DERIVATIVES
75  C--
76        IF (MODE.EQ.2) THEN
77  C
78  C++
79  C        MODE 2 code portion is inserted here
80
81           !VAR(L+6) calculation
82
83           IF (KPAUSE == 1) THEN
84               CONTINUE
85           ELSE
86               IF (VAR(L+7) > length) THEN
87                   VAR(L+7) = L+9
88                   VAR(L+8) = 1
89               ELSE
90                   index = INT(VAR(L+7))
91                   VAR(index) = WPCMND(WMC)*(-CON(J)/CON(J+1))
92                   VAR(L+7) = VAR(L+7)+1
93               ENDIF
94
95               IF (VAR(L+7) > length) THEN
96                   CONTINUE
97               ELSE
98
```

...E models\Nordic44_SE_battery_model\Electric_Model.for 3

```
 99                    IF (VAR(L+8) >= 1) THEN
100                        index = INT(VAR(L+7))
101                        VAR(L+6) = VAR(index)
102                    ELSE
103                        VAR(L+6) = 0.0
104                    ENDIF
105                ENDIF
106         ENDIF
107 C       Check for SOC limits and direction of Power flow
108
109
110
111           IF ((VAR(L+2) > CON(J+6)) .AND. (VAR(L+6) > 0)) THEN
112               VAR(L+6) = 0.0
113               STATE(K) = 0.0
114               DSTATE(K) = 0.0
115               STORE(K) = 0.0
116               STATE(K+1) = 0.0
117               DSTATE(K+1) = 0.0
118               STORE(K+1) = 0.0
119               STATE(K+2) = 0.0
120               DSTATE(K+2) = 0.0
121               STORE(K+2) = 0.0
122               STATE(K+3) = 0.0
123               DSTATE(K+3) = 0.0
124               STORE(K+3) = 0.0
125               Vsense = CON(J+8)*CON(J+9)*LOG(VAR(L+2)/(CON(J+10)-VAR(L+2)))
126               VAR(L) = CON(J+2)+Vsense
127               VAR(L+1) = STATE(K)*CON(J+4)
128               VAR(L+3) = VAR(L) + VAR(L+1) + STATE(K+2)
129               VAR(L+4) = VAR(L+3)*STATE(K)
130               VAR(L+5) = VAR(L+4)*(1/CON(J+2))*(-1/CON(J+13))
131           ELSEIF ((VAR(L+2) < CON(J+7)) .AND. (VAR(L+6) < 0)) THEN
132               VAR(L+6) = 0.0
133               STATE(K) = 0.0
134                DSTATE(K) = 0.0
135               STORE(K) = 0.0
136               STATE(K+1) = 0.0
137               DSTATE(K+1) = 0.0
138               STORE(K+1) = 0.0
139               STATE(K+2) = 0.0
140               DSTATE(K+2) = 0.0
141               STORE(K+2) = 0.0
142               Vsense = CON(J+8)*CON(J+9)*LOG(VAR(L+2)/(CON(J+10)-VAR(L+2)))
143               VAR(L) = CON(J+2)+Vsense
144               VAR(L+1) = STATE(K)*CON(J+4)
145               VAR(L+3) = VAR(L) + VAR(L+1) + STATE(K+2)
146               VAR(L+4) = VAR(L+3)*STATE(K)
147               VAR(L+5) = VAR(L+4)*(1/CON(J+2))*(-1/CON(J+13))
```

```
...E models\Nordic44_SE_battery_model\Electric_Model.for                    4
148               STATE(K+3) = 0.0
149               DSTATE(K+3) = 0.0
150               STORE(K+3) = 0.0
151           ELSE
152               !STATE(K) derivative
153               dP =  VAR(L+6)-VAR(L+4)
154               Ti = 1/CON(J+12)
155               VINP = dP/CON(J+2)
156               VOUT = INT_MODE2(Ti, VINP, K)
157
158               !STATE(K+1) derivative
159               VINP = STATE(K)
160               VOUT = INT_MODE2(1.0, VINP, K+1)
161
162               !VAR(L+2) calculation
163                IF (CON(J+5) > CON(J+6)) THEN
164                    CON(J+5) = CON(J+6)
165                ELSEIF (CON(J+5) < CON(J+7)) THEN
166                    CON(J+5) = CON(J+7)
167                ELSE
168                    VAR(L+2) = CON(J+5)+STATE(K+1)/(3600*CON(J+10))
169                ENDIF
170
171                !VAR(L) calculation
172                Vsense = CON(J+8)*CON(J+9)*LOG(VAR(L+2)/(CON(J+10)-VAR(L
                     +2)))
173                VAR(L) = CON(J+2)+Vsense
174
175                !VAR(L+1) calculation
176                VAR(L+1) = STATE(K)*CON(J+4)
177
178                !STATE(K+2) derivative
179                VINP = STATE(K)
180                VOUT = LAG_MODE2(CON(J+11), CON(J+3), VINP, K+2)
181
182                !VAR(L+3) calculation
183                VAR(L+3) = VAR(L) + VAR(L+1) + STATE(K+2)
184
185                !VAR(L+4) calculation
186                VAR(L+4) = VAR(L+3)*STATE(K)
187
188                !VAR(L+5) calculation
189                VAR(L+5) = VAR(L+4)*(1/CON(J+2))*(-1/CON(J+13))
190
191                !STATE(K+3) derivative
192                VINP = PELEC(MC)
193                VOUT = INT_MODE2(1/CON(J+14) , VINP, K+3)
194
195
```

```
196            ENDIF
197
198            WIQCMD(WMC) = 0.0
199
200   C--
201           RETURN
202         ENDIF
203   C
204
205
206
207   C++
208   C     MODE 3 - SET Model output
209   C--
210         IF (MODE.EQ.3) THEN
211   C
212   C++
213   C        MODE 3 code portion is inserted here
214           WIPCMD(WMC) = VAR(L+5)
215           WIQCMD(WMC) = 0.0
216   C--
217           RETURN
218         ENDIF
219   C
220   C++
221   C     MODE 1 - INITIALIZATION
222   C--
223         IF (MODE.EQ.1) THEN
224   C
225   C++
226   C        MODE 1 code portion is inserted here
227
228           !VAR(L+5) Initialization
229           VAR(L+5) = WIPCMD(WMC)
230
231           !VAR(L+4) Initialization
232           IF ((CON(J+1) == 0.0) .OR. (CON(J) == 0.0)) THEN
233               VAR(L+4) = 0.0
234               WRITE(LPDEV, *) 'ERROR: USEMDL: K and n cannot be 0'
235           ELSE
236               VAR(L+4) = -CON(J+2)*(CON(J)/CON(J+1))*VAR(L+5)
237           ENDIF
238
239           !VAR(L+6) initialization
240           VAR(L+6) = WPCMND(WMC)*(-CON(J)/CON(J+1))
241
242           !STATE(K) initialization
243           IF ((CON(J+1) == 0.0) .OR. (CON(J) == 0.0)) THEN
244               STATE(K) = 0.0
```

```
245               WRITE(LPDEV, *) 'ERROR: USEMDL: K and n cannot be 0'
246           ELSE
247               dP = VAR(L+6)-VAR(L+4)
248               STATE(K) = dP/CON(J+2)
249           ENDIF
250
251           !STATE(K+1) initialization
252           STATE(K+1) = STATE(K)
253
254           !VAR(L+2) initialization
255           IF (CON(J+5) > CON(J+6)) THEN
256               CON(J+5) = CON(J+6)
257           ELSEIF (CON(J+5) < CON(J+7)) THEN
258               CON(J+5) = CON(J+7)
259           ELSE
260               VAR(L+2) = CON(J+5)+STATE(K+1)/(3600*CON(J+10))
261           ENDIF
262
263           !VAR(L) initialization
264           Vsense = CON(J+8)*CON(J+9)*LOG(VAR(L+2)/(CON(J+10)-VAR(L+2)))
265           VAR(L) = CON(J+2)+Vsense
266
267           !VAR(L+1) initialization
268           VAR(L+1) = STATE(K)*CON(J+4)
269
270           !STATE(K+2) initialization
271           STATE(K+2) = CON(J+11)*STATE(K)
272
273           !VAR(L+3) initialization
274           VAR(L+3) = VAR(L)+VAR(L+1)+STATE(K+2)
275
276           WIQCMD(WMC) = 0.0
277
278           !STATE(K+3) initialization
279           STATE(K+3) = PELEC(MC)
280
281           VAR(L+7) = L+9
282           VAR(L+8) = 0
283
284           IF (CON(J+15) > 5) THEN
285            CON(J+15) = 5
286            WRITE(LPDEV, *) 'ERROR: USPMDL: Time delay should be <= 5 s'
287           ELSE
288            VAR(L+9:length) = 0.0;
289           ENDIF
290
291           RETURN
292         ENDIF
293 C
```

```
...E models\Nordic44_SE_battery_model\Electric_Model.for                    7
294  C++
295  C     MODE 4 - set NINTEG
296  C--
297        IF (MODE.EQ.4) THEN
298           IF (MIDTRM) THEN
299              CALL NOTMID
300           ELSE
301  C++
302  C     Set NINTEG
303           IF(NINTEG < K+2) NINTEG = K+2
304  C     NINTEG = MAX(NINTEG, K+1) - does the same thing
305  C--
306           ENDIF
307  C
308           RETURN
309        ENDIF
310  C
311  C++
312  C        MODE 6 - DYDA
313  C--
314        IF (MODE.EQ.6) THEN
315  C++
316  C        MODE 6 code portion is inserted here
317  C--
318           RETURN
319        ENDIF
320  C
321  C++
322  C        MODE 5 OR 7 - ACTIVITY DOCU
323  C--
324        IF (MODE==5 .OR. MODE==7) THEN
325           IF (MODE==5) THEN
326              CALL DOCUHEADING
327           ELSE
328  C++
329  C        If you don't have MODE 7 checks, just RETURN
330  C--
331              RETURN
332  C ======================================================================
333
334           ENDIF
335  C++
336  C     This portion of code is common to both MODE 5 and MODE 7
337  C--
338  C     Add code to output the model variables
339  C
340           RETURN
341        ENDIF
342  C
```

```
...E models\Nordic44_SE_battery_model\Electric_Model.for                    8
343         RETURN
344  C++
345  C      FORMAT STATEMENTS
346  C--
347         END SUBROUTINE USEMDL
348
```